NSF/CEE-81057

PB82-147919

WASHINGTON UNIVERSIT

SCHOOL OF ENGINEERING AND APPLIED SCIENCE
DEPARTMENT OF CIVIL ENGINEERING

SHORE IV

Finite Element Program for Dynamic and Static Analysis of Shells of Revolution

THEORETICAL MANUAL

by

O. M. El-Shafee, P. K. Basu, B. J. Lee

and

P. L. Gould

Research Report No. 57   Structural Division   October 1981

This report is part of final report for
National Science Foundation Grant
PRF7900012

PREFACE

This manual describes the theoretical background of the software (SHORE-IV) for the static and dynamic analysis of axisymmetric shells and plates.

In this program the shell is discretized by high-precision rotational shell finite elements of any quadratic shape. The thickness of the element may vary in the meridional direction. Special open type elements are used to take into account the effect of regularly spaced members at the base or at some intermediate level of the shell. The shell may be isotropic, or orthotropic (single or multi-layer), or framed. The program can take care of both axisymmetric and asymmetric external effects like mechanical and thermal loads, horizontal and vertical base accelerations, and support settlements. For shells founded over shallow ring footing the soil-structure interaction can be included in the analysis. The soil medium may be shallow or deep strata. The program can handle layered soil material as well as half-space soil medium.

TABLE OF CONTENTS

INTRODUCTION

SHORE-IV is a finite element program for the linear static and dynamic analysis of arbitrarily loaded axisymmetric plates and shells. It is written in FORTRAN IV language.

The meridian curve of the shell may have any geometric shape including closed ends. In addition to common boundary conditions, the shell may be supported on a series of regularly spaced inclined and/or vertical members around the circumference, (see Fig. 1). Such a framework may be located at some intermediate level as well (see Fig. 2). Also framed structures which follow the form of a surface of revolution can be analyzed.

The shell is discretized by a series of curved rotational elements and cap elements, if necessary. The thickness of an element may vary linearly in the meridional direction. Special 'open type elements' are used for frameworks at the base and at intermediate levels. Discontinuous meridian curves are permissible, provided a nodal circle is located at such a discontinuity.

For the shell elements, the strain-displacement relationships used in the formulation include the effects of transverse shear deformations. Fourth-order Lagrangian interpolation polynomials are used to represent various combinations of the definitive geometric parameters of the shell. The coefficients of these polynomials are evaluated from exact geometric data. In forming the element stiffness and mass matrices, displacement fields of arbitrary order, actually linear to sixth, can be used. As only C° continuity is required to be satisfied, the extra coefficients in quadratic and higher order displacement fields are eliminated by kinematic condensation at the element level. Thus, the size of the global problem is independent of the order of interpolation polynomials. Proportional damping is assumed and the damping matrix is arrived at through a linear combination of the condensed stiffness and mass matrices.

In the case of the open type elements, the displacement fields are taken as Hermitian polynomials. The stiffness and mass matrices are formed by distributing the properties of the individual members around the circumference.

Axisymmetric isoparametric quadratic solid elements are employed to represent the finite element region of the soil medium below the structure, (see Fig. 3). The vertical boundaries which can be placed directly at the foundation extremities, represent the far field as a semi-analytic energy transmitting boundary[(1)*], which is based on the exact displacement functions in the horizontal direction and an expansion in the vertical direction consistent with that used for the finite elements in the core

---

*Numerals in parentheses indicate references in the Bibliography.

region. The lower boundary is assumed to be fixed, which is necessary for the numerical stability of the finite element solution.

The connection problem between the three dimensional soil medium and the two dimensional foundation element is solved by introducing a frequency dependent dynamic boundary system at the common degrees of freedom between the ring footing and the underlaying soil. The soil model is formulated at the fundamental frequency of the structure on a fixed foundation.

The static or transient loads include - concentrated line loads (applied at designated nodal points), distributed loads (replaced by consistent equivalent nodal loads), and thermal effects (expressed as equivalent initial loads). Transient loads may also include earthquake effects in the form of vertical or horizontal base accelerations. Alternatively, the earthquake effect can be considered through response spectrum analysis. Static analysis due to support settlements can also be carried out.

All loads (or effects) which are not axisymmettric are expanded in symmetric (and, if necessary, also antisymmetric) Fourier harmonics and the final result is obtained by superimposing the results of each harmonic. The distributed loads and temperature may vary linearly along the meridian of each element. The temperature may also vary linearly through the thickness.

For reducing the differential equations of motion into an equivalent set of algebraic equations, any three step scheme or one step higher derivative scheme can be used. The time step can be varied at will. In solving the set of linear simultaneous equations, a very efficient modification of the Gaussian elimination scheme which takes advantage of

the symmetric narrow banded nature of the global matrices is used. Free vibration analysis is carried out by the combined Sturm sequence and inverse iteration technique[2].

For dynamic analysis including soil-structure interaction the inertial coupling method is used and, as a result, no deconvolution is required.

GEOMETRY OF ELEMENTS

The geometry of a general rotational shell element is shown in Fig. 4. Points on the meridian of the element are defined in terms of the nondimensional parameter s such that

$$\frac{\partial}{\partial S} = \frac{1}{L}\frac{\partial}{\partial s} \tag{1}$$

where

L = the length of the meridian of element 'i'

$$= \int_{Z_i}^{Z_{i+1}} \sqrt{1 + \left(\frac{dR}{dZ}\right)^2}\, dZ$$

The equation of the meridian curve of a shell element is defined by

$$AZ^2 + BRZ + CR^2 + DZ + ER + F = 0 \tag{2}$$

where A, B, C, D, E, and F are constants for the meridian curve. In the case of open type elements A = B = C = 0.

The derivation of the element matrices will, in general, involve numerical integration due to the presence of definitive geometric parameters like $1/R_\phi$, $1/R$, $\cos\phi$, $\cos\phi/R$, etc., in the strain-displacement relationships (Appendix-A). In order to arrive at the terms of the element matrices in explicit forms, these parameters are expressed by fourth degree Lagrangian polynomials(3) which satisfy the values of these parameters exactly at five equidistant points along the meridian, including the ends.

At the center of a cap element, $R = 0$ and $R' = \infty$, so L and certain other geometric parameters cannot be determined as described. This is overcome(4) by a suitable rotation of the coordinate axes into the $\overline{R} - \overline{Z}$ system as shown in Fig. 5.

Various axisymmetric shell and plate elements that can be used for discretizing the shell are shown in Fig. 6. Open type elements with different member arrangements are also shown in the same figure. Different end conditions of the members of open type elements are shown in Fig. 7. It may be noted here that no meridional discontinuity is allowed at the lower end of an open type element, except at the base.

DISPLACEMENT FIELDS

Shell Elements

As-the effect of transverse shear strains are included in the strain-displacement relationships, u, v, w, β_ϕ, β_θ-displacement fields, Fig. 8, expressed as functions of s and θ, are considered. Each displacement component is considered as a product of the meridional and circumferential fields. The meridional field is a polynomial in s and the circumferential field is represented by a finite Fourier series.

$$\{D\} = \sum_{j=-m_1}^{m_2} \{u^{(j)}(s)q^{(j)}(\theta)v^{(j)}(s)\bar{q}^{(j)}(\theta)w^{(j)}(s)q^{(j)}(\theta)\beta_\phi{}^{(j)}(s)q^{(j)}(\theta)$$

$$\beta_\theta{}^{(j)}(s)\bar{q}^{(j)}(\theta)\} \quad (3)$$

where

$$q^{(j)}(\theta) = \cos j\theta \text{ for } j \geq 0$$

$$= -\sin j\theta \text{ for } j < 0$$

$$\bar{q}^{(j)}(\theta) = -\sin j\theta \text{ for } j \geq 0$$

$$= \cos j\theta \text{ for } j < 0$$

$u^{(j)}(s)$, $v^{(j)}(s)$, ..., etc. = nth degree interpolation polynomials in s corresponding to jth harmonic.

For a typical harmonic

$$\{D^{(j)}(s,\theta)\} = \lceil\Theta\rfloor\{\bar{D}^{(j)}(s)\} \quad (4)$$

where

$$\lceil\Theta\rfloor = \lceil q^{(j)}(\theta)\bar{q}^{(j)}(\theta)q^{(j)}(\theta)q^{(j)}(\theta)\bar{q}^{(j)}(\theta)\rfloor$$

and

$$\{\overline{D}^{(j)}(s)\} = \{u^{(j)}(s)\ v^{(j)}(s)\ w^{(j)}(s)\ \beta_{\phi}^{(j)}(s)\ \beta_{\theta}^{(j)}(s)\}$$

$$= \{\overline{d}^{\,1}(s)\ \overline{d}^{2}(s)\ \overline{d}^{3}(s)\ \overline{d}^{4}(s)\ \overline{d}^{5}(s)\}$$

Each displacement function is represented as an interpolation polynomial of the form

$$\overline{d}^{i}(s) = \sum_{k=1}^{n_i} \overline{d}^{i}{}_{k}\ N_k \qquad (i=1,\ldots 5) \tag{5}$$

where N_k are the shape functions, as defined below.

$$N_1 = (1-s)$$

$$N_2 = s$$

$$N_k = s^{k-2}(1-s), \text{ for } k>2.$$

Also,

$\overline{d}^{i}_{1}$ = the displacement at $s = 0$

$\overline{d}^{i}_{2}$ = the displacement at $s = 1$

For further details see Ref. 5.

In individual members of open type elements, the following Hermitian fields which ensure displacement and slope continuities at the ends of a member are used:

$$
\begin{aligned}
u &= su_t + (1-s)\ u_b \\
v &= (1-3s^2 + 2s^3)v_t + (3s^2 - 2s^3)v_b \\
&\quad + s(s-1)^2\ L_c\ \theta_{zt} + s(s^2-s)\ L_c\ \theta_{zb} \\
w &= (1-3s^2+2s^3)w_t + (3s^2-2s^3)w_b \\
&\quad -s(s-1)^2\ L_c\ \theta_{yt} - s(s^2-s)\ L_c\ \theta_{yb} \\
\theta_x &= s\theta_{xt} + (1-s)\ \theta_{xb}
\end{aligned}
\tag{6}
$$

The nodal variables u_t, θ_t, w_t, θ_{yt}, θ_{zt}, etc. are defined in Fig. 9 and the nondimensional variable $s = x/L_c$. In the case of inclined members, it is necessary to transform the above displacements in local coordinate system into those corresponding to the curvilinear coordinates of the axisymmetric system. The variation of displacements can be accommodated by using Fourier series expansions in θ as was done in the case of shell elements. Thus, the top and bottom end displacements of an inclined member corresponding to the jth harmonic, with its center located at 'θ', can be written as

$$\begin{aligned} \{D_t^{(j)}(s,\theta)\} &= \lceil\theta_t\rfloor\{\bar{D}_t^{(p)}(s)\} \\ \{D_b^{(j)}(s,\theta)\} &= \lceil\theta_b\rfloor\{\bar{D}_b^{(p)}(s)\} \end{aligned} \tag{7}$$

where

$$\lceil\theta_t\rfloor = \lceil q^{(j)}(\theta - \tfrac{e}{2})\ \bar{q}^{(j)}(\theta - \tfrac{e}{2})\ q^{(j)}(\theta - \tfrac{e}{2})\ q^{(j)}(\theta - \tfrac{e}{2})\ \bar{q}^{(j)}(\theta - \tfrac{e}{2})\}$$

and

$$\lceil\theta_b\rfloor = \lceil q^{(j)}(\theta + \tfrac{e}{2})\ \bar{q}^{(j)}(\theta + \tfrac{e}{2})\ q^{(j)}(\theta + \tfrac{e}{2})\ q^{(j)}(\theta + \tfrac{e}{2})\ \bar{q}^{(j)}(\theta + \tfrac{e}{2})\}$$

In these diagonal matrices e is the horizontal angle subtended by the member at the axis of revolution.

ELEMENT STIFFNESS AND MASS MATRICES

On substituting the assumed displacement fields into the strain-displacement relationships (Appendix A) the following expressions are obtained. The membrane strain components,

$$\begin{aligned} \{\varepsilon\} &= \sum_{j=-m_1}^{m_1} [\ E_1^{(j)}\ E_2^{(j)}\ E_3^{(j)}\ E_4^{(j)}\ \ldots.\ ]\ \{\ \Delta^{[j]},\ \Omega^{[j]}\ \}. \\ &= \sum_{j=-m_1}^{m_2} [\ G_1^{(j)}\ ]\ \{\ \Delta^{[j]},\ \Omega^{[j]}\ \} \end{aligned} \tag{8}$$

where

$$E_i^{(j)} = \begin{bmatrix} \frac{1}{L}\frac{\partial N_i}{\partial s} & 0 & \frac{N_i}{R_\phi} & 0 & 0 \\ \frac{N_i \cos\phi}{R} & \frac{-j\,N_i}{R} & \frac{N_i \sin\phi}{R} & 0 & 0 \\ \frac{-jN_i}{R} & \left(\frac{1}{L}\frac{\partial N_i}{\partial s} - \frac{N_i\cos\phi}{R}\right) & 0 & 0 & 0 \end{bmatrix}$$

$$\{\Delta^{[j]}, \Omega^{[j]}\} = \lceil\Theta_j\rfloor \{\Delta^{(j)}, \Omega^{(j)}\}$$

$$\lceil\Theta_j\rfloor = \lceil\theta_j\ \theta_j\ \theta_j\ \ldots.\rfloor$$

$$\lceil\theta_j\rfloor = \lceil f^{(j)}(\theta)\, f^{(-j)}(\theta)\, f^{(j)}(\theta)\, f^{(j)}(\theta)\, f^{(-j)}(\theta)\rfloor$$

$\{\Delta^{(j)}\}$ = the vector of Fourier coefficients for external nodal variables at the top (s=0) and bottom (s=1) nodes corresponding to the jth harmonic

$$= \{u_0^{(j)}\ v_0^{(j)}\ w_0^{(j)}\ \beta_{\phi 0}^{(j)}\ \beta_{\theta 0}^{(j)}\ u_1^{(j)}\ v_1^{(j)}\ w_1^{(j)}\ \beta_{\phi 1}^{(j)}\ \beta_{\theta 1}^{(j)}\};$$

$\{\Omega^{(j)}\}$ = the vector of Fourier coefficients for internal nodal variables of the jth harmonic

$$= \{a_1^{(j)}, b_1^{(j)}, c_1^{(j)}, d_1^{(j)}, e_1^{(j)}, a_2^{(j)}, b_2^{(j)}, c_2^{(j)}, \ldots\};$$

and $\{\varepsilon\} = \{\varepsilon_\phi, \varepsilon_\theta, \varepsilon_{\phi\theta}\}$

The curvature components,

$$\{\chi\} = \sum_{j=-m_1}^{m_2} [X_1^{(j)}, X_2^{(j)}, X_3^{(j)}, \ldots] \{\Delta^{[j]}, \Omega^{[j]}\}$$

$$= \sum_{j=-m_1}^{m_2} [G_2^{(j)}] \{\Delta^{[j]}, \Omega^{[j]}\} \qquad (9)$$

where

$$X_i^{(j)} = \begin{bmatrix} 0 & 0 & 0 & \frac{1}{L}\frac{\partial N_i}{\partial s} & 0 \\ 0 & 0 & 0 & N_i\cos\phi & \frac{-jN_i}{R} \\ 0 & 0 & 0 & \frac{-jN_i}{R} & \frac{1}{L}\frac{\partial N_i}{\partial s} - N_i\cos\phi \end{bmatrix} ;$$

and $\{\chi\} = \{\chi_\phi, \chi_\theta, \chi_{\phi\theta}\}$.

The transverse shear strain components,

$$\{\gamma^{(j)}\} = \sum_{j=-m_1}^{m_2} [Y_1^{(j)}, Y_2^{(j)}, Y_3^{(j)}, \ldots]\{\Delta^{[j]}, \Omega^{[j]}\}$$

$$= \sum_{j=-m_1}^{m_2} [G_3^{(j)}] \; \{\Delta^{[j]}, \Omega^{[j]}\} \tag{10}$$

where

$$Y_i^{(j)} = \begin{bmatrix} \frac{-N_i}{R_\phi} & 0 & \frac{1}{L}\frac{\partial N_i}{\partial s} & N_i & 0 \\ 0 & \frac{-N_i\sin\phi}{R} & \frac{-jN_i}{R} & 0 & N_i \end{bmatrix} ;$$

and $\{\gamma^{(j)}\} = \{\gamma_\phi^{(j)}, \gamma_\theta^{(j)}\}$.

Expressing

$$G^{[j]} = \begin{bmatrix} [G_1^{(j)}] \\ [G_2^{(j)}] \\ [G_3^{(j)}] \end{bmatrix}_{8xM} [\Theta_j] \tag{11}$$

where

$$M = 2 + \sum_{i=1}^{5} (2+n_i) \text{ , and}$$

n_i = the number of internal nodal variables for the i-th field,

the element stiffness matrix for the j-th harmonic becomes

$$[k^{(j)}] = L \int_0^1 \int_{-\pi}^{\pi} [G^{[j]}]^T [H] [G^{[j]}] \, R d\theta ds. \tag{12}$$

The kinematically consistent element mass matrix[5] corresponding to any harmonic is expressed by

$$[m] = \pi L \int_0^1 [G^m]^T [H^m] [G^m] R ds \tag{13}$$

CONSTITUTIVE RELATIONSHIPS

Shell Elements

The relationship between the force resultants and the strain components are expressed by

$$\{N\} = [H] \{\varepsilon\} - \{N_t\} \tag{14}$$

where

$\{N\}$ = the stress resultants and stress-couple resultants as shown in Figs. 8 and 10

$= \{N_\phi, N_\theta, N_{\theta\phi}, M_\phi, M_\theta, M_{\phi\theta}, Q_\phi, Q_\theta\}$

$\{\varepsilon\}$ = the linear and shearing strains, and changes in curvature and torsion corresponding to the above force resultants.

$= \{\varepsilon_\phi, \varepsilon_\theta, \varepsilon_{\theta\phi}, \chi_\phi, \chi_\theta, \chi_{\phi\theta}, \gamma_\phi, \gamma_\theta\}$

$[H]$ = the (8x8) elasticity matrix. The non-zero terms of this matrix in the case of isotropic and orthotropic materials, and for framed shells are given in Appendix B,

and

$\{N_t\}$ = the initial stress-resultants and stress-couples due to thermal effects.

$$= \{N^*_{t\phi}, N^*_{t\theta}, 0, M^*_{t\phi}, M^*_{t\theta}, 0, \quad 0, \quad 0\}$$

For an isotropic shell material

$$N^*_{t\phi} = N^*_{t\theta} = \frac{E\alpha}{1-\mu} \int_{-h/2}^{h/2} T(\zeta)d\zeta$$

$$M^*_{t\phi} = M^*_{t\theta} = \frac{E\alpha}{1-\mu} \int_{-h/2}^{h/2} T(\zeta)\,\zeta d\zeta \tag{15}$$

where

α = the coefficient of thermal expansion

$T(\zeta)$ = the temperature difference from the reference value for any point located at a distance ζ from the middle surface.

Open Type Elements

The relationship between the force resultants at any section of a member in the open type element and the strain components are expressed by

$$\{N^o\} = [C^o]\ \{\varepsilon^o\} - \{N^o_t\} \tag{16}$$

where

$\{N^o\}$ = the stress resultants and stress-couple resultants as shown in Fig. 8

$$= \{F_x, F_y, F_z, M_x, M_y, M_z\}$$

$\{\varepsilon^o\}$ = the linear and shear strains, the twist per unit length, and the changes in curvature on y and z

$= \{\varepsilon_x, \gamma_y, \gamma_z, \chi_x, \chi_y, \chi_z\}$

$[C^o]$ = (6x6) elasticity matrix

$$\begin{bmatrix} EA & & & & & \\ & \lambda GA & & & 0 & \\ & & \lambda GA & & & \\ & & & GJ & & \\ & 0 & & & EI_y & \\ & & & & & EI_z \end{bmatrix}$$

$\{N_t^o\}$ = the initial stress-resultants and stress-couples due to thermal effect

$= \{N_{tx}^* \;\; 0 \;\; M_{ty}^* \;\; 0\}$

$$N_{tx}^* = E\alpha \int_{-d/2}^{d/2} T(Z)bdZ$$

$$M_{ty}^* = E\alpha \int_{-d/2}^{d/2} T(Z)\, bZ\, dZ$$

where

$$[G^m]_{5xNN} = [n_1, n_2, n_3, n_4, n_5, \ldots\ldots]$$

$$n_i = [N_i, N_i, N_i, N_i, N_i]$$

$$[H^m] = [\rho h, \rho h, \rho h, \rho\frac{h^3}{12}, \rho\frac{h^3}{12}] \text{ for isotropic shells}$$

The lumped mass matrix is arrived at by considering a unit acceleration corresponding to each degree of freedom at a time and assigning the corresponding mass to the same degree of freedom.

ELEMENT LOAD VECTORS

The consistent load vector[5] for an element due to distributed loads, $f_\phi^{(j)}$, $f_\theta^{(j)}$, and $f_\zeta^{(j)}$ acting along the ϕ, θ, and ζ directions corresponding to harmonic j is expressed as

$$\{p_s^{(j)}\} = L \int_0^1 [G^m]^T [G^f] \{F_s^{(j)}\} R ds \tag{17}$$

where

$$[G^m] = [\tilde{n}_1, \tilde{n}_2, \tilde{n}_3, \tilde{n}_4, \tilde{n}_5, \ldots]$$

$$\tilde{n}_i = [N_i, N_i, N_i, 0, 0]$$

$$[G^f] = [\bar{n}_1, \bar{n}_2]$$

$$\bar{n}_i = \pi[\bar{N}_i, \bar{N}_i, \bar{N}_i, 0, 0]$$

$$\bar{N}_1 = (1-s)$$

$$\bar{N}_2 = s$$

$$\{F_s^{(j)}\} = \{f_{\phi 1}^{(j)}, f_{\theta 1}^{(j)}, f_{\zeta 1}^{(j)}, f_{\phi 2}^{(j)}, f_{\theta 2}^{(j)}, f_{\zeta 2}^{(j)}\}$$

The consistent load vector due to the thermal effect is expressed as

$$\{p_T^{(j)}\} = \pi L \left(\int_0^1 [G^{(j)}]^T [H^t][G^t] ds \right) \{T^{(j)}\} \tag{18}$$

where

$$[H^t] = -\frac{E\bar{\alpha}}{1-\mu^2}\begin{bmatrix} h & \mu h \\ \mu h & h \\ 0 & 0 \\ \frac{-h^2}{12} & \frac{-\mu h^2}{12} \\ \frac{\mu h^2}{12} & \frac{h^2}{12} \\ 0 & 0 \\ 0 & 0 \\ 0 & 0 \end{bmatrix}$$

$$[G^t] = \begin{bmatrix} \bar{N} & 0 & \bar{N}_2 & 0 \\ 0 & \bar{N}_1 & 0 & \bar{N}_2 \end{bmatrix}$$

$$\{T^{(j)}\} = \{T_{00}{}^{(j)},\ T_{10}{}^{(j)},\ T_{01}{}^{(j)},\ T_{11}{}^{(j)}\}$$

$\bar{\alpha}$ = the coefficient of thermal expansion

EQUATIONS OF MOTION

Using Hamilton's variational principle[6] the equation of motion can be expressed as below. In the case of mechanical and thermal loads,

$$[K]\{D\} + [C]\{\dot{D}\} + [M]\{\ddot{D}\} = \{F\} \tag{19}$$

where

[K] = the stiffness matrix;

[M] = the mass matrix;

[C] = the proportional damping matrix;

= α [M] + β[K];

$\{D\},\{\dot{D}\},\{\ddot{D}\}$ = the vector of nodal displacements, velocities, and accelerations;

{F} = the load vector due to mechanical and thermal effects;

α, β = constants depending upon the damping ratios corresponding to two unequal natural frequencies of vibration;

$$\alpha = \frac{2\omega_1\omega_2\ (\omega_2\xi_1 - \omega_1\xi_2)}{(\omega_2^{\ 2} - \omega_1^{\ 2})}\ ;$$

$$\beta = \frac{2(\omega_2\xi_2 - \omega_1\xi_1)}{(\omega_2^{\ 2} - \omega_1^{\ 2})}\ ;$$

ω_1, ω_2 = the circular frequencies;

ξ_1, ξ_2 = the corresponding modal damping ratios.

In the case of base acceleration, $\{D\}$, $\{\dot{D}\}$ and $\{\ddot{D}\}$ are measured relative to the base and the load vector {F} becomes $-[M]\{\ddot{D}_g\}$ where $\{\ddot{D}_g\}$ is the vector of base accelerations as discussed later.

In the case of free vibration analysis, the loading and damping terms are dropped and the resulting eigenvalue problem becomes

$$[K]\{D\} + [M]\{\ddot{D}\} = 0 \tag{20}$$

For static analysis the damping and inertia terms are dropped from the equation of motion.

The global stiffness and mass matrices [K]and [M] for each harmonic are of size (5Nx5N), where N is the total number of nodal circles. These

matrices are assembled after computing the condensed element stiffness and mass matrices. The case with a discontinuous meridional curve at a node needs special treatment and is taken care of by defining a master set of coordinates at such a nodal circle and transforming the stiffness and mass coefficients of the adjacent elements to coincide with these coordinates.

The (5Nx1) global load vector, {F}, for each harmonic is computed by algebraically combining the condensed nodal loading vectors for the elements. In the event of a finite discontinuity at a node, the forces for each element are transformed to the master system for the node.

By a simple transformation from Cartesian to curvilinear coordinates the base acceleration vectors for vertical acceleration ($j=0$) and horizontal acceleration ($j=1$) are expressed as

$$\begin{aligned}
\{\ddot{D}_g^{(0)}\} &= \{\sin\phi_1 \; -\cos\phi_1 \; 0 \; \ldots\ldots \sin\phi_i \; -\cos\phi_i \; 0 \; \ldots\ldots \\
&\qquad \sin\phi_{5N} \; -\cos\phi_{5N} \quad 0\}\, \ddot{g}_v \\
\{\ddot{D}_g^{(1)}\} &= \{-\cos\theta\cdot\cos\phi,\ \sin\theta,\ -\cos\theta\cdot\sin\phi,\ \ 0\ \ 0\ldots\ldots \\
&\qquad -\cos\theta\cos\phi_i,\ \sin\theta,\ -\cos\theta\cdot\sin\phi_i \ \ 0\ \ 0\ldots\ldots \\
&\qquad -\cos\theta\cos\phi_{5N},\sin\theta,\ -\cos\theta\sin\phi_{5N}\ 0\ \ 0\}\ddot{g}_h
\end{aligned} \tag{21}$$

where $\ddot{g}_v$ and $\ddot{g}_h$ are the vertical and horizontal components of base acceleration.

CONDENSATION OF MATRICES

The kinematic condensation of the stiffness and mass matrices and the load vectors to eliminate the internal degress of freedom at the element level reduces the overall size and bandwidth of the resulting set of equations. In the case of dynamic response analysis assuming proportional damping, the equation of motion for an element may be written in partioned form, with the harmonic index suppressed, as

$$\begin{bmatrix} k_{rr} & k_{rc} \\ k_{cr} & k_{cc} \end{bmatrix} \begin{Bmatrix} D_r \\ D_c \end{Bmatrix} + \beta \begin{bmatrix} k_{rr} & k_{rc} \\ k_{cr} & k_{cc} \end{bmatrix} \begin{Bmatrix} \dot{D}_r \\ \dot{D}_c \end{Bmatrix}$$

$$+ \alpha \begin{bmatrix} m_{rr} & m_{rc} \\ m_{cr} & m_{cc} \end{bmatrix} \begin{Bmatrix} \dot{D}_r \\ \dot{D}_c \end{Bmatrix} + \begin{bmatrix} m_{rr} & m_{rc} \\ m_{cr} & m_{cc} \end{bmatrix} \begin{Bmatrix} \ddot{D}_r \\ \ddot{D}_c \end{Bmatrix} = \begin{Bmatrix} P_r \\ P_c \end{Bmatrix} \tag{22}$$

where the subscript r denotes external degrees of freedom and c denotes the internal degrees of freedom to be condensed.

The above equation can now be expanded as

$$k_{rr}D_r + k_{rc}D_c + \beta\, k_{rr}\dot{D}_r + \beta\, k_{rc}\dot{D}_c + \alpha\, m_{rr}\dot{D}_r + \alpha\, m_{rc}\dot{D}_c$$
$$+ m_{rr}\ddot{D}_r + m_{rc}\ddot{D}_c = P_r \tag{23}$$
$$k_{cr}D_r + k_{cc}D_c + \beta\, k_{cr}\dot{D}_r + \beta\, k_{cc}\dot{D}_c + \alpha\, m_{cr}\dot{D}_r + \alpha\, m_{cc}\dot{D}_c$$
$$+ m_{cr}\ddot{D}_r + m_{cc}\ddot{D}_c = P_c$$

Solving the second equation successively it can be shown that

$$D_c + \beta\, \dot{D}_c = k_{cc}^{-1}\, (F_c - k_{cr}(D_r + \beta\, \dot{D}_r)\,)$$
$$+ (k_{cc}^{-1}\, m_{cc}\, k_{cc}^{-1}\, k_{cr} - k_{cc}^{-1}\, m_{cr})\, (\ddot{D}_r + \alpha\, \dot{D}_r) \tag{24}$$
$$+ \text{Higher order terms}$$

$$\alpha\, \dot{D}_c + \ddot{D}_c = -k_{cc}^{\ -1} k_{cr}\, (\alpha\, \dot{D}_r + \ddot{D}_r) + \text{Higher order terms}$$

It should be noted that the last two equations are essentially based on the assumption of simple harmonic motion which is necessary to effect a kinematic condensation in this form.

When the higher order terms are neglected and the last two equations are substituted in the first, the condensed equation of motion becomes

$$[\bar{k}]\ \{D_r\} + (\beta\ [\bar{k}] + \alpha\ [\tilde{m}])\ \{\dot{D}_r\} + [\tilde{m}]\ \{\ddot{D}_r\} = \{\tilde{P}\} \tag{25}$$

in which

$$[\bar{k}] = k_{rr} - k_{rc}k_{cc}^{-1}\ k_{cr}$$

$$[\tilde{m}] = m_{rr} + k_{rc}k_{cc}^{-1}\ m_{cc}k_{cc}^{-1}\ m_{cc}k_{cc}^{-1}\ k_{cr} - k_{rc}k_{cc}^{-1}\ m_{cr}$$

$$-m_{rc}k_{cc}^{-1}\ k_{cr}$$

and

$$\{\tilde{P}\} = P_r - k_{rc}k_{cc}^{-1}\ P_c$$

SOIL MODEL

For viscoelastic material and a cylindrical coordinate system (Fig. 11), Hamilton's principle becomes:

$$\int_V \delta\varepsilon_{ij}\ \sigma_{ij}\ dv - \int_V \delta\ u_i(b_i + \rho\Omega^2\ u_i)dv - \int_S p_i\ \delta u_i\ dA = 0 \tag{26}$$

in which

$i = r,\ z,\ \theta$

u_i = displacement vector

ε_{ij} = strain tensor

σ_{ij} = stress tensor

b_i = body force vector

ρ = mass density

Ω = driving frequency

p_i = load vector

In equation (26) the quantities are, in general, complex. However, for real elastic moduli, the stresses will be real and in phase with the strains and displacements. An alternate form of equation (26) is obtained using integration by parts, resulting in

$$\int_V \delta u_i(\sigma_{ij,j} + b_i + \rho\Omega^2 u_i)dv + \int_{S'} \delta u_i(p_i - n_j\sigma_{ij})dA = 0 \qquad (27)$$

in which

n_j = unit outward normal on the boundary

For arbitrary variations of virtual displacements δu_i, equation (27) yields the body and boundary equilibrium equations.

If ϕ denotes the shape function for the isoparametric formulation and

$$\{u\} = [\Phi]^T\{u_0\} \tag{28}$$

where $$[\Phi]^T = \begin{bmatrix} \Phi^T & & 0 \\ & \Phi^T & \\ 0 & & \Phi^T \end{bmatrix} \tag{29}$$

equation (27), for a cross-anisotropic material, becomes

$$\sum_{\text{elements}} \delta\{u_0\}^T \iint ([\Phi][A]^T[D][A][\Phi]^T - \rho\Omega^2[\Phi][\Phi]^T)\{u_0\}\ rdrdz$$

$$- \int [\Phi]\{\bar{p}\}\ rds\} = 0 \tag{30}$$

where

$[A]$ = operator matrix relating the strain tensor to the displacement vector

and

$[D]$ = constitutive matrix

For the $k^{\underline{th}}$ element, the consistent mass matrix $[M_k]$, the stiffness matrix $[K_k]$ and the load vector P_k are defined as

$$[M_k] = \iint \rho[\Phi][\Phi]^T\ rdrdz$$

$$[K_k] = \iint [\Phi][A]^T[D][A][\Phi]^T\ rdrdz \tag{31}$$

$$[P_k] = \int [\Phi]\{\bar{p}\}\ rds$$

respectively.

The global mass matrix [M], stiffness matrix [K], and the load vector {P} are related by the familiar free vibration equation

$$([K] - \Omega^2[M])\ \{u\} = \{P\} \tag{32}$$

where {u} stands for the total nodal displacements and Ω is the driving frequency.

Equation (32) should be modified to include the effect of the far field on the finite element region. This can be achieved by considering the equilibrium of the vertical boundaries of the core region. If the core region of Figure 1 is removed and replaced by equivalent distributed forces corresponding to the internal stresses, the dynamic equilibrium of the far-field will be preserved. The relation between these boundary forces and the corresponding boundary displacements is the dynamic boundary matrix to be added to the dynamic stiffness matrix of Equation (32).

For a consistent boundary, it is always possible to express the displacements in the far-field in terms of eigenfunctions corresponding to the natural modes of wave propagation in the stratum. A discrete eigenvalue problem can be obtained by replacing the actual dependence of the displacements in the vertical direction by an expansion consistent with that used for the finite elements,while retaining the exact solution in the radial direction.

Consider the toroidal section of the far-field limited by two cylindrical surfaces of radii r_0 and r_1, as shown in Figure 3. An

isoparametric representation for the nodal displacements in the finite element region is convenient (1):

$$\{u_{app_n}\} = [N]\{u_{o_n}\} \tag{33}$$

= the approximate nodal displacements for the $n^{\underline{th}}$ layer

where

[N] = the expansion matrix

and

$$\{u_{o_n}\} = \left\{ \begin{array}{c} x_{1_i} H'_j + \frac{j}{r_0} x_{3_i} H_j \\ k\, x_{2_i} H_j \\ \frac{j}{r_0} x_{1_i} H_j + x_{3_i} H'_j \\ x_{1_{i+1}} H'_j + \frac{j}{r_0} x_{3_{i+1}} H_j \\ k\, x_{2_{i+1}} H_j \\ \frac{j}{r_0} x_{1_{i+1}} H_j + x_{3_{i+1}} H'_j \\ x_{1_{i+2}} H'_j + \frac{j}{r_0} x_{3_{i+2}} H_j \\ k\, x_{2_{i+2}} H_j \\ \frac{j}{r_0} x_{1_{i+2}} H_j + x_{3_{i+2}} H'_j \end{array} \right\} \tag{34}$$

in which

$\{x_1, x_2, x_3\}_i$ = nodal displacements of node i

r_o = radius of the vertical boundary

k = wave number (unknown)

j = Fourier mode number

$H_j = H_j^{(2)} (kr_o)$

= second Hankel function

Equation (27) is now rewritten in matrix form (1)

$$\iint \delta\{u\}^T \cdot [H]\cdot\{Z\} \, rdrdz + \int \delta\{u\}^T(\{P\} - \{\bar{\sigma}\})rds = 0 \tag{35}$$

where [H] is a matrix depending on the wave number k, on the driving frequency Ω and the radius r_0 and {Z} is a vector depending only on z.

In addition, the modal wave equation (1) is considered

$$[H]\{Z\} = \{0\} \tag{36}$$

Equation (36) represents the body equilibrium equation, while the second integral in Equation (35) represents the boundary equilibrium equation.

Summing over the ℓ layers, with the requirement for the integrands over S_0 and S_1 to vanish (Figure 3) and with no external prescribed forces acting at the layer interfaces (S_2 and S_3), Equation (35) becomes

$$\sum_{n=1}^{\ell} \left[\iiint \delta\{u\}^T [H]\{Z\} r\,dr\,dz - \int_{S_2} \delta\{u\}^T \{\bar{\sigma}\} r\,ds - \int_{S_3} \delta\{u\}^T \{\sigma\} \cdot r\,ds \right] = 0 \tag{37}$$

which leads to an algebraic eigenvalue problem with 6ℓ eigenvectors (modes of propagation $\{x\}_i$) and the corresponding eigenvalues (the wave number k_i). The details of the wave propagation problem are available elsewhere (1).

The equivalent distributed forces corresponding to the internal stresses $\{\bar{\sigma}\}_i$ at the vertical boundaries can be formulated in terms of the mode shape $\{x\}_i$ and weighted by the modal participation factor α_i, such that

$$\{P\}_i = \alpha_i \, r_0 \int_0^{h_i} [N]^T \{\sigma\}_i \, dz \tag{38}$$

with

$$[N]^T \{\bar{\sigma}\}_i = ([N]^T [N] [\bar{S}]_i + [N]^T [N'] [\bar{T}]_i) \{x\}_i \tag{39}$$

where

$$[\bar{S}]_i = \begin{bmatrix} S_i & & \\ & S_i & \\ & & S_i \end{bmatrix}_{9\times 9} \tag{40}$$

and

$$[\bar{T}]_i = \begin{bmatrix} T_i & & \\ & T_i & \\ & & T_i \end{bmatrix}_{9\times 9}$$

in which S_i and T_i are 3×3 matrices containing the wave numbers k_i and Hankel functions with first and second derivatives.

Summing the contributions of each mode gives the boundary load vector,

$$\{P\}_b = \sum_{i=1}^{6\ell} \alpha_i r_0 \{\bar{x}\}_i \tag{41}$$

where

ℓ = total number of layers

$\{\bar{x}\}_i$ = the boundary vector which contains the wave number k_i, the wave mode shape $\{x\}_i$, and the layer properties (1).

An alternate form of equation (15) in matrix notation, is

$$\{P\}_b = r_0[x^*]\{\alpha\} \tag{42}$$

with $[x^*] = [\{\bar{x}\}_1\{\bar{x}\}_2.....\{\bar{x}\}_i.....\{\bar{x}\}_{6\ell}]$ (43)

= the boundary matrix

and

$$\{\alpha\}^T = \{\alpha_1\ \alpha_2....\alpha_i...\alpha_{6\ell}\} \tag{44}$$

= the modal participation factors vector

The boundary displacement vector $\{u\}_b$ is formulated in a similar way and the resulting displacement is found to be

$$\{u\}_b = [u^*]\{\alpha\} \tag{45}$$

with

$[u^*]$ = the displacement matrix (1).

Equations (42) and (45) lead to the boundary dynamic stiffness matrix of the energy absorbing boundary $[R]_b$:

$$[R]_b = r_0[x^*][u^*]^{-1} \tag{46}$$

The total global dynamic stiffness matrix of the soil medium is given by

$$[K]_s = [\,K\,] - \Omega^2[M] + [R] \tag{47}$$

where

[R] = the matrix given by Equation (46), expanded to the dimensions of [K] and [M] of Equation (32).

Finally, Equation (32) becomes

$$[K]_s\{u\} = \{P\} \tag{48}$$

Considering Equation (48), with the RHS all equated to zero except for the value at one of the common d.o.f. which is set to unity, and solving for the displacements at the common d.o.f., the complex compliance matrix for the foundation [C] can be obtained. The complex impedance matrix $[\bar{K}]$ is then found by inverting the compliance matrix [C], i.e.,

$$[\bar{K}] = [C]^{-1} \tag{49}$$

In Fig. 12 the common d.o.f. are associated with nodes m-2, m-1 and m, and the resulting impedance matrix $[\bar{K}]$ will be of the order 9×9.

Herein prescribed forces rather than displacements are used to avoid the complex mixed boundary value problem which could result from the traction free condition outside the structure-foundation interface.

The Connection Model

The connection between the soil medium and the ring footing is established by eliminating the six degrees of freedoms at the corners D and F shown in Fig. 13 while forming the rotational d.o.f. at E from the eliminated degrees of freedom; in other words, the nine d.o.f. are lumped into five d.o.f. at the mid point of the footing base. The base uplift is treated by restricting the contact stresses between the soil and the footing to be compressive or shearing, but not tensile. Mild tension may be admissible but no quantitative results are available as yet.

In order to formulate the soil stiffnesses and damping at the connecting nodal point, the following method is commonly used:

$$K = \bar{K}_r - 2D\bar{K}_i \tag{50a}$$

$$C = (\bar{K}_i + 2D\bar{K}_r)/\Omega \tag{50b}$$

where $\bar{K}_r + i\bar{K}_i$ is the complex soil-stiffness with none material damping; D is the material damping parameter independent of the driving frequency Ω. It is obvious that both K and C of Equation (50) are frequency dependent since $\bar{K}_r$ and $\bar{K}_i$ are frequency dependent and the material damping affects both stiffness and damping.

The nine stiffness elements of Fig. 14 are obtained from Equation (50a) by considering each stiffness element on the main diagonal as

a linear spring in the corresponding direction. The stiffness elements of the connection model are formulated from these nine stiffnesses:

$$
\begin{aligned}
K_u &= K_1 + K_4 + K_7 \\
K_w &= K_2 + K_5 + K_8 \\
K_v &= K_3 + K_6 + K_9 \\
K_\theta &= \frac{B^2}{4}(K_2 + K_8) \\
K_\phi &= \frac{B^2}{4}(K_3 + K_9)
\end{aligned}
\tag{51}
$$

The damping system is formulated from matrix C (Equation (50b) in a way similar to the stiffness elements of the connection model discussed above. The resultants in the five degrees of freedom at the center point E of Figure 13 are evaluated as follows:

$$
\begin{aligned}
C_u &= C_1 + C_4 + C_7 \\
C_w &= C_2 + C_5 + C_8 \\
C_v &= C_3 + C_6 + C_9 \\
C_\theta &= \frac{B^2}{4}(C_2 + C_8) \\
C_\phi &= \frac{B^2}{4}(C_3 + C_9)
\end{aligned}
\tag{52}
$$

For obvious reasons the connecting model is named the Equivalent Boundary System (EBS) for the ring footing. The EBS is frequency dependent and must be updated for each Fourier harmonic. In Equations (51) and (52) the K's and C's are the modal values and they are expressed in Fourier series in the θ direction. Figure 3 shows the modal translational and the rotational stiffnesses and damping elements at the midpoint of the footing base.

SOLUTION OF EQUATIONS OF MOTION

After assembling the system matrices and vectors by the direct addition of the terms corresponding to each degree of freedom in the element stiffness and mass matrices and vectors, if the soil structure interaction is not considered, the boundary conditions are enforced by 'zeroizing' the rows and columns of the stiffness, mass, and damping matrices corresponding to the constrained degrees of freedom, with the exception that the diagonal term in such rows and columns of the stiffness matrix is set equal to one. At the same time, the terms in the load vector corresponding to these degrees of freedom are replaced by the given values of the constraints, which may be non-zero. In the case of non-zero values of the constraints, the other terms in the load vector are suitably modified. However, in the case of eigenvalue problems, it is more convenient to disregard the rows and columns in the system matrices corresponding to the degrees of freedom defined as zero.

Free Vibration Analysis

Apart from its use for the first step towards linear dynamic analysis by mode superposition and also for a response spectrum analysis, the solution of the eigenvalue problem is helpful in selecting a suitable time step for direct integration algorithms. The characteristic features of the eigenvalue problem at hand are that the stiffness and mass matrices are positive definite, narrow banded, and symmetric. Moreover, only a few eigenvalues, usually the first few are desired. All of these features are exploited in an algorithm put forward by Gupta[2]. This algorithm makes use of the Sturm sequence property of the principal minors of $([m] - \Lambda[k])$ to determine the number of Λ^2 lying within a given range (Λ_U, Λ_L), where Λ is equal to $1/\omega^2$. Then the upper and lower bounds of

individual roots are determined by repeated bisection and application of Sturm sequence properties. Finally, the roots are accurately located and the corresponding eigenvectors are found simultaneously by inverse iteration using the mean value of the roots based on the bounds established earlier and starting with a unit eigenvector. During each iteration step a new estimate of Λ^r is obtained using the Rayleigh quotient. For every root only one triangular decomposition of $([m] - \Lambda[k])$ is performed.

Static Analysis

The set of 5N equations are solved for each harmonic using a modified version of the Gaussian elimination method which takes advantage of the symmetric narrow bandedness of the stiffness matrix and the fact that terms in the rows and columns corresponding to the constrained degrees of freedom are zero except the diagonal term which is equal to one.

Time History Analysis

The solution of the 5N second order equations of motion may be carried out by direct integration. The equations are first reduced to 5N algebraic equations by the direct application of unconditionally stable difference formulas. Such formulas may either be single step higher derivative types like those in the Newmark-β scheme (with β=0.25), Wilson-θ scheme (θ=1.4), etc., or multistep types like Houbolt's formula. Then these equations are solved step-by-step for the given digitized load function. The various steps involved in the solution procedure are as follows:

(1) Setting up the linear stiffness matrix [k], the mass matrix [m], and the scaled load vector for the harmonic under consideration.

(2) Introducing the boundary conditions and setting the vectors $\{D^\circ\}$, $\{\dot{D}^\circ\}$, and $\{\ddot{D}^\circ\}$ to the given initial conditions. The initial conditions for at least two vectors are required to be defined.

(3) Choosing a suitable time step, Δt, based on the period of vibration of one of the higher modes for the harmonic under consideration, determining the proportional damping coefficients, and calculating the parameters A_1 and A_2 to A_8, or $\tilde{A}_2$ to $\tilde{A}_8$, of the integration scheme used. The expressions for these parameters are given in Appendix C.

(4) If only two of the initial conditions are specified, it is necessary to solve the following equations for the vector which is unknown.

$$[K]\ \{D\}^\circ + (\alpha\ [M] + \beta\ [K])\ \{\dot{D}\}^\circ + [M]\ \{\ddot{D}\}^\circ = \{F\}^\circ \tag{53}$$

(5) If a multistep scheme is being used it is necessary to estimate the displacements at $-\Delta t$ and $-2\Delta t$ using the following equations.

$$\begin{aligned} \{D\}^{-1} &= \{D\}^\circ - \Delta t\ \{\dot{D}\}^\circ + \frac{\Delta t^2}{2}\ \{\ddot{D}\}^\circ \\ \{D\}^{-2} &= -\{D\}^\circ + 2\{D\}^{-1} + \Delta t^2\ \{\ddot{D}\}^\circ \end{aligned} \tag{54}$$

(6) Setting up the equivalent stiffness matrix

$$[\tilde{K}] = [K] + A_1\ [M] \tag{55}$$

(7) Triangularizing $[\tilde{K}]$ which must only be done once.

(8) Calculating the equivalent load vector

$$\{R\}^r = \bar{\theta} l_r\ \{F\}^r + (1 - \bar{\theta})\ l_{r-1}\ \{F\}^r \tag{56}$$

where l_r is the load coefficient for the rth step and $\bar{\theta} = 1.4$ for Wilson-θ scheme and equal to 1 for other schemes.

(9) Solving for $\{D\}^r$ by back substitution of $\{R\}^r$ into the decomposed equivalent stiffness matrix.

(10) Calculating the displacement, velocity, and acceleration vector for the rth step using

$$\{D\}^r = (\{\tilde{D}\}^r + A_6\ \{D\}^{r-1} + A_7\ \{\dot{D}\}^{r-2} + A_8\ \{\ddot{D}\}^{r-1})/A_2$$

$$\{\dot{D}\}^r = A_{12}\ \{D\}^r - A_{12}\ \{D\}^{r-1} - A_{13}\ \{\dot{D}\}^{r-1} - A_{14}\ \{\ddot{D}\}^{r-1} \tag{57}$$

$$\{\ddot{D}\}^r = A_9\ \{D\}^r - A_9\ \{D\}^{r-1} - A_{10}\ \{\dot{D}\}^{r-1} - A_{11}\ \{\ddot{D}\}^{r-1}$$

in the case of single step higher derivative schemes, or

$$\{D\}^r = (\{\tilde{D}\}^r + \tilde{A}_6\ \{D\}^{r-1} + \tilde{A}_7\ \{D\}^{r-2} + \tilde{A}_8\ \{D\}^{r-3})/\tilde{A}_2$$

$$\{\dot{D}\}^r = (P_1\{D\}^r + P_2\{D\}^{r-1} + P_3\{D\}^{r-2} + P_4\{D\}^{r-3})/\Delta t \tag{58}$$

$$\{\ddot{D}\}^r = (P_5\{D\}^r + P_6\{D\}^{r-1} + P_7\{D\}^{r-2} + P_8\{D\}^{r-3})/(\Delta t)^2$$

in the case 3-step schemes. The parameters appearing here are defined in Appendix C.

DETERMINATION OF STRESS RESULTANTS AND STRESSES

The stress resultants are computed at the nodal points using the global displacement vector {D}. The stresses at the intermediate points are determined after finding the coefficients of higher order displacement terms.

Once the stress resultants are known, the stresses at any point in the shell can be determined. For instance, in the case of orthotropic layered shells,

at the midsurface,

$$\sigma_{\phi} = \frac{1}{\eta_o} \left(\frac{N_{\phi}}{A_e}\right)$$

$$\alpha_{\phi\theta} = \frac{1}{\eta_o'} \left(\frac{N_{\phi\theta}}{A_o'}\right) \tag{59}$$

and at the outer surface of any layer,

$$\sigma_{\phi} = \frac{1}{\eta_k} \left(\frac{N_{\phi}}{A_e} \pm \frac{M_{\phi}}{S_e} \quad \zeta_k\right)$$

$$\sigma_{\phi\theta} = \frac{1}{\eta_k'} \left(\frac{N_{\phi\theta}}{A_e'} \pm \frac{M_{\phi\theta}}{S_e'} \quad \zeta_k\right) \tag{60}$$

where

$\eta_k = \dfrac{E_{\phi k}}{E_{\phi n}}$, i.e., ratio of Young's moduli of k^{th} layer to that for the outermost layer (See Fig. 10)

$\eta_k' = \dfrac{G_{\phi\theta k}}{G_{\phi\theta n}}$, i.e., ratio of shear moduli of k^{th} layer to that for outermost layer

$$A_e = h_o \ \eta_o + 2 \sum_{k=1}^{n-1} h_k \ \eta_k + 2 \ h_n$$

A_e' = same as A_e with η_k replaced by η_k'

$$S_e = \frac{1}{12} \{(\eta_o - 1)h_o{}^3 - \sum_{k=1}^{n-1} (1 - \eta_k) \ [\ (2 \sum_{k=1}^{k} h_i) + h_o]^3 + h^3\}$$

S_e' = Same as S_e with η_k replaced by η_k'

S_k = the distance of outer fibre of a layer 'k'.

n = (total number of layers - 1)/2, that is the number of of pairs of symmetrical layers in addition to the central one.

In the case of isotropic shells under thermal loading, the above formulae become

at the midsurface,

$$\sigma_\phi = \frac{N_\phi}{h} - \frac{E\alpha\ T(0)}{1 - \mu}$$
$$\alpha_{\phi\theta} = \frac{N_{\phi\theta}}{h} \qquad (61)$$

and at the outer surfaces,

$$\sigma_\phi = \frac{N_\phi}{h} \pm \frac{6\ M_\phi}{h^2} - \frac{E\alpha T(\pm h/2)}{1 - \mu}$$
$$\sigma_{\phi\theta} = \frac{N_{\phi\theta}}{h} \pm \frac{6\ M_{\phi\theta}}{h^2} \qquad (62)$$

In the case of framed shells the forces in the framing members in the ϕ and θ-directions can be obtained by simply multiplying the stress-resultants by the spacing of the meridional and circumferential members, respectively.

GENERAL FEATURES OF THE PROGRAM

SHORE-III program is designed for the linear static and dynamic analysis of axisymmetric shells (and shell-like structures) and plates. It is written in FORTRAN IV language and has been developed on an IBM

360/65 computer. It is an in-core solver requiring less than 500k in high speed storage. For running the program it is necessary to use an overlay structure (see fig. 5, SHORE-IV User's Manual). All calculations are done in double precision with 32 bits word length.

As can be seen from the flow diagram for SHORE-IV shown in Figures 15 to 19, the complete solution process, which is done harmonic-wise, can be divided into five steps:

Step 1: Data Input

The input data for geometry, nodal location, material, loading (Harmonic-wise), control data, etc., are read and, if necessary, additional data are generated. All data are stored in common arrays and temporary disk files.

Step 2: Generation of Element Matrices

Corresponding to the current harmonic, the stiffness matrix and, if necessary, the mass matrix and/or the loading vector for each element are generated. These are stored in temporary disk files.

Step 3: Assembly of Global Matrices

For each harmonic, the stiffness matrix and, if necessary, the mass matrix and/or the loading vector for the structure are assembled and stored in temporary disk files.

Step 4: Calculation of Response

For each harmonic, the desired structural response is calculated and the results printed out in desired formats. Partial and total effects of the harmonics are also computed and printed.

Step 5: Time History Plots

In the case of time history analysis by direct integration, the time history response plots can be obtained on the line printer. Alternatively, a plot tape can be created for obtaining off-line time history response plots on a Calcomp plotter.

Further details about the program are discussed in the SHORE-IV Users Manual.

EXAMPLE PROBLEMS

Free Vibration Analysis of Cylindrical Shell

The free vibration analysis of the shell shown in Fig. 20 is carried out with seven and twelve elements for p = 2,3,4,5,6. The results for the first four harmonics with p = 3 and seven elements are shown in Fig. 21. Comparisons with the results obtained by Donnell's theory and experiment[7], and numerical integration[8] are also shown. SHORE-IV solutions show good agreement with others. The convergence characteristics with different values of p in the case of the zeroeth harmonic is shown in Fig. 22. In the case of the first mode, the solution appears to be independent of p, but in the case of higher modes the solution seems to converge as the degree of polynomial interpolation is reduced.

Free Vibration Analysis of Hemispherical Shell

The hemispherical shell shown in Fig. 23 is discretized with three, five and ten equal elements and analyzed for the zeroeth harmonic using third and sixth degree polynomial interpolations. The natural frequencies for the first four modes are shown in Fig. 24. The analytical solution obtained by Kalnins and Kraus (9,10) based on Reissner-Naghdi theory

which includes both transverse shear and rotary inertia effects are also shown. It may be noted that in the case of the 6th degree polynomial interpolation, the solution shows excellent convergence as the number of elements is increased; whereas, in the case of third degree polynomial interpolation the solution shows improvement as the number of elements is increased. The convergence characteristics of SHORE-III solution with increasing degree of polynomial is shown in Fig. 25. It may be noted that higher values of p showed consistent behavior. But, in the case of the third degree polynomial, good results are obtained in the case of second and third modes. The first four mode shapes for the shell as obtained for $p = 3$ and five elements are shown in Fig. 26. It was found that these mode shapes are nearly the same as those with ten elements.

Free Vibration Analysis of Empty Water Tank with Soil Interaction Effect:

The tank shown in Fig. 27 was analyzed using sixth-order general elements; the seventh element is the ring footing of the tank. The soil is modeled using sixteen isoparametric quadratic solid elements. The soil model is analyzed at a driving frequency of 358.8 rad./sec., which is the fundamental frequency of the tank on a rigid foundation.

The first five mode of vibrations along with the corresponding frequencies are shown in Fig. 28. It may be noticed that the fundamental frequency of this stiff structure dropped from 358.8 rad./sec. to 151.6 rad./sec. when the soil interaction is considered. A better soil model may be obtained if the analysis is repeated at the new fundamental frequency (151.6 rad./sec.).

Static Analysis of Hyperboloidal Shell

The column supported hyperbolic cooling tower shown in Fig. 29 was analyzed for a mean wind pressure expressed in terms of the following six harmonics.

Harmonic Number	Fourier Coefficient
0	-0.064317
1	-2.072903
2	-3.846021
3	-3.404910
4	-3.962074
5	0.3289617

The shell was discretized using ten general axisymmetric shell elements and one open type element at the base (Fig. 29). The variation of the mean wind pressure in the meridional direction was assumed to be constant. Sixth degree polynomial interpolations of the displacement fields were used in the case of shell elements. The C.P.U. time required for running the problem was 1.5 secs. per element for each harmonic loading case. The membrane and bending stress resultants, N_ϕ, N_θ, M_ϕ, M_θ, at $\theta = 0°$ obtained by the analysis are shown in Fig. 30. The nature and distribution of forces and moments in the shell agree well to those reported in past literature(11). The nature and distribution of the forces and moments in the columns are shown in Fig. 31.

Cylindrical Shell Under Blast Load

The cylindrical shell (Fig. 32) is analyzed for the zeroeth harmonic only as shown in Fig. 33. For this harmonic, the time period corresponding to the third mode is 2.42×10^{-4} sec. whereas in the case of the fifth mode it was found to be 2.415×10^{-4} sec. Thus a suitable

value of the time step, Δt, at one tenth of the period is approximately 2.5×10^{-5} sec. However, the first time step cannot exceed 5×10^{-6} sec. but larger time steps can be used after this step. The normal displacement at the top of shell as obtained by SHORE-IV and by Johnson and Greif(12) are shown in Fig. 34. It may be noted that there is excellent agreement between the SHORE-IV solution and Johnson and Greif's solution based on numerical integration.

Hyperboloidal Shell under Dynamic Wind Load

The tower shown in Fig. 29 is analyzed for the wind loading shown in Fig. 35. The digitized wind data is at 0.5 second intervals. The damping coefficients used are $\alpha = 0.276$ and $\beta = 0.0058$. The time step used was 0.025 sec., which is about 1/50th of the fundamental period. The pressure was assumed constant over the height of the tower, and the eight harmonics, as shown in Fig. 35, were used. The resulting time history of the normal displacement at throat level and the meridional force (N_ϕ) are shown in Figs. 36 and 37. The SHORE-IV solution was based on eleven third order elements (Fig. 29), whereas, in Ref. 13 twenty elements were used.

Response Spectrum Analysis of Hyperboloidal Shell with Soil Interaction:

The tower shown in Fig. 38 is analyzed under the ground motion given by the response spectrum of Fig. 39. The damping ratios for both the shell and the soil are 5% of the critical damping ratio. The analysis of the soil is carried out under arbitrary driving frequency of 20 rad./sec. The soil medium is an elastic half space with shear modulus of 1600 k/ft^2 and Poisson's ratio of 0.4. The RSS of the N_ϕ, N_θ, $N_{\theta\phi}$, M_ϕ and M_θ are plotted along the circumferential axis for selected nodal points in

Figs. 40 to 42. For comparison the same problem with fixed base results are plotted with dashed lines on the same figures.

Time History Analysis of Hyperboloidal Shell

a. With soil effect (EBS)

b. Without soil effect (fixed)

The tower of Fig. 38 is analyzed under El-Centro earthquake (5-18-1940) EW Comp. The soil medium is considered as an elastic half space as in the response spectrum analysis, and then the analysis repeated with fixed lower boundary at node #10. The time of the analysis is taken as five seconds and the time step for Newmark β method integration is taken 0.02 second in case a, and 0.005 second in case b (fixed base). The damping coefficients (α=0.715779 and β=0.003356) are obtained based on 5% damping ratio for the first two modes of vibration (the modes of vibrations are obtained during the response spectrum analysis). The time history results are shown in Figs. 43 to 49.

For further details about these problems see Ref. 5.

ACKNOWLEDGEMENT

This work was partly supported under NSF Grant No. PFR-7900012. However, any opinions, findings, conclusions or recommendations expressed herein are those of the author's and do not necessarily reflect the views of NSF.

The authors gratefully acknowledge the cooperation of Washington University Computing Facility staff.

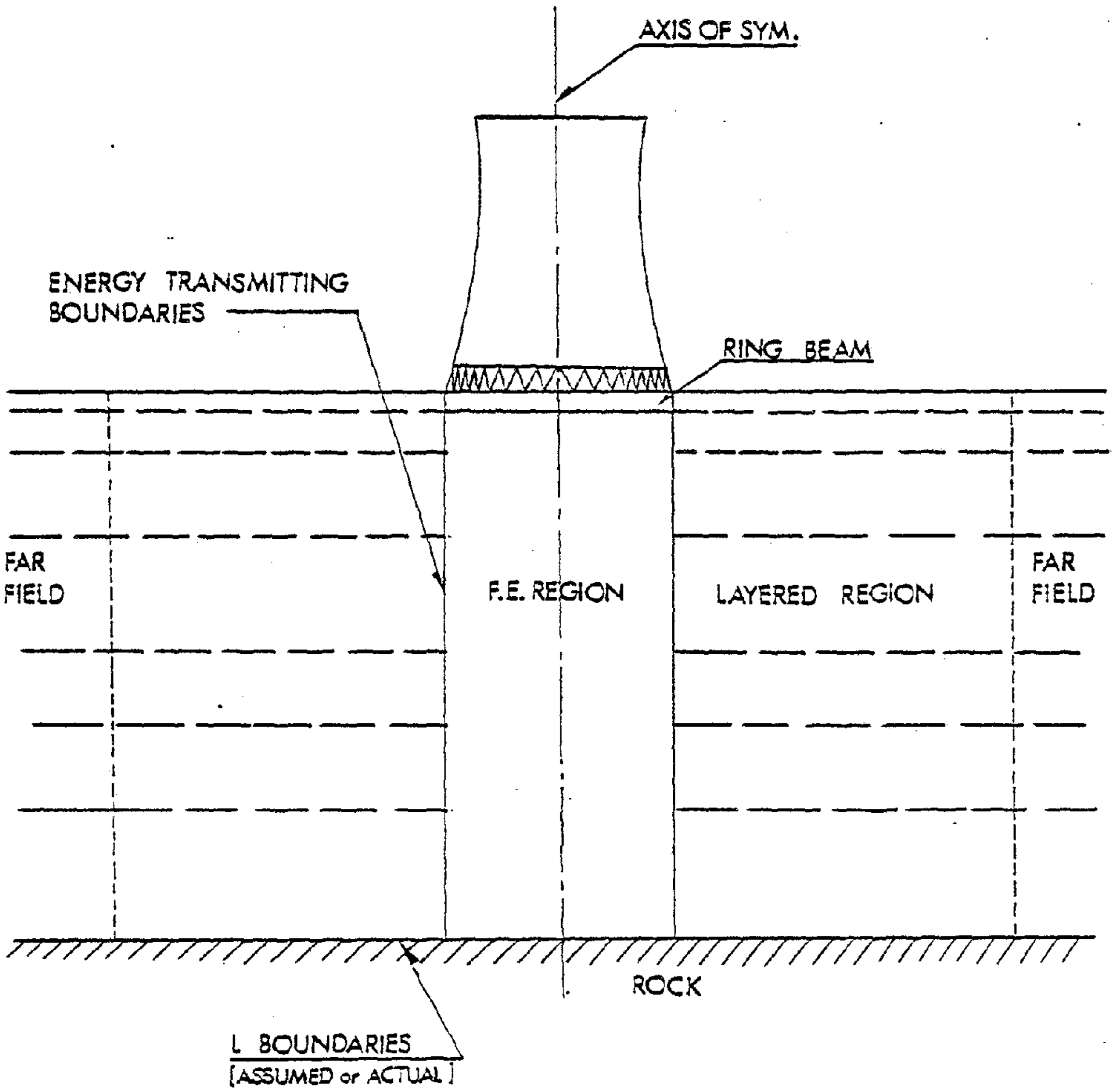

Figure 1. Finite Element Model for the Soil Medium

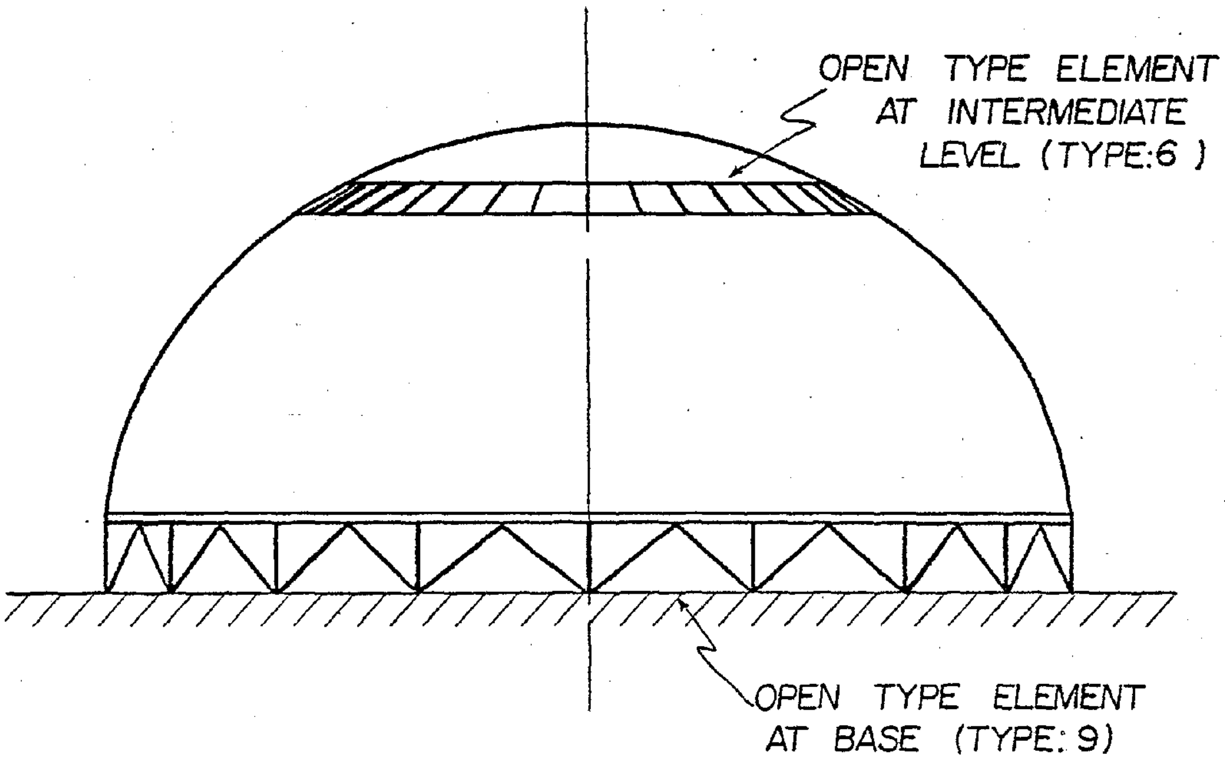

Figure 2. Elliptic Dome with Column Supports and Roof Openings

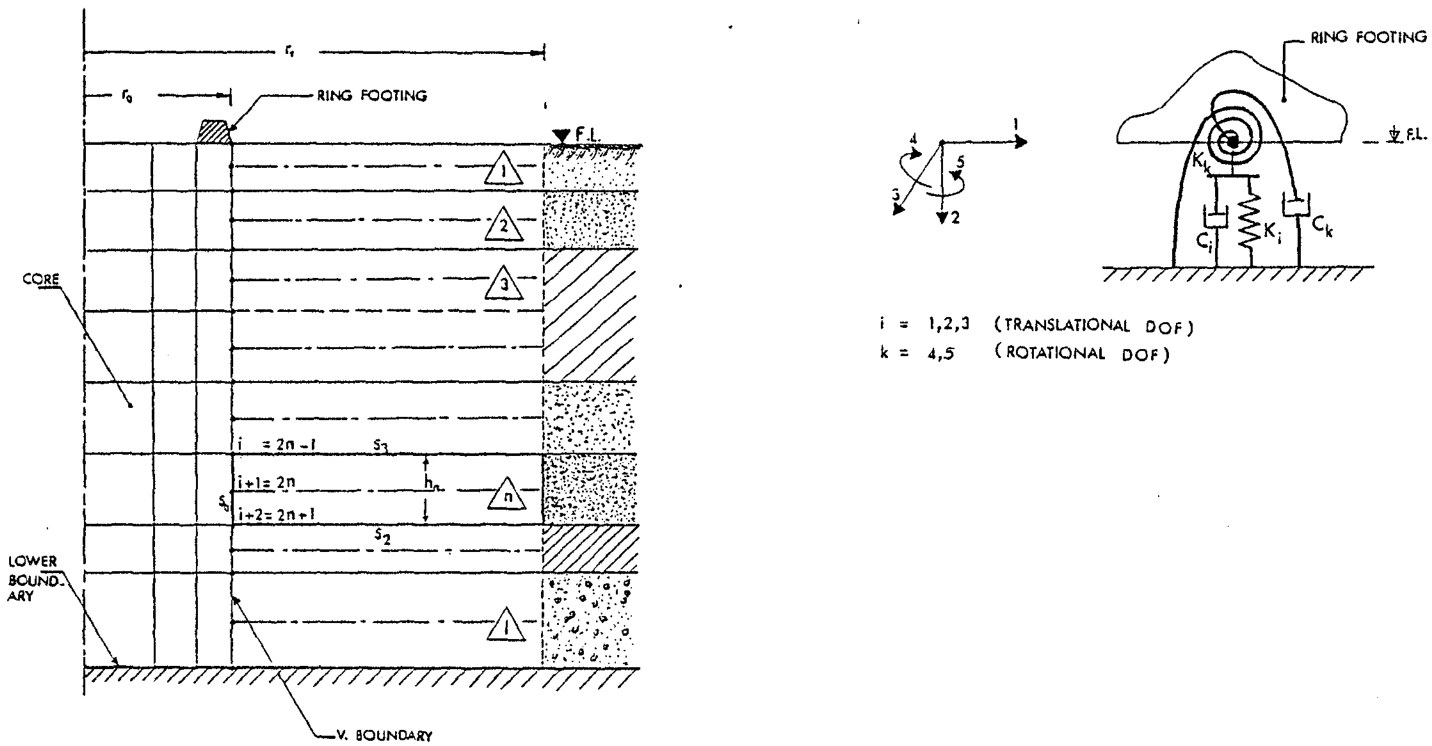

Figure 3. Soil Model

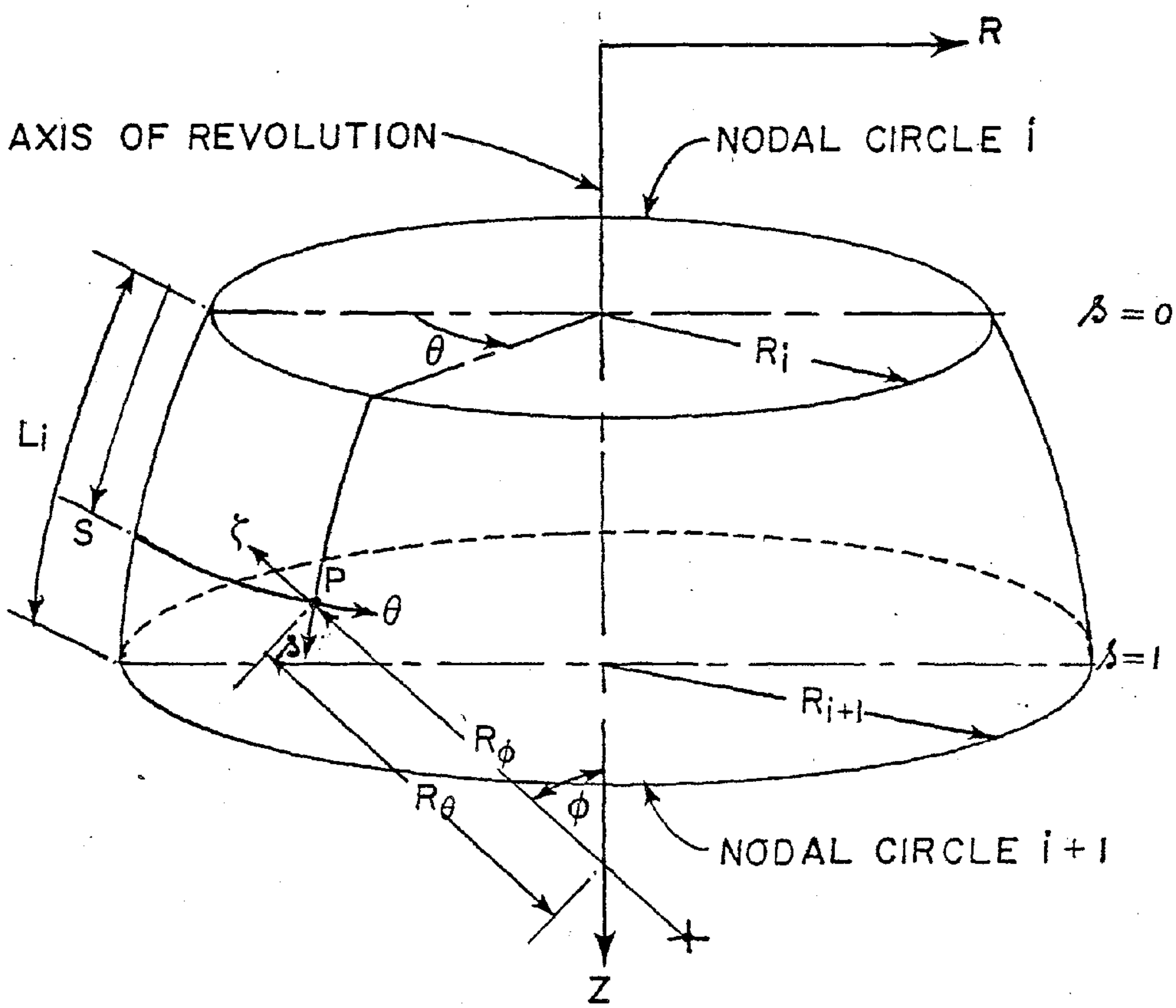

Figure 4. Geometry of Axisymmetric Shell Element

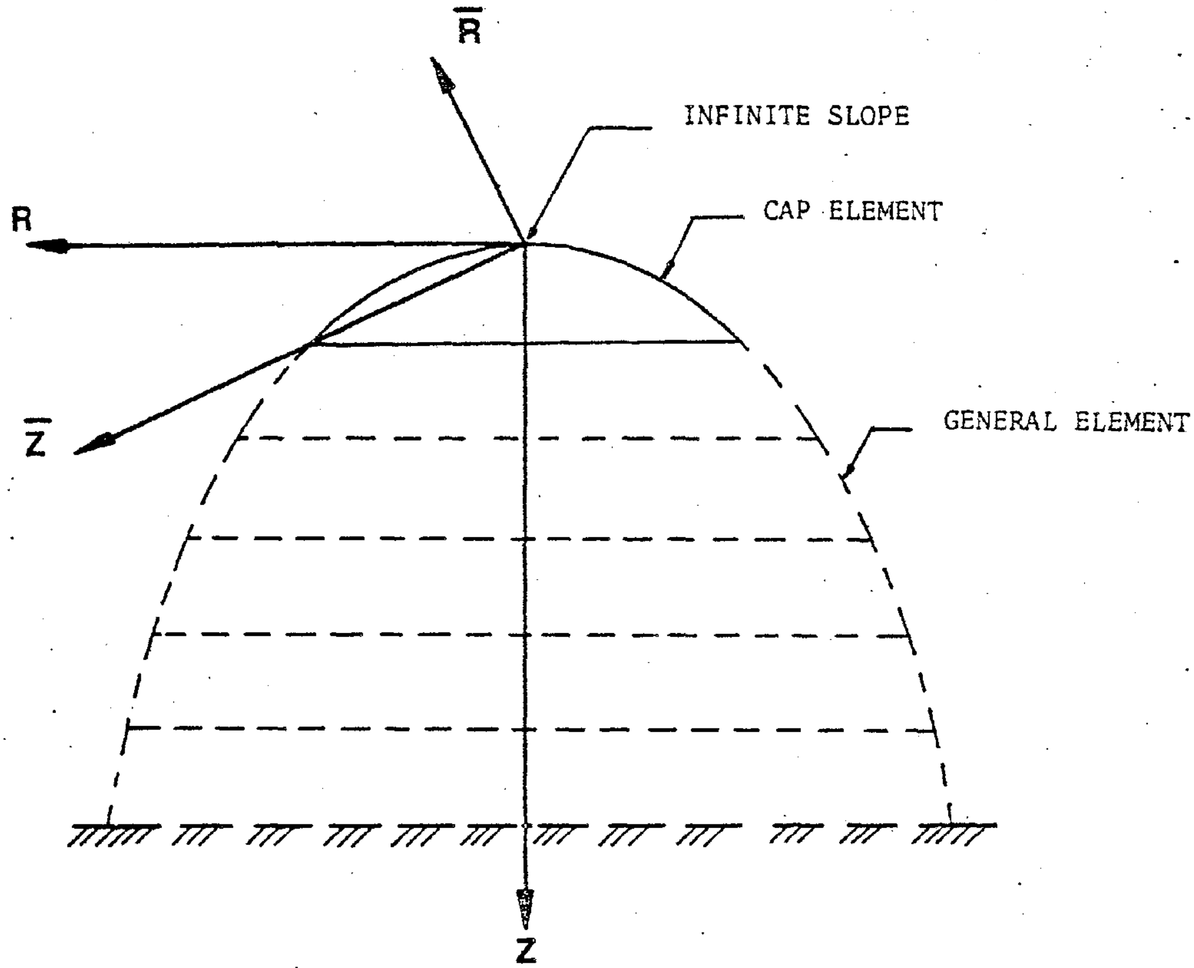

Figure 5. Rotation of Axes for Cap Element

CODE	TYPE	SHAPE
1	GENERAL (CURVED)	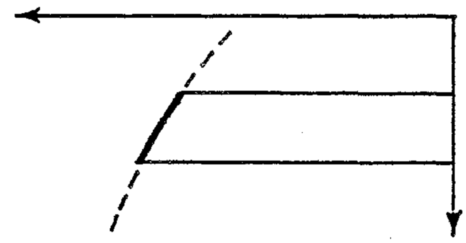
2	CAP (INFINITE SLOPE)	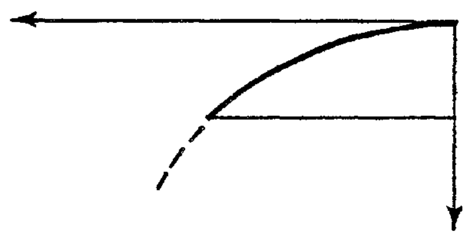
3	CAP (FINITE SLOPE)	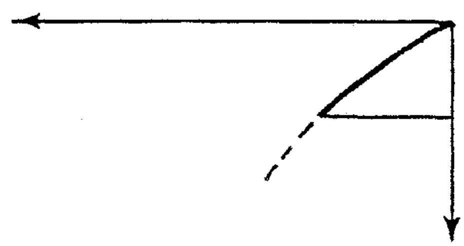
4	CAP (FLAT PLATE)	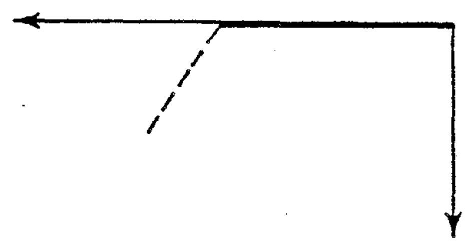
5	GENERAL (FLAT PLATE)	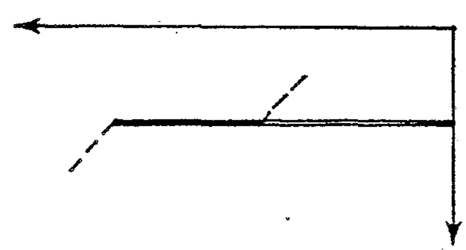

Figure 6. Library of Elements

CODE	TYPE	SHAPE
6	OPEN	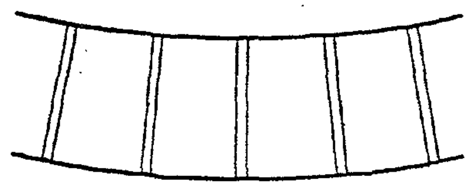
7	OPEN	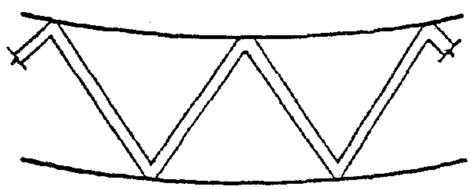
8	OPEN	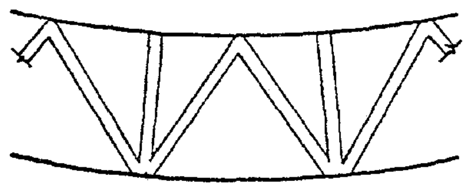
9	OPEN	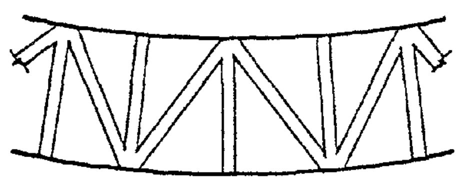

Figure 6. (Contd.)

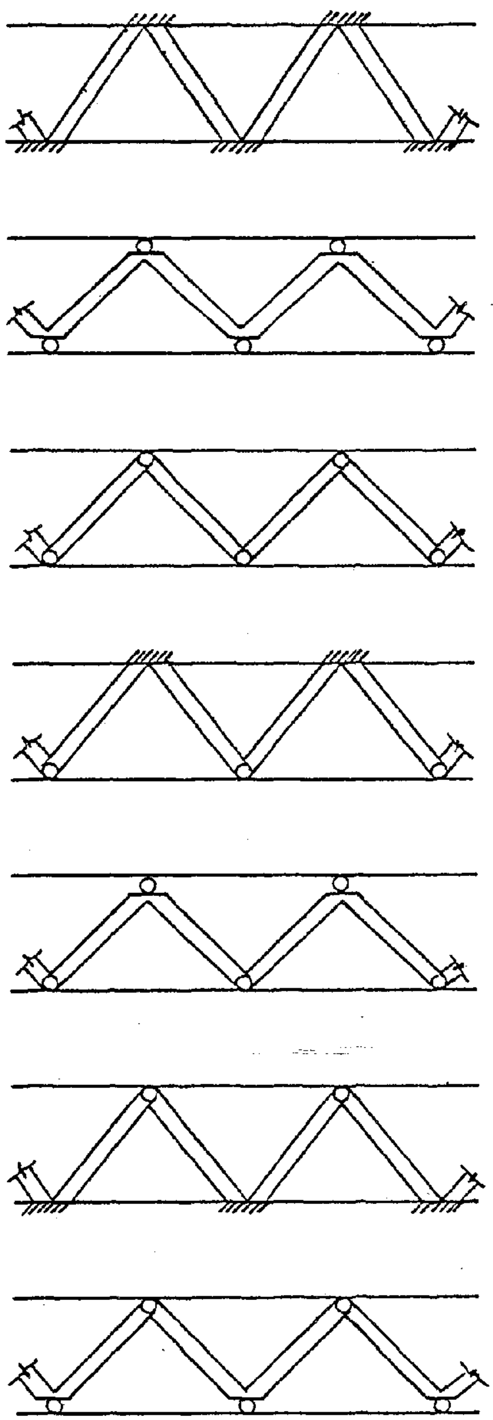

FULL CONTINUITY AT BOTH ENDS
CODE NUMBER: 1

MEMBERS MONOLITHIC PINNED ENDS
CODE NUMBER: 2

MEMBERS AND ENDS PINNED
CODE NUMBER: 3

TOP. ENDS LIKE CODE NO.1
BOT. ENDS LIKE CODE NO.3
CODE NUMBER: 4

TOP ENDS LIKE CODE NO.2
BOT. ENDS LIKE CODE NO.3
CODE NUMBER: 5

TOP ENDS LIKE CODE NO.3
BOT. ENDS LIKE CODE NO.1
CODE NUMBER: 6

TOP ENDS LIKE CODE NO.3
BOT. ENDS LIKE CODE NO.2
CODE NUMBER: 7

Figure 7. End Conditions of Open Type Elements

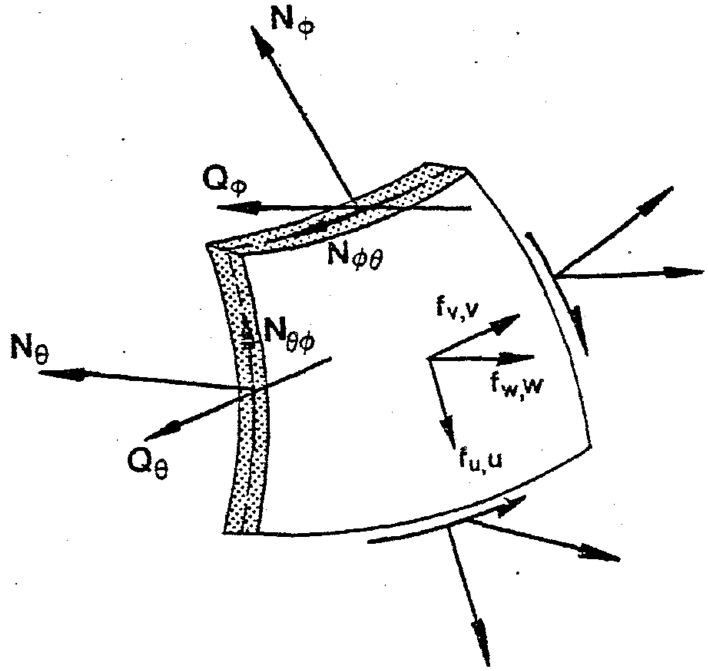

Stress Resultants

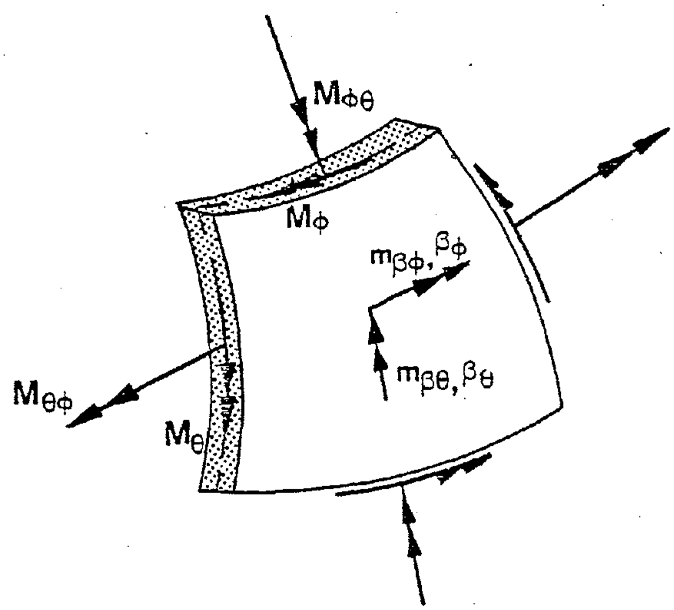

Stress-Couple Resultants

Figure 8. Sign Conventions

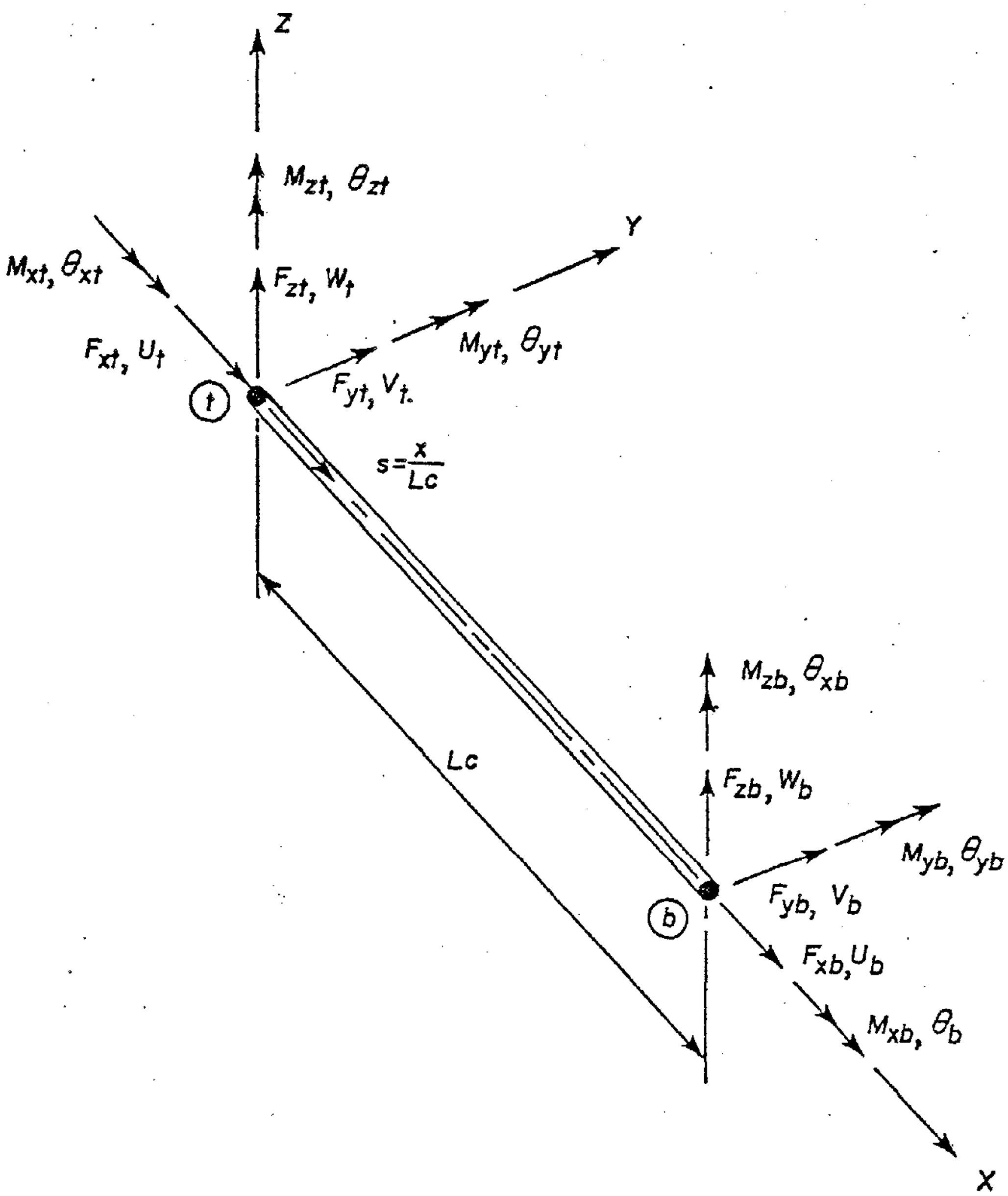

Figure 9. Bar Element

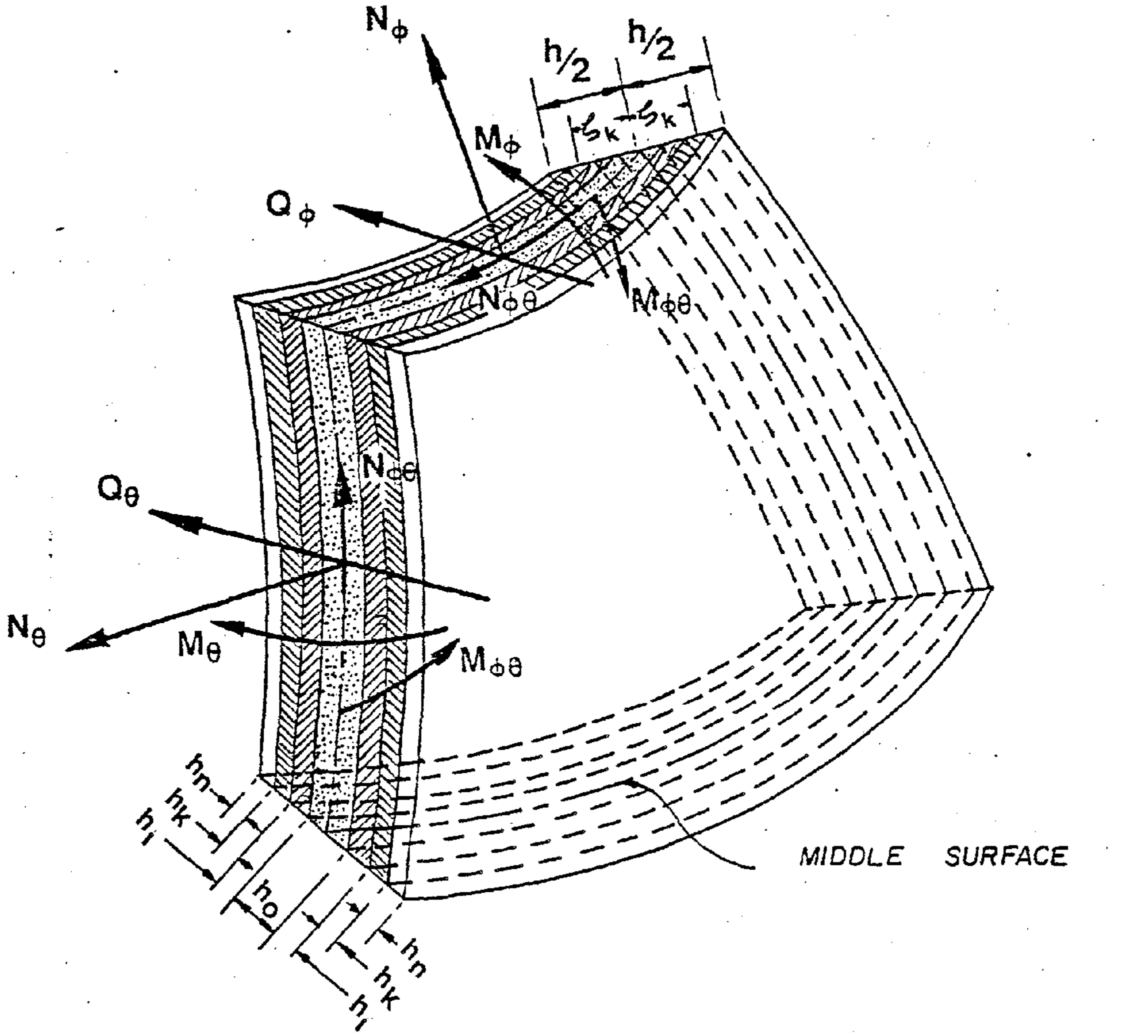

h_n — THICKNESS OF OUTER LAYER
h_k — THICKNESS OF INTERMEDIATE LAYER
h_o — THICKNESS OF MIDDLE LAYER

Figure 10. Multilayer Shell Element

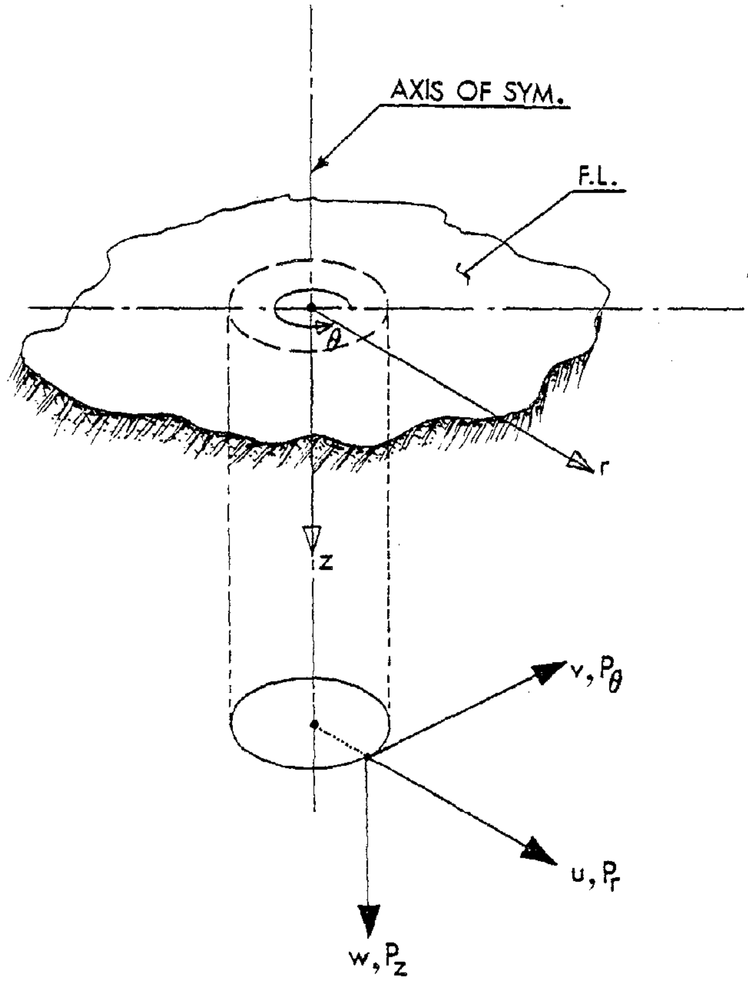

Figure 11. Coordinate System for the Soil Model

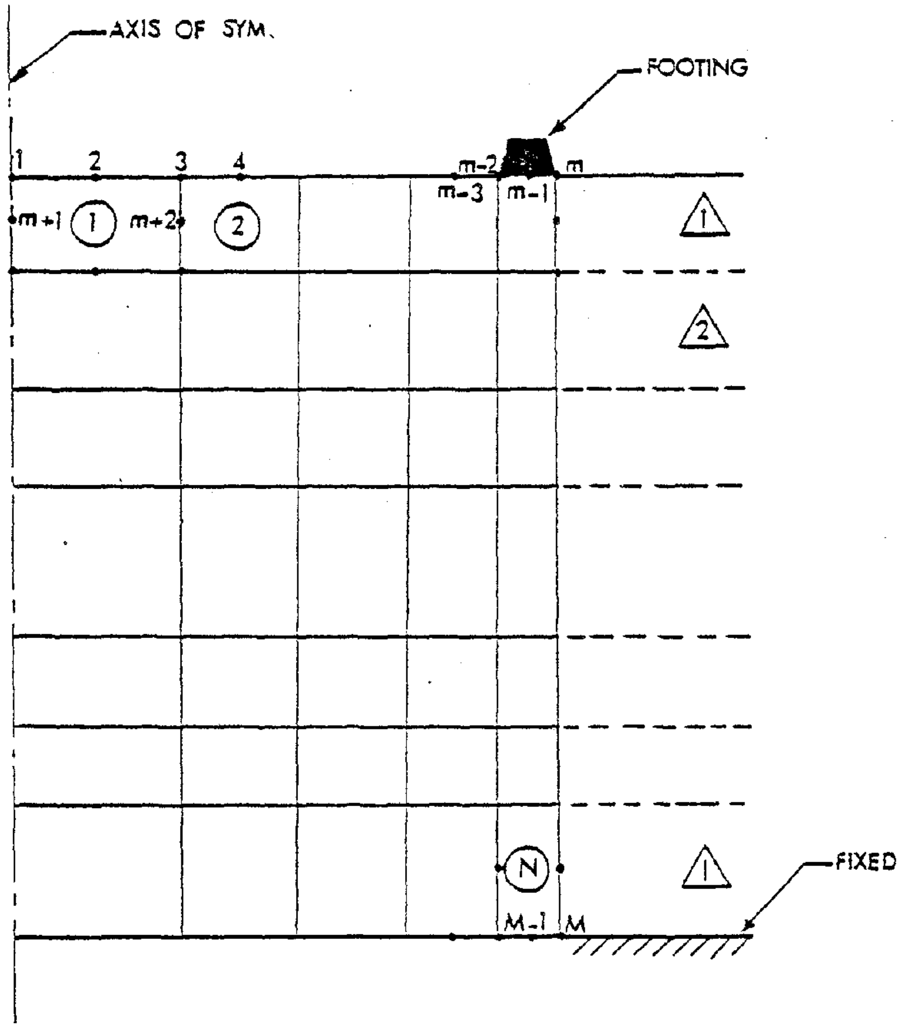

Figure 12. Soil Mesh with the
Ring Footing

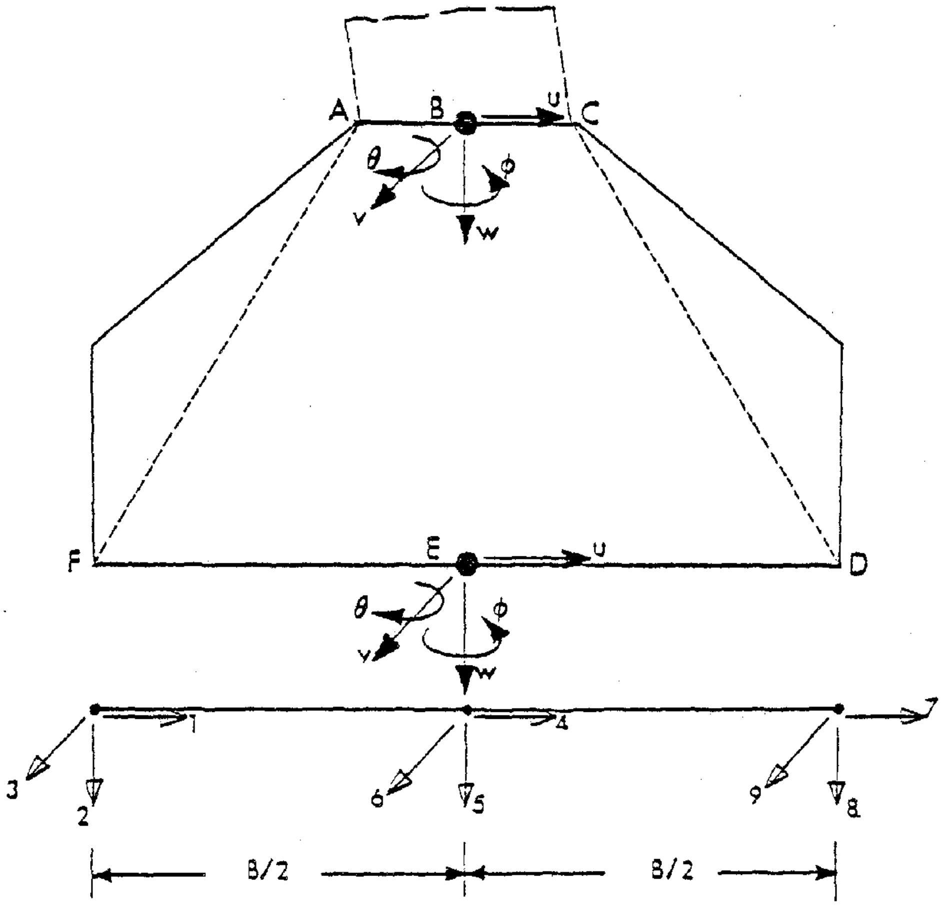

Figure 13. Ring Footing Cross Section

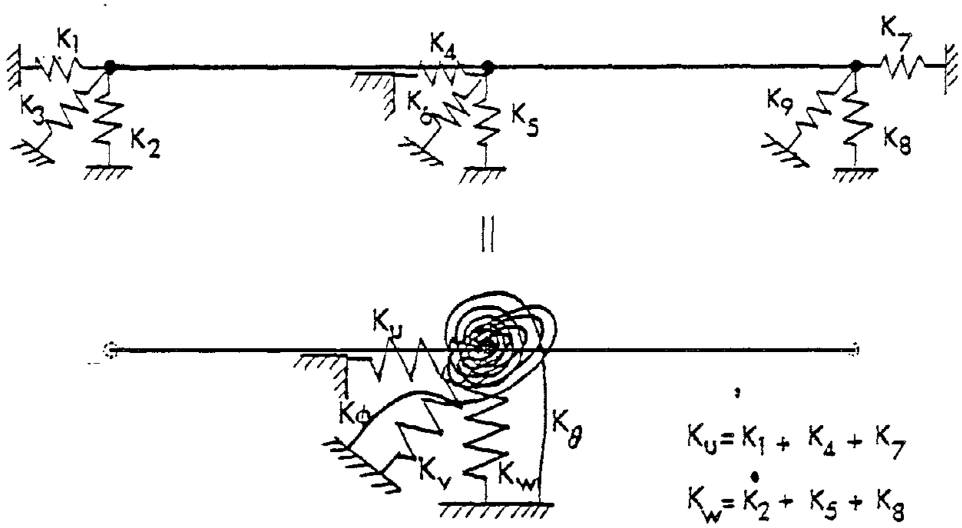

$$K_u = K_1 + K_4 + K_7$$

$$K_w = K_2 + K_5 + K_8$$

$$K_v = K_3 + K_6 + K_9$$

$$K_\theta = [K_2 + K_8]B^2/4$$

$$K_\phi = [K_3 + K_9]B^2/4$$

Figure 14. Equivalent Boundary
Stiffnesses

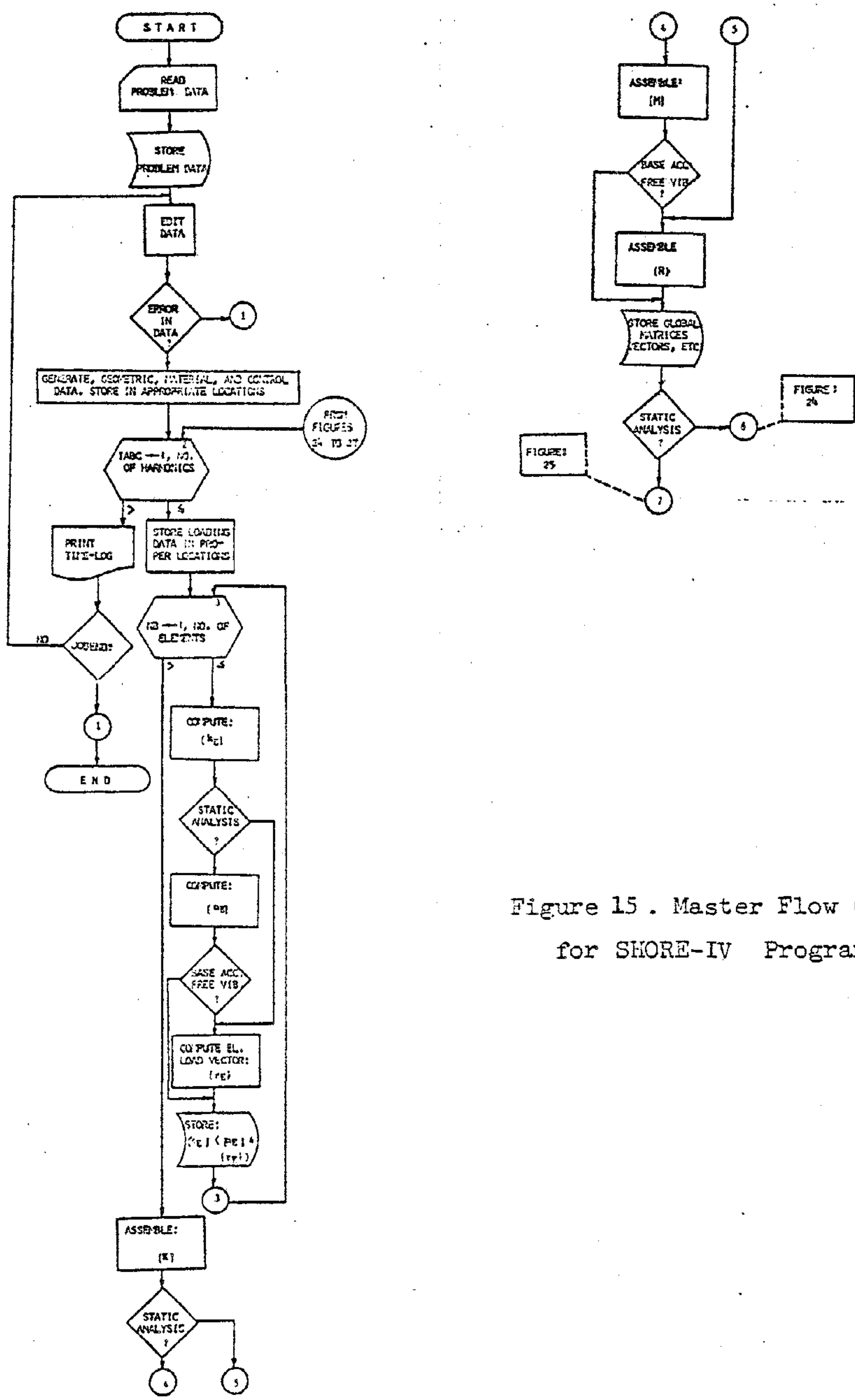

Figure 15 . Master Flow Chart for SHORE-IV Program

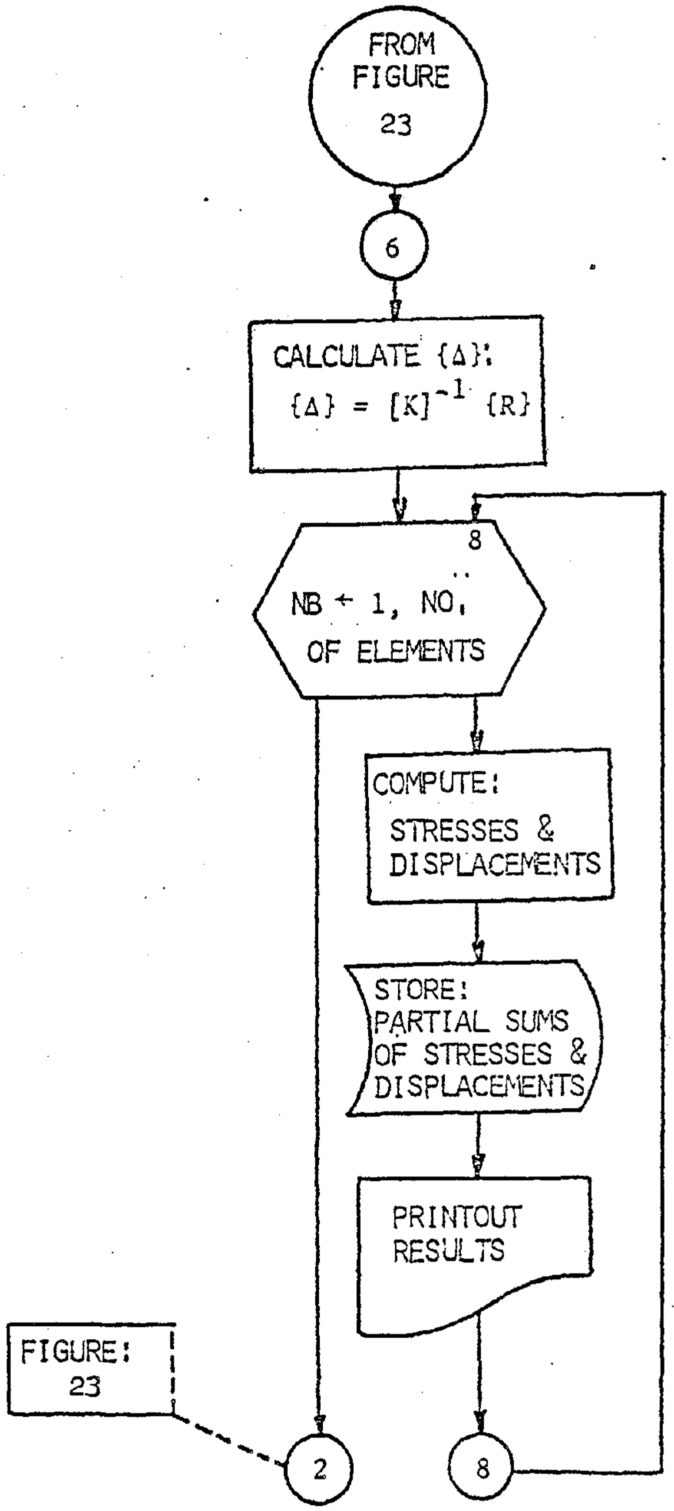

Figure 16. Flow Chart Segment for SHORE-IV Program
(STATIC ANALYSIS)

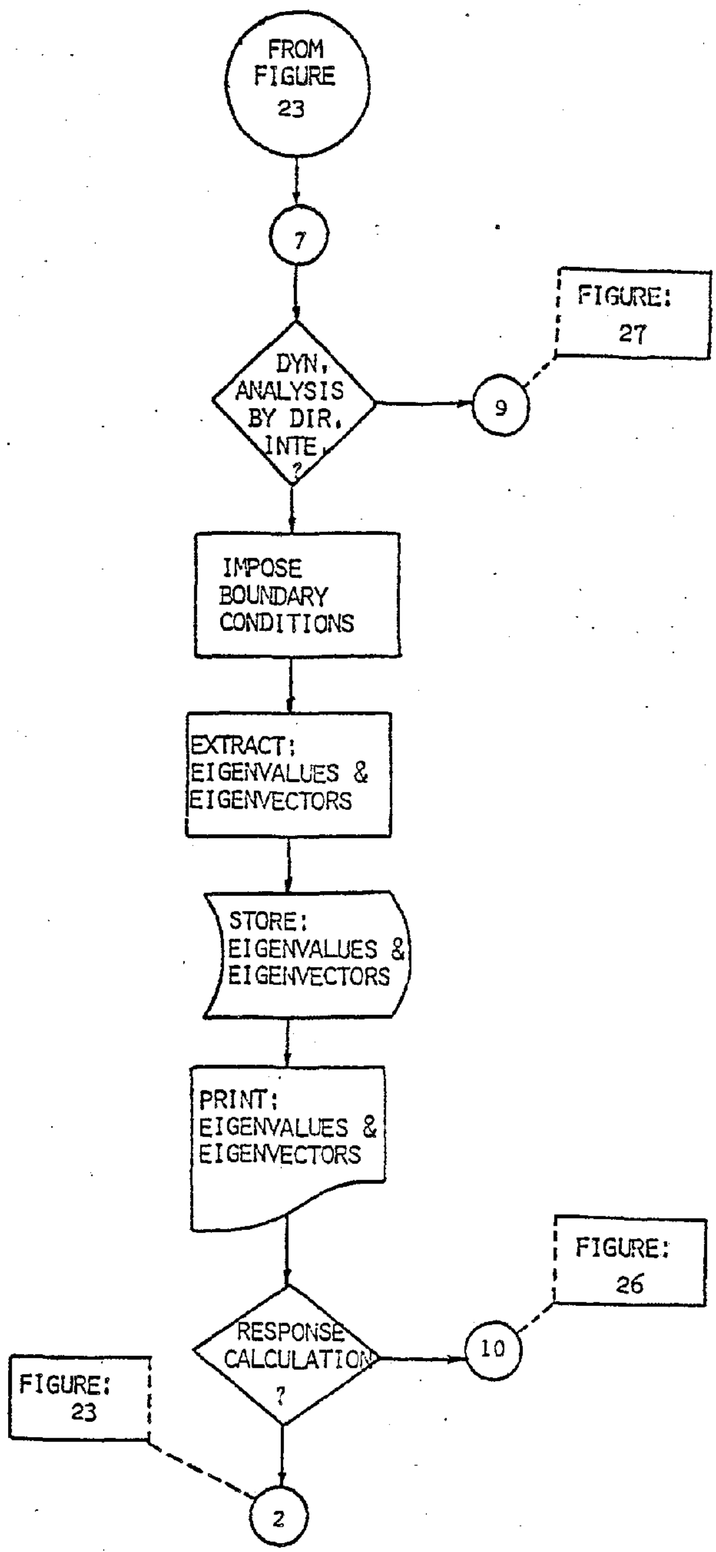

Figure 17. Flow Chart Segment for SHORE-IV Program
(FREE VIBRATION)

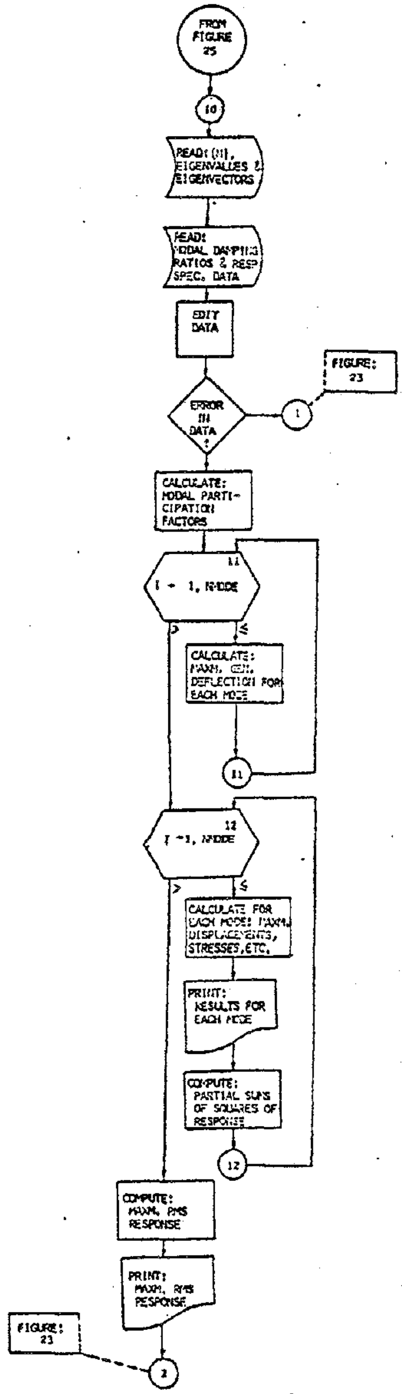

Figure 18. Flow Chart Segment foe SHORE-IV Program
(RESPONSE SPECTRUM)

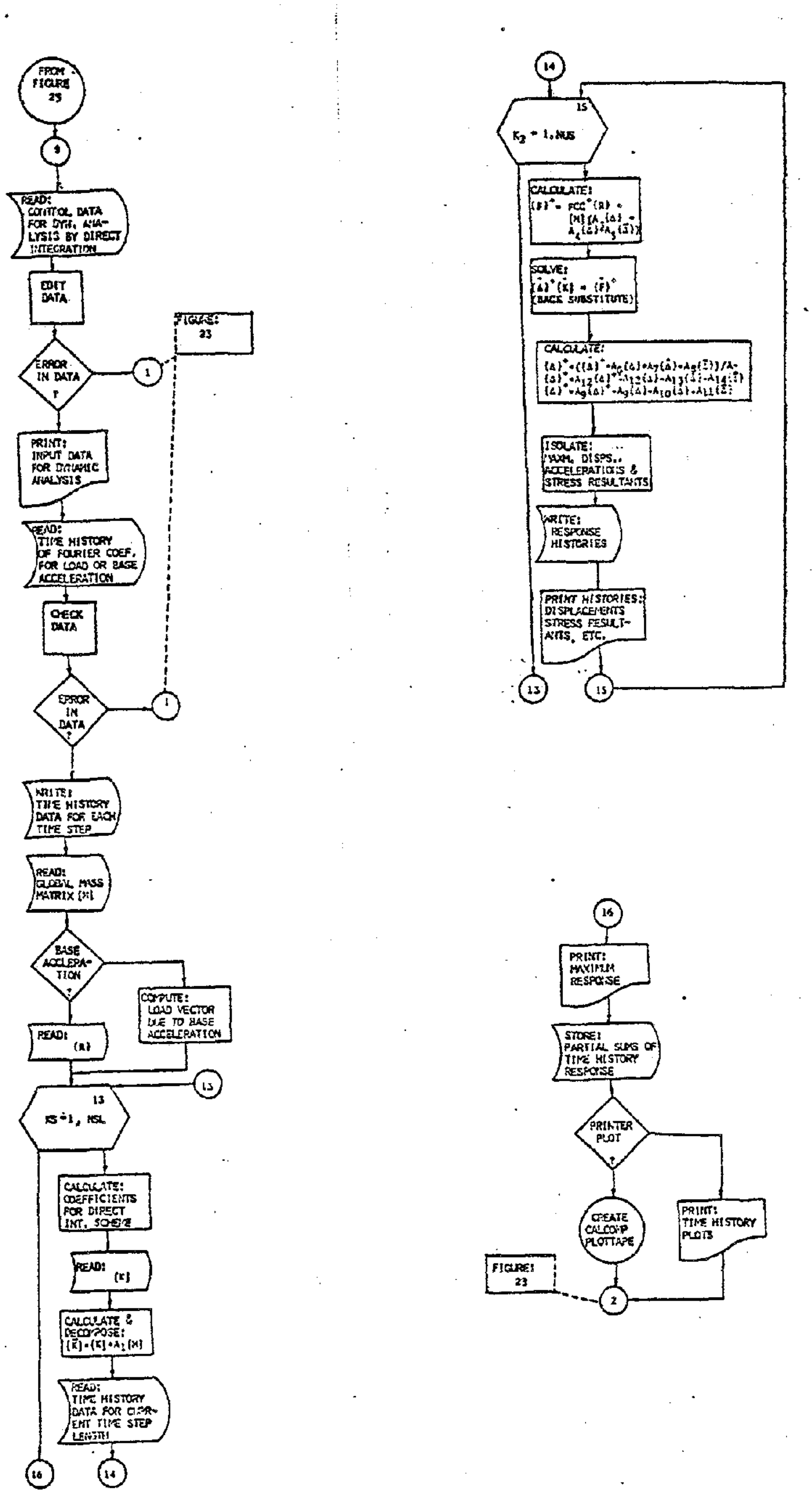

Figure 19. Flow Chart Segment for SHORE-IV Program
(FORCED VIBRATION)

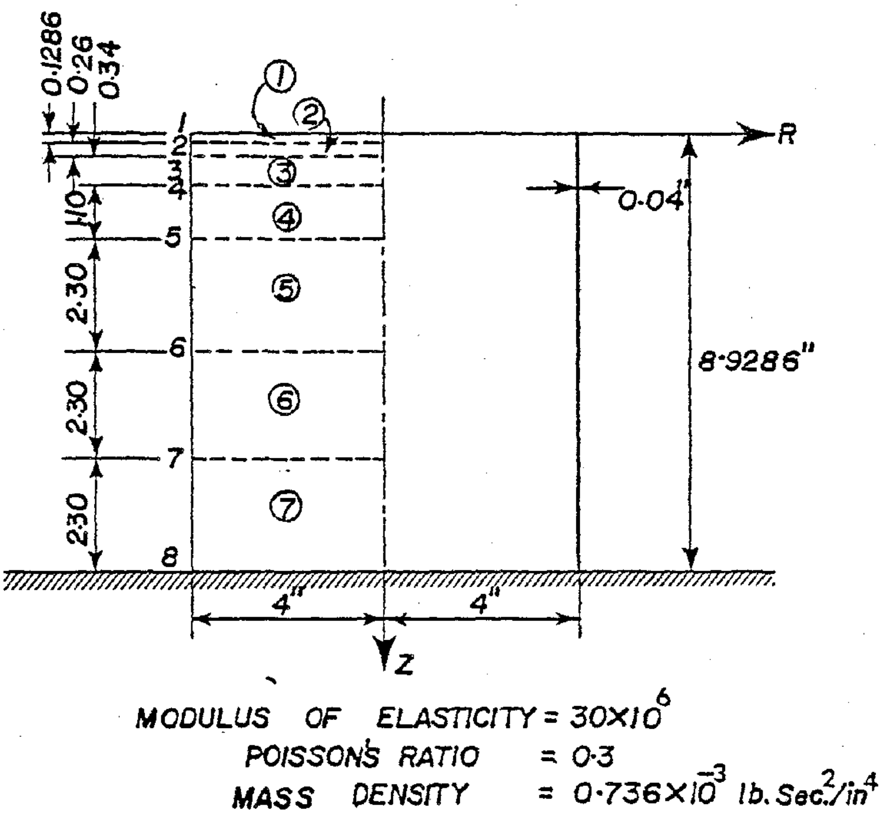

Figure 20. Circular Cylindrical Shell

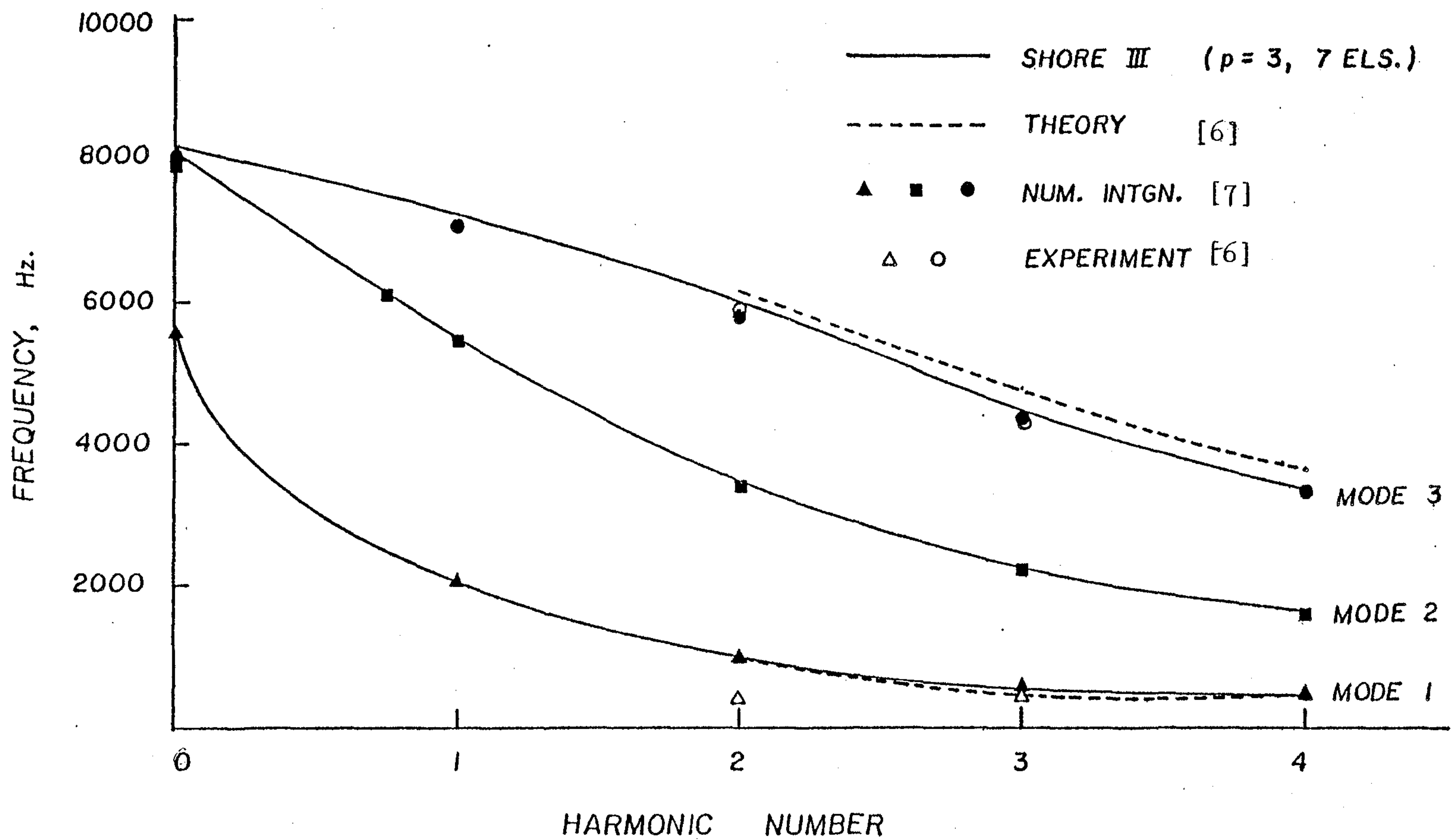

Figure 21. Comparison of Natural Frequencies of a Clamped-Free Cylindrical Shell

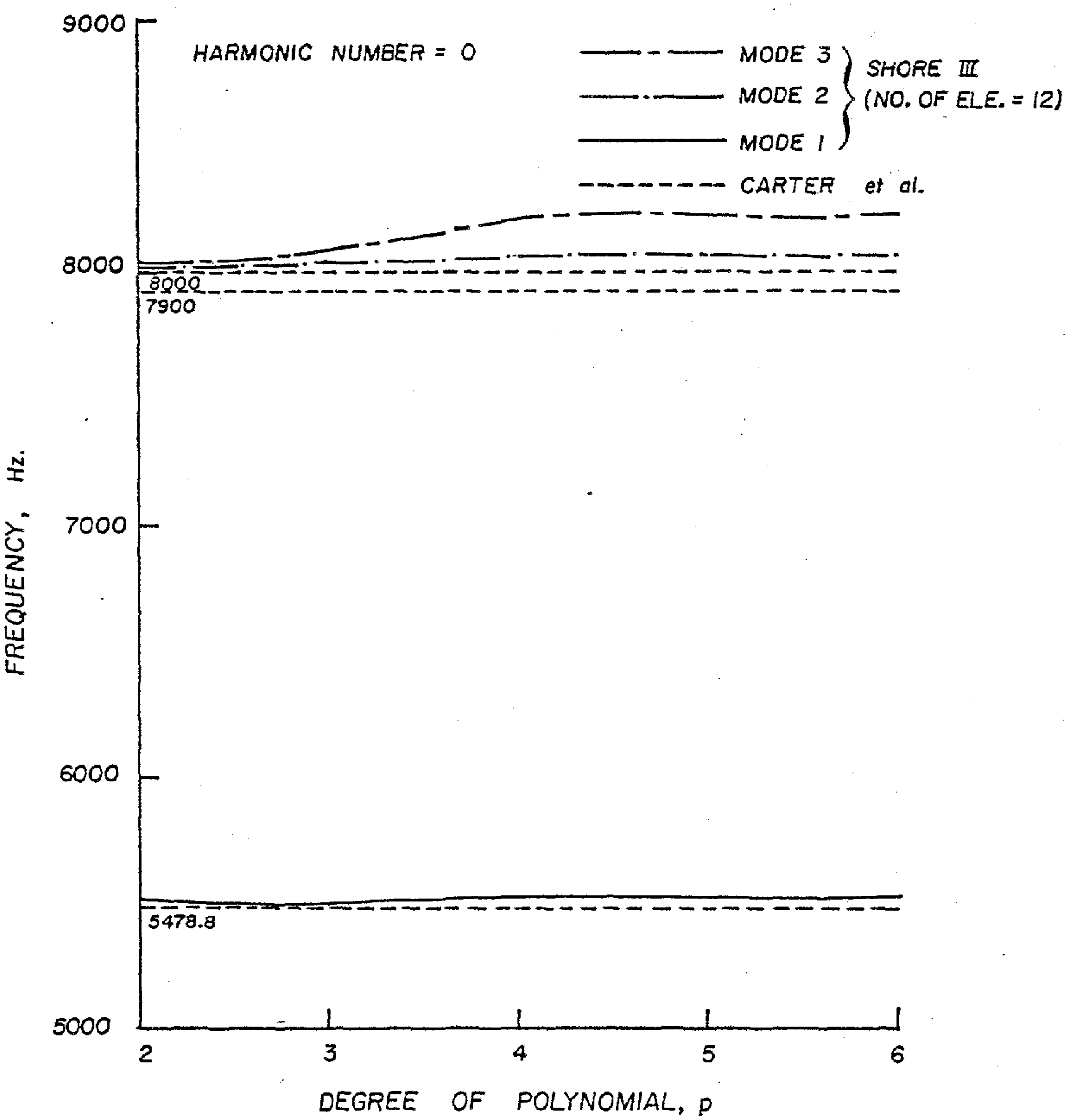

Figure 22. Convergence Characteristics of Natural Frequencies of a Cylindrical Shell with Varying Element Order

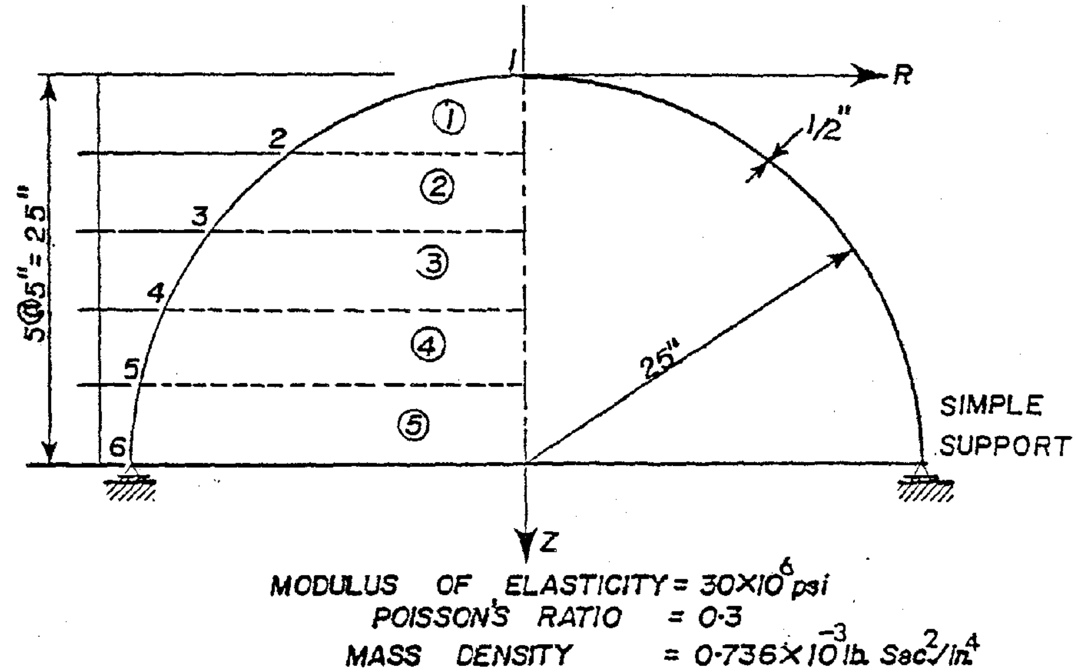

Figure 23. Hemispherical Shell

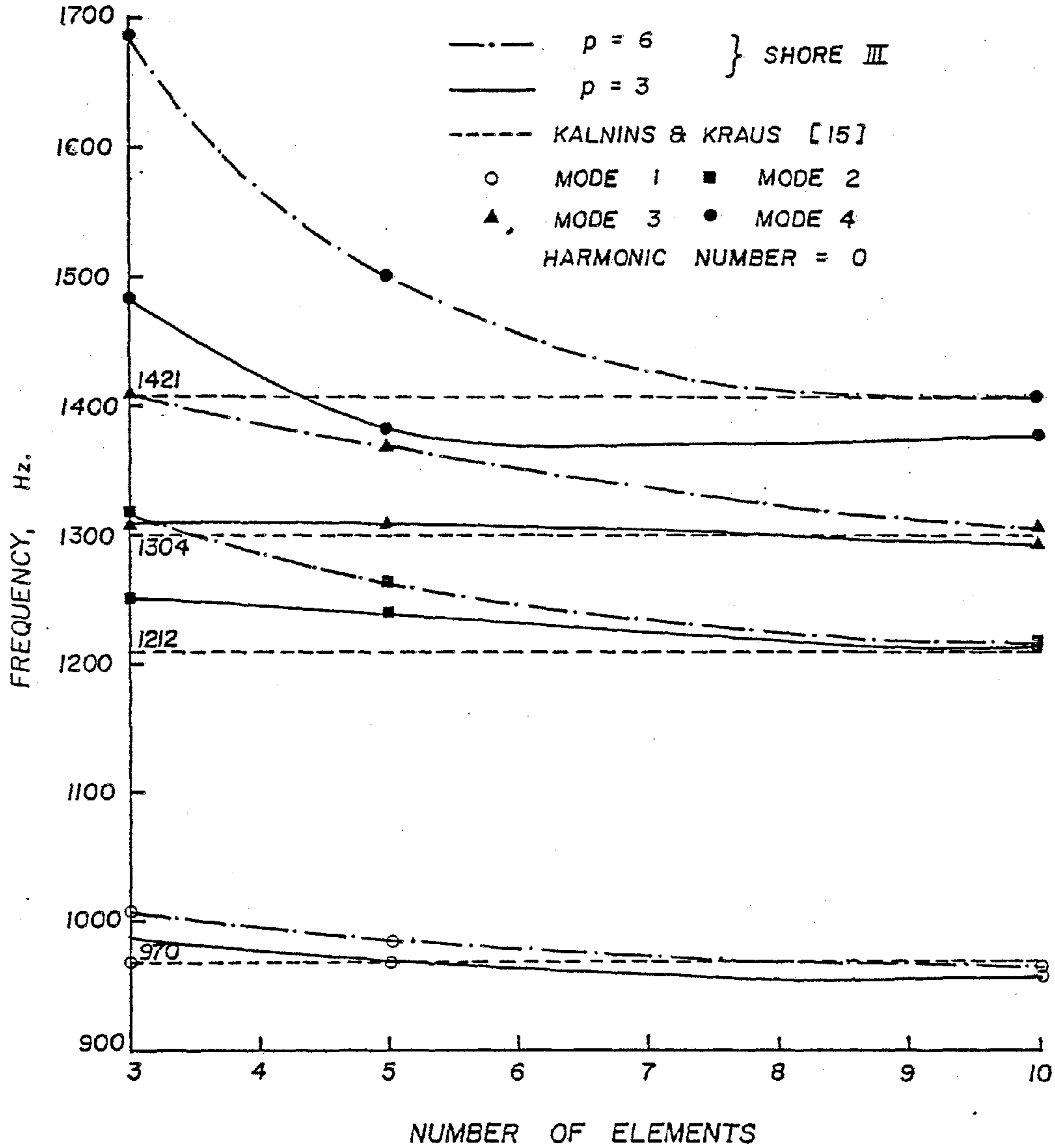

Figure 24. Natural Frequencies of Simply Supported Hemispherical Shell

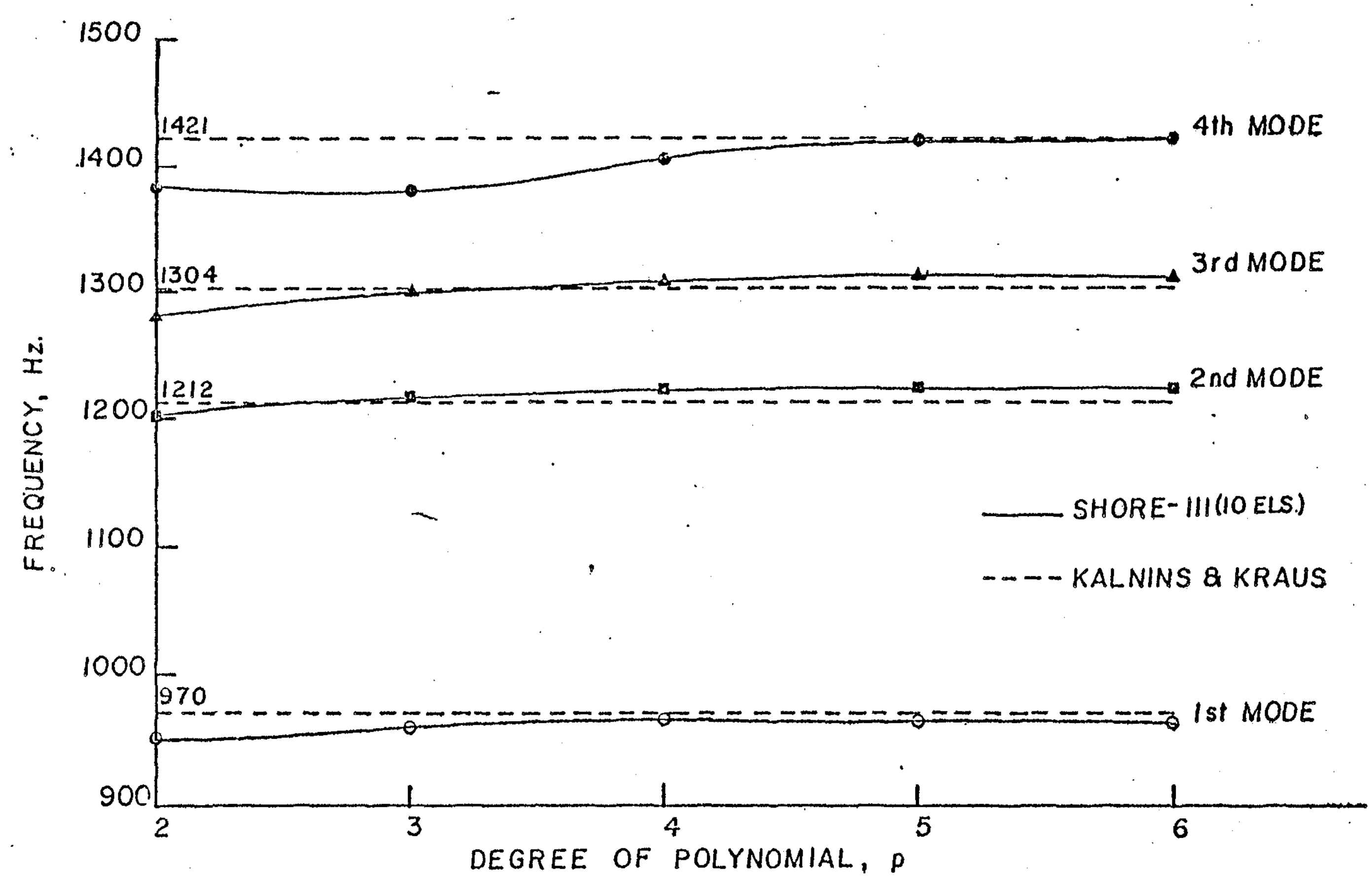

Figure 25. Convergence Characteristics of Natural Frequencies of Hemispherical Shell with Varying Element Order

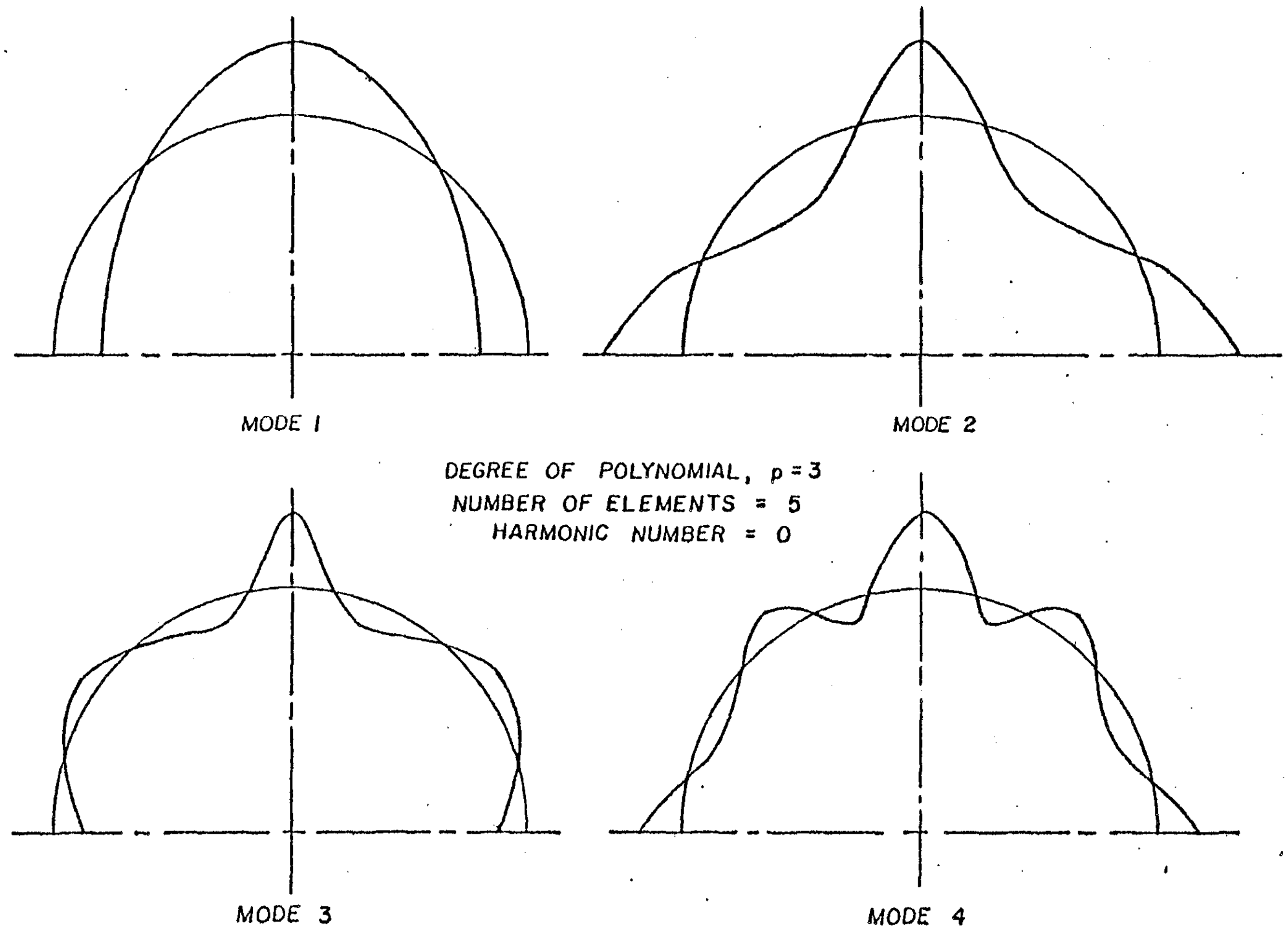

Figure 26. Mode Shapes of Hemispherical Shell Using SHORE-III

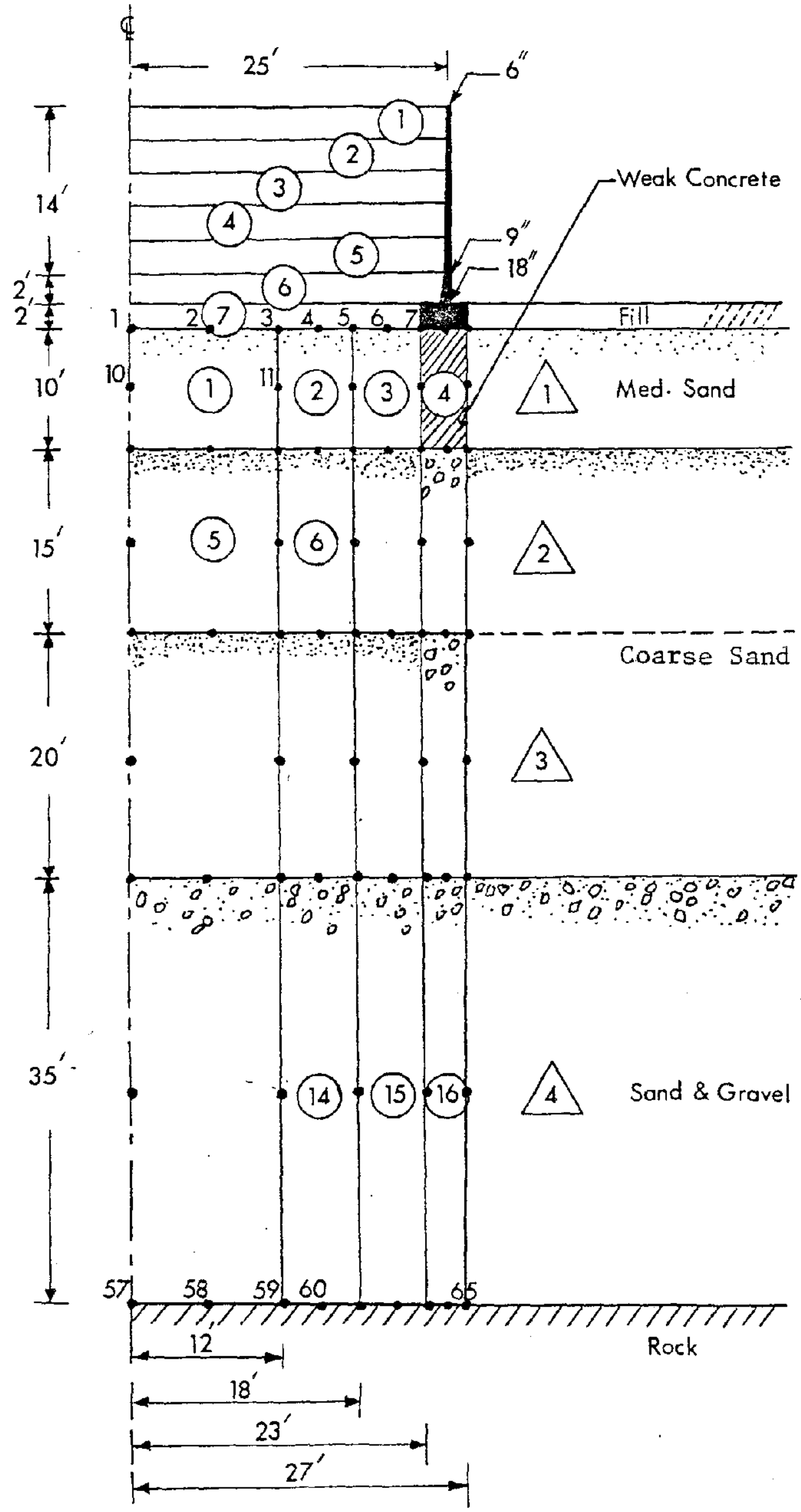

Figure 27. Water Tank on Layered Strata

RESULTS OF EIGENVALUE ANALYSIS FOR MODE NO. = 1

EIGENVALUE, LAMDA = 0.43522596E-04
CIRCULAR FREQUENCY= 0.15158025E 03 (RAD./SEC)
CYCLIC FREQUENCY = 0.24126756E 02 (CYCLES/SEC)

EIGENVECTOR NO. = 1

NODE NUMBER	U	V	W	BETA(PHI)	BETA(THETA)
1	0.696703	-0.872298	1.000000	0.032522	0.004885
2	0.694765	-0.814916	0.934982	0.032360	0.004778
3	0.690802	-0.723427	C.839754	0.030680	0.004623
4	0.685211	-0.626554	0.750686	0.029514	0.004929
5	0.677729	-0.525169	C.650682	0.041561	0.004960
6	0.668961	-0.420406	0.471531	0.085381	0.001624
7	0.665114	-0.356557	0.278658	0.103118	-0.007986
8	0.665599	-0.298938	0.070658	0.103365	-0.002728

RESULTS OF EIGENVALUE ANALYSIS FOR MODE NO. = 2

EIGENVALUE, LAMDA = 0.21325977E-04
CIRCULAR FREQUENCY= 0.21654369E 03 (RAD./SEC)
CYCLIC FREQUENCY = 0.34464020E C2 (CYCLES/SEC)

EIGENVECTOR NC. = 2

NODE NUMBER	U	V	W	BETA(PHI)	BETA(THETA)
1	-0.904268	-0.297101	0.387501	-0.049519	0.003848
2	-0.904951	-0.368118	0.486832	-0.050576	0.004652
3	-0.904454	-0.468663	0.649006	-0.059252	0.007146
4	-0.903300	-0.559671	0.840887	-0.065534	0.011161
5	-0.902584	-0.63782C	1.000000	-0.025408	0.014298
6	-0.900669	-0.701185	0.891612	0.123966	0.006578
7	-0.896807	-0.747669	0.567095	0.186172	-0.018486
8	-0.889631	-0.812496	0.189739	0.187158	-0.010356

Figure 28. Water Tank Results

RESULTS OF EIGENVALUE ANALYSIS FOR MODE NO. = 3

EIGENVALUE, LAMDA = 0.57813577E-05
CIRCULAR FREQUENCY= 0.41589624E 03 (RAD./SEC)
CYCLIC FREQUENCY = 0.66192001E 02 (CYCLES/SEC)

EIGENVECTOR NO.= 3

NODE NUMBER	U	V	W	BETA(PHI)	BETA(THETA)
1	-0.037648	-0.044113	1.000000	0.149447	0.036690
2	-0.048365	-0.041010	0.701970	0.148019	0.026494
3	-0.057609	-0.020942	0.274819	0.132554	0.010165
4	-0.060219	0.005011	-0.069064	0.091587	-0.002499
5	-0.058566	0.026326	-0.254628	0.028788	-0.009028
6	-0.055794	0.038012	-0.236141	-0.041064	-0.007623
7	-0.054597	0.038565	-0.131831	-0.057610	-0.000584
8	-0.054111	0.034346	-0.016113	-0.057669	-0.003283

RESULTS OF EIGENVALUE ANALYSIS FOR MODE NO. = 4

EIGENVALUE, LAMDA = 0.39595334E-05
CIRCULAR FREQUENCY= 0.50254858E 03 (RAD./SEC)
CYCLIC FREQUENCY = 0.79983154E C2 (CYCLES/SEC)

EIGENVECTOR NO.= 4

NODE NUMBER	U	V	W	BETA(PHI)	BETA(THETA)
1	0.006806	-0.051712	1.000000	0.420445	0.033552
2	-0.000377	-0.046068	0.173942	0.387798	0.005335
3	0.006137	-0.035999	-0.677269	0.142595	-0.028219
4	0.020938	-0.044309	-0.653007	-0.134881	-0.027607
5	0.02974C	-0.069250	-0.094336	-0.184940	-0.006628
6	0.029858	-0.094232	0.240589	-0.007988	0.005435
7	0.028853	-0.101286	0.175914	0.054118	-0.000036
8	0.028628	-0.099448	0.065213	0.054701	0.002501

Figure 28. (cont.)

RESULTS OF EIGENVALUE ANALYSIS FOR MODE NO. = 5

EIGENVALUE, LAMDA = 0.29355861E-05
CIRCULAR FREQUENCY= 0.58365015E (3 (RAD./SEC)
CYCLIC FREQUENCY = 0.92890884E (2 (CYCLES/SEC)

EIGENVECTER NO. = 5

NODE NUMBER	U	V	W	BETA(PHI)	BETA(THETA)
1	0.058033	0.324250	1.000000	0.294811	0.050003
2	0.043864	0.331992	0.428532	0.256374	0.030728
3	0.032466	0.343440	-0.009267	0.009899	0.013767
4	0.021149	0.344756	0.289425	-0.161472	0.025539
5	0.001331	0.343846	0.683960	-0.057181	0.040941
6	-0.021584	0.350914	0.552383	0.136389	0.035414
7	-0.032779	0.355797	0.234042	0.166839	0.014567
8	-0.038528	0.353624	-0.097145	0.166291	0.022245

Figure 28. (cont.)

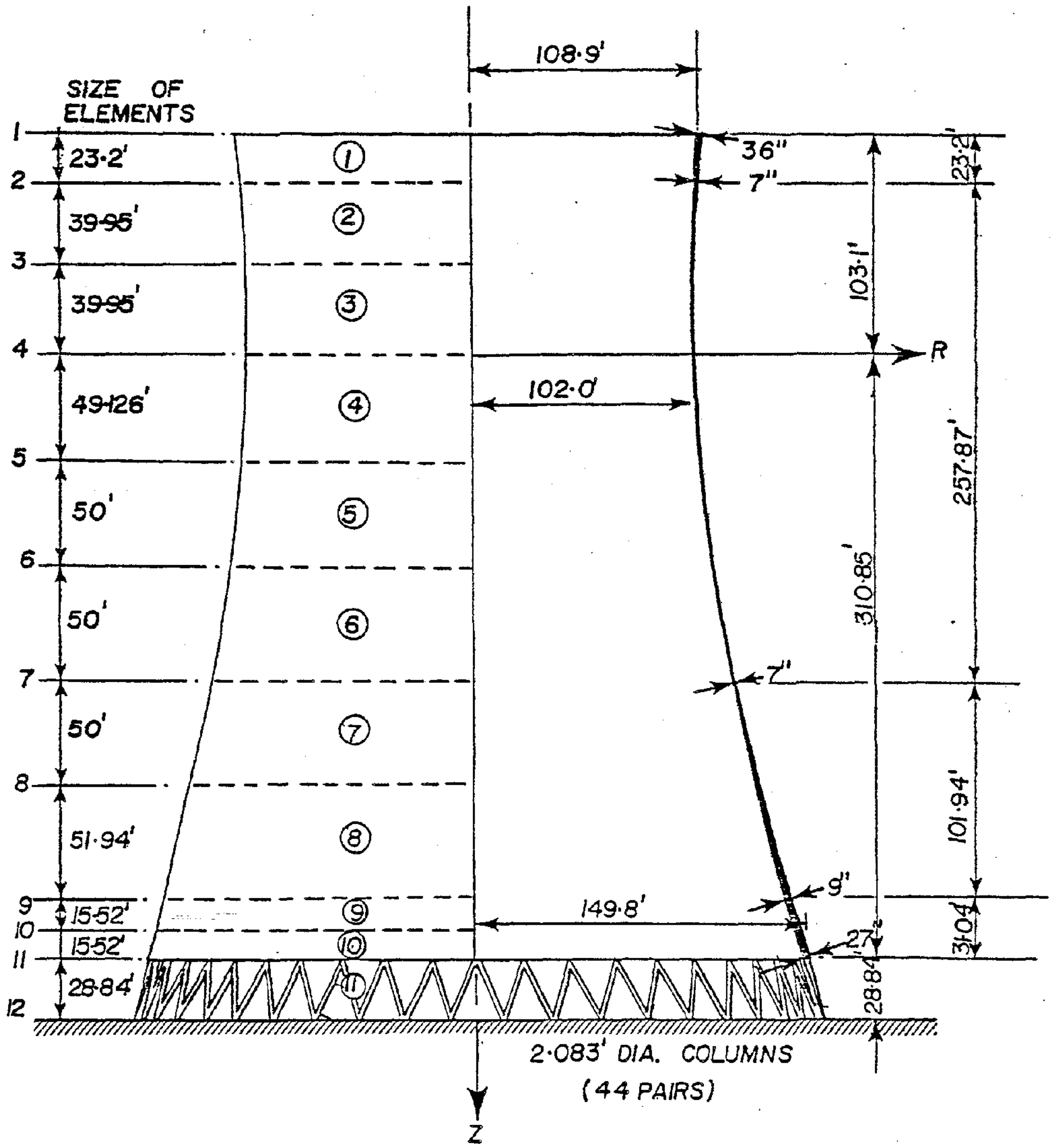

MODULUS OF ELASTICITY:
$5{\cdot}2\times10^8$ (SHELL); $6{\cdot}4\times10^8$ (COLS) psi
POISSON'S RATIO = 0·15
DENSITY = 150 lbs/cft

Figure 29. Discretization of Hyperboloidal Tower

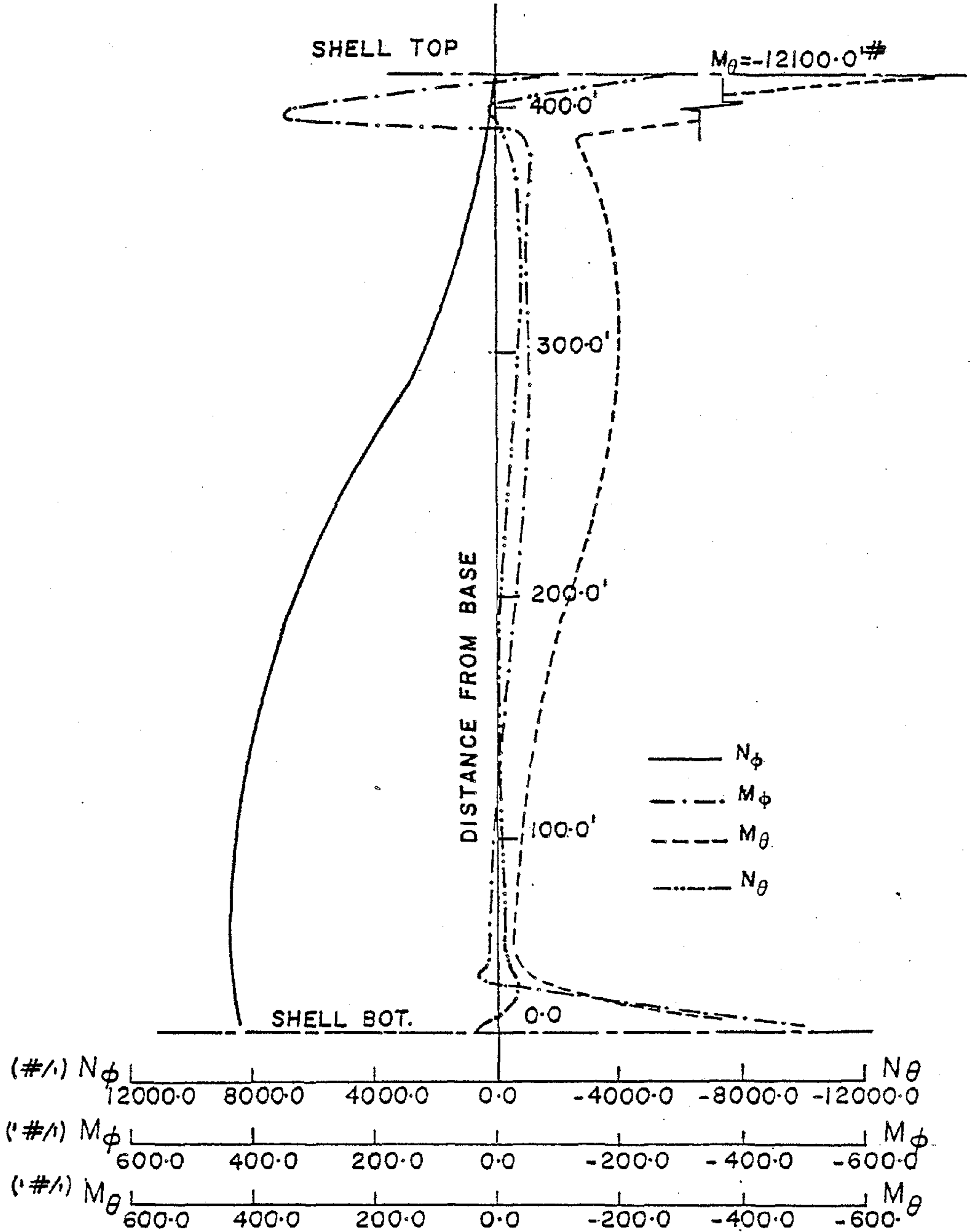

Figure 30. Stress Resultants for Hyperboloidal Tower at $\theta = 0°$ Under Mean Static Wind Load

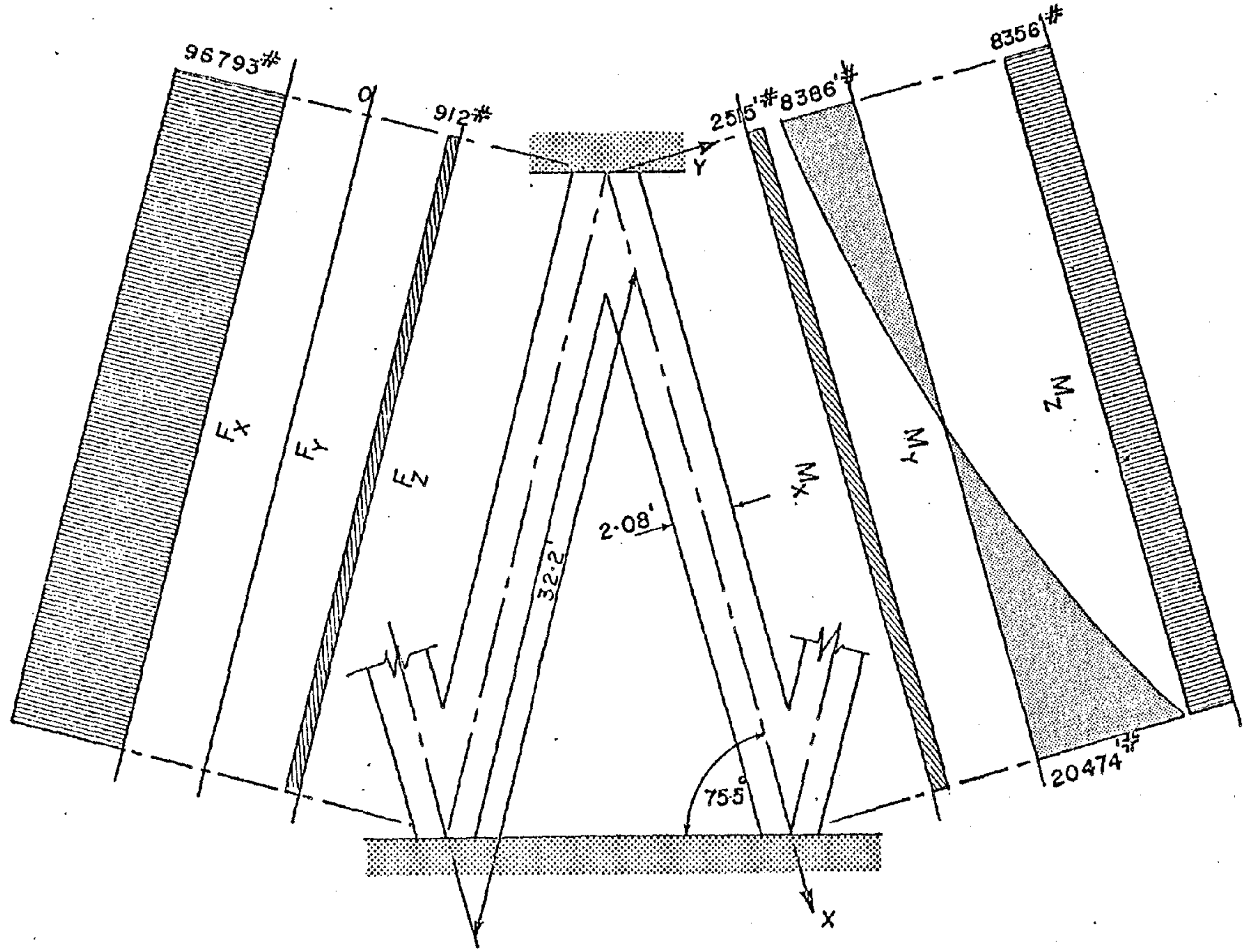

Figure 31. Forces in Supporting Columns of Hyperboloidal Cooling Tower at θ = 0°

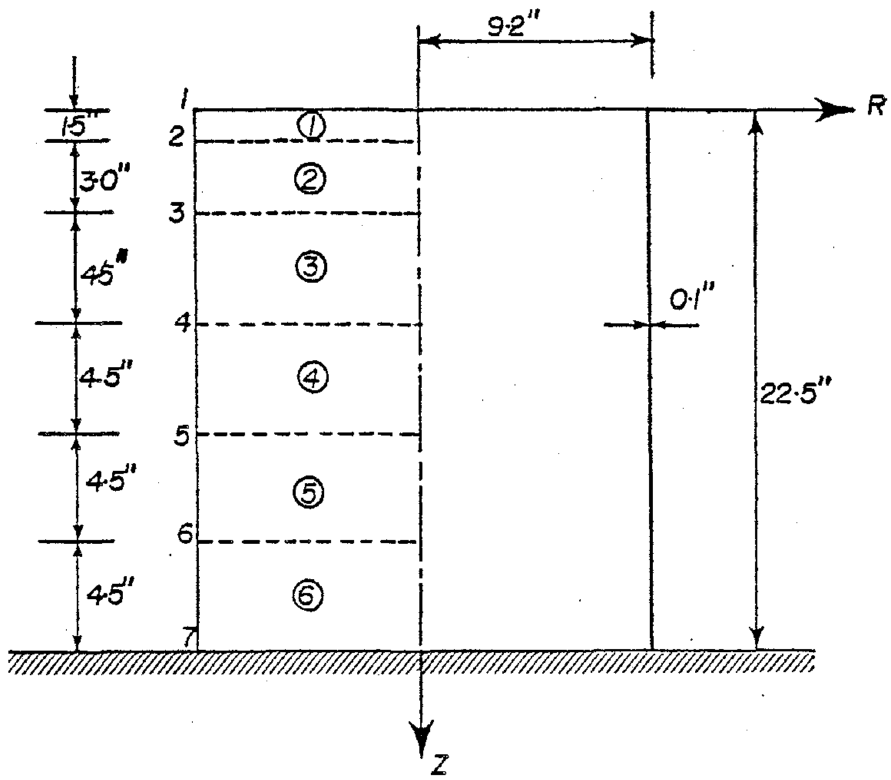

MODULUS OF ELASTICITY = $10 \cdot 5 \times 10^6$ psi
POISSON'S RATIO = 0·3
MASS DENSITY = $2 \cdot 4 \times 10^{-4}$ lb. Sec^2/in^4

Figure 32. Fixed Base Cylindrical Shell

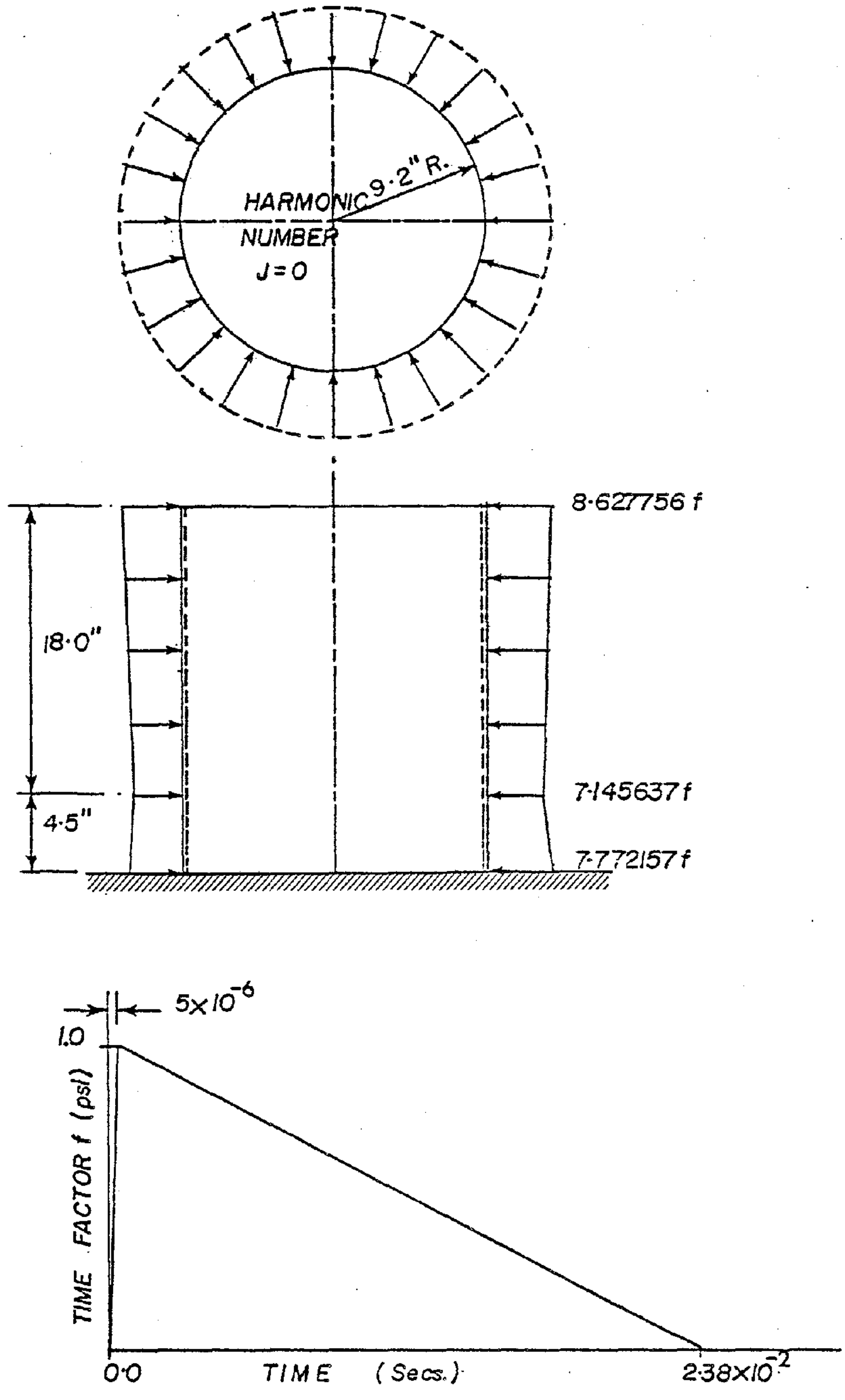

Figure 33. Zero Harmonic of the Blast Loading
on Cylindrical Shell

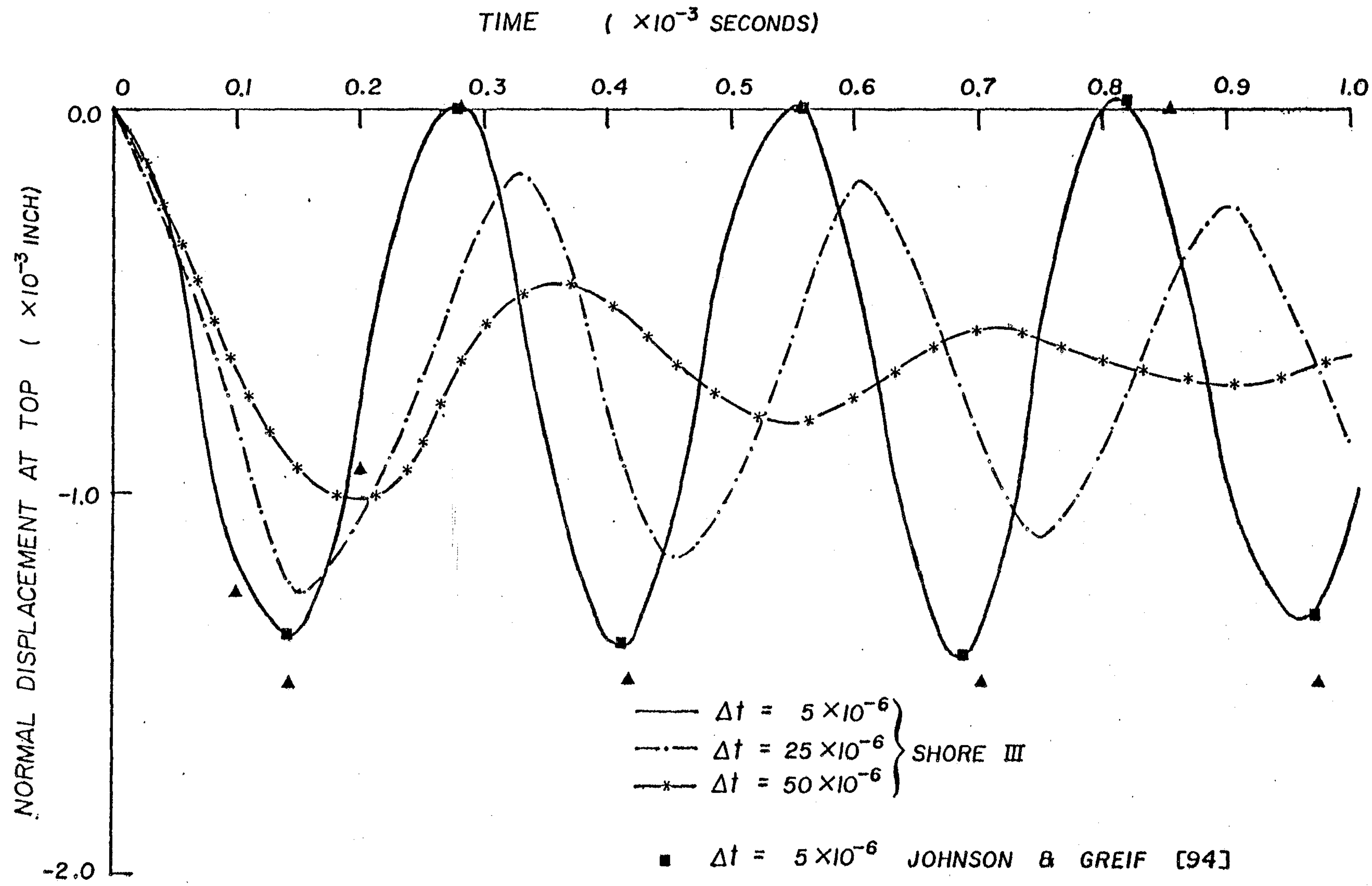

Figure 34. Time History of Normal Displacement at the Top of Cylindrical Shell

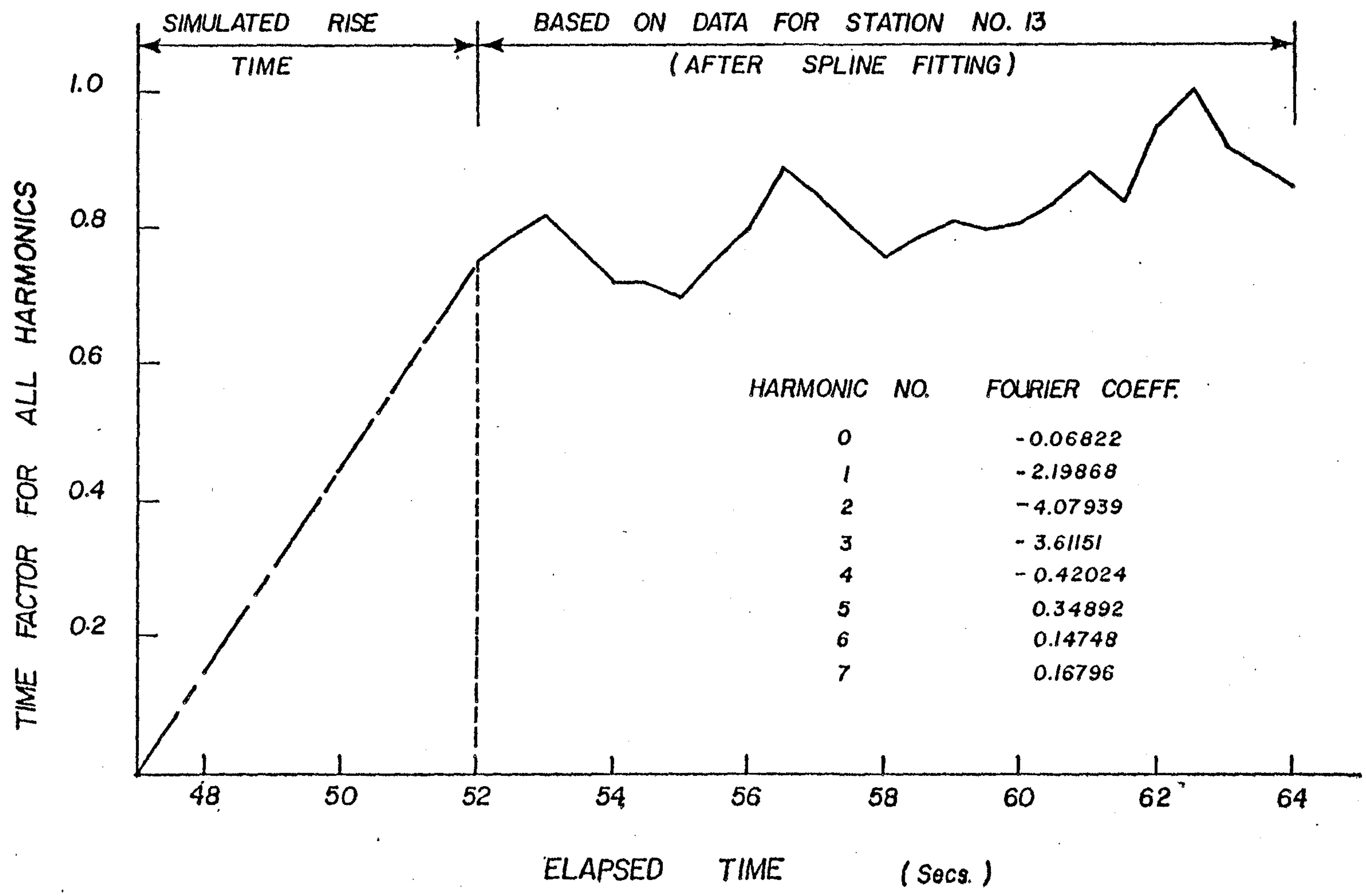

Figure 35. Time History of Wind Loading for Hyperboloidal Tower

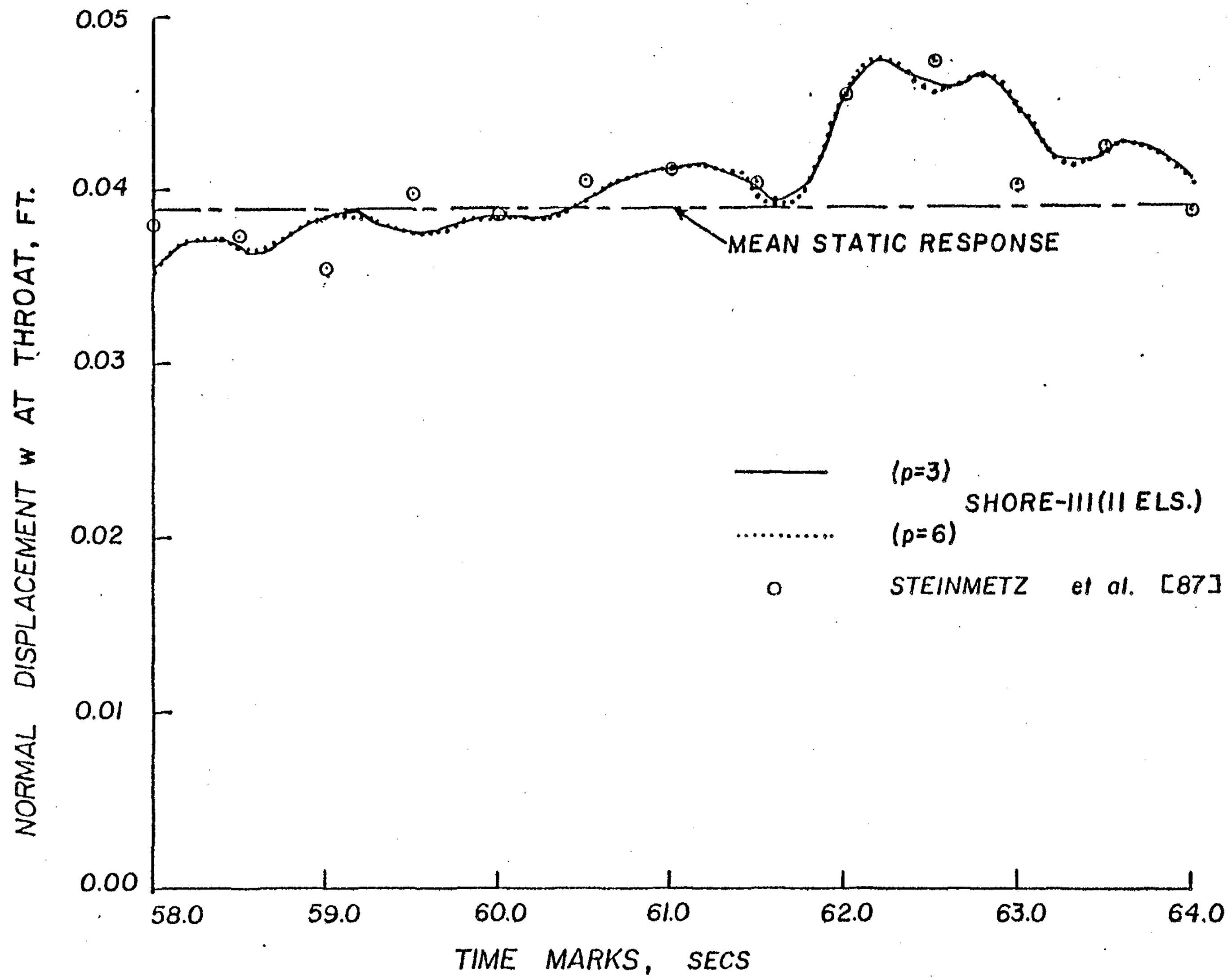

Figure 36. Time History of Normal Displacement at Throat Level for Hyperboloidal Tower Under Wind Load

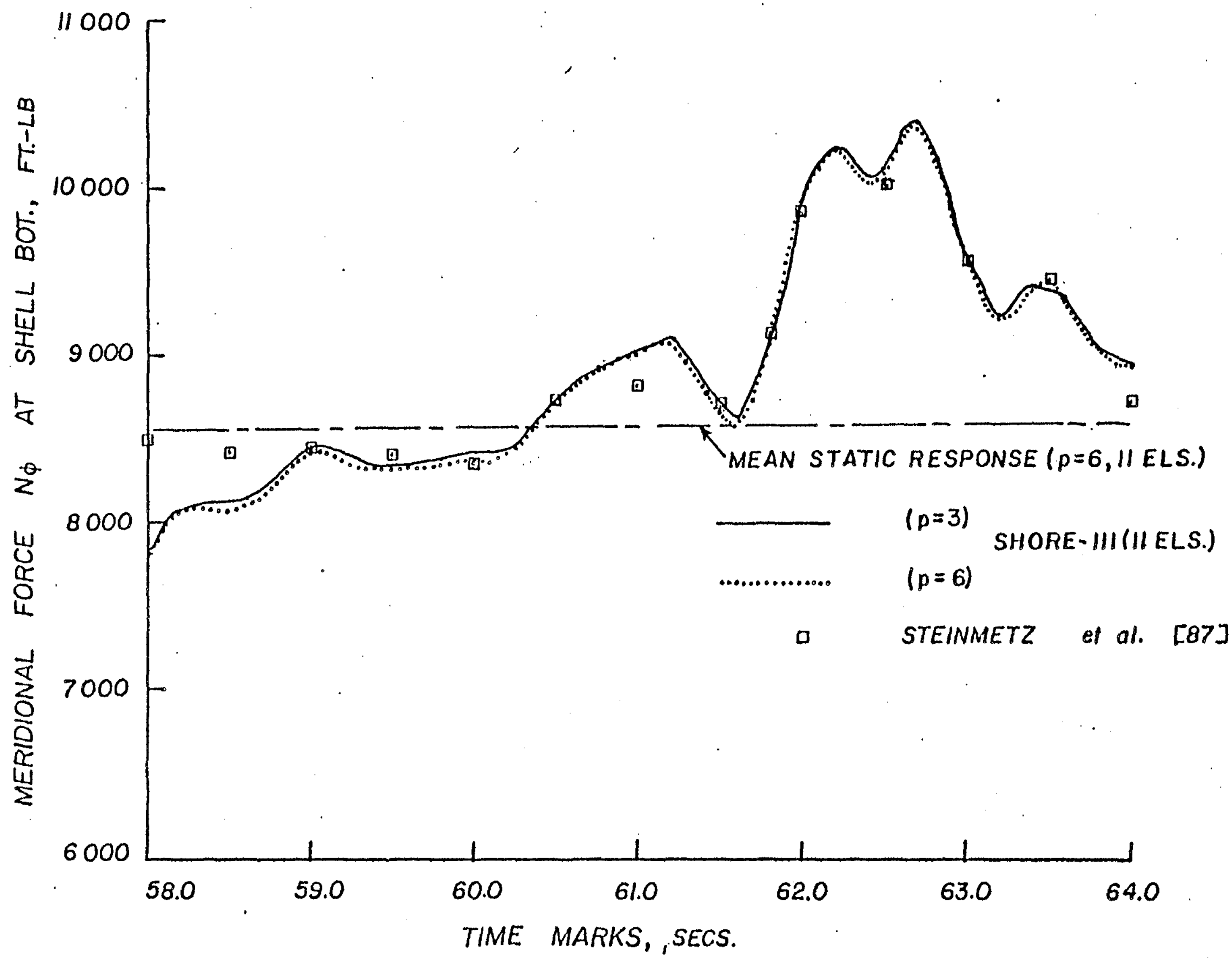

Figure 37. Time History of Meridional Force at Shell Bottom for Hyperboloidal Tower under Wind Load

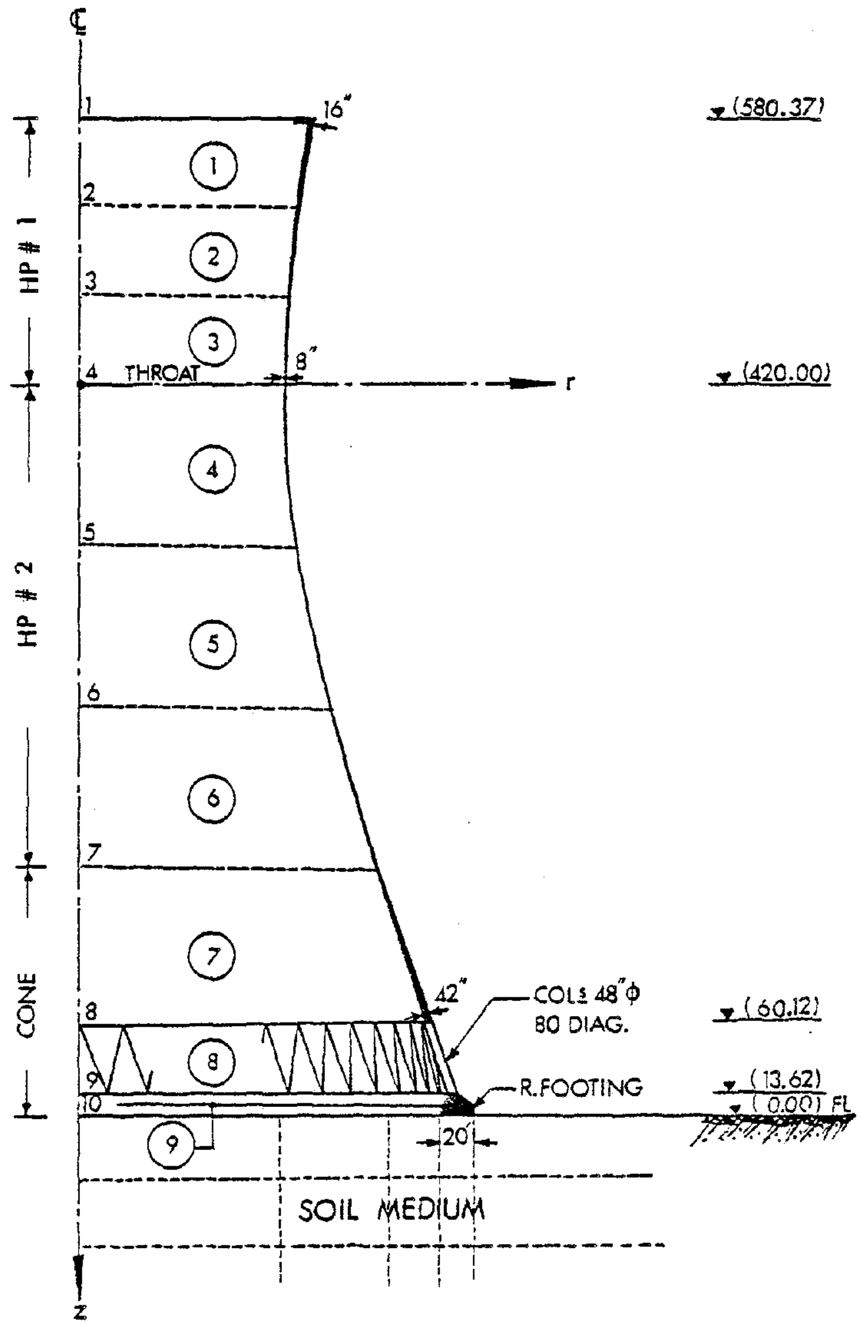

Figure 38. Cooling Tower on a Hypothetical Foundation

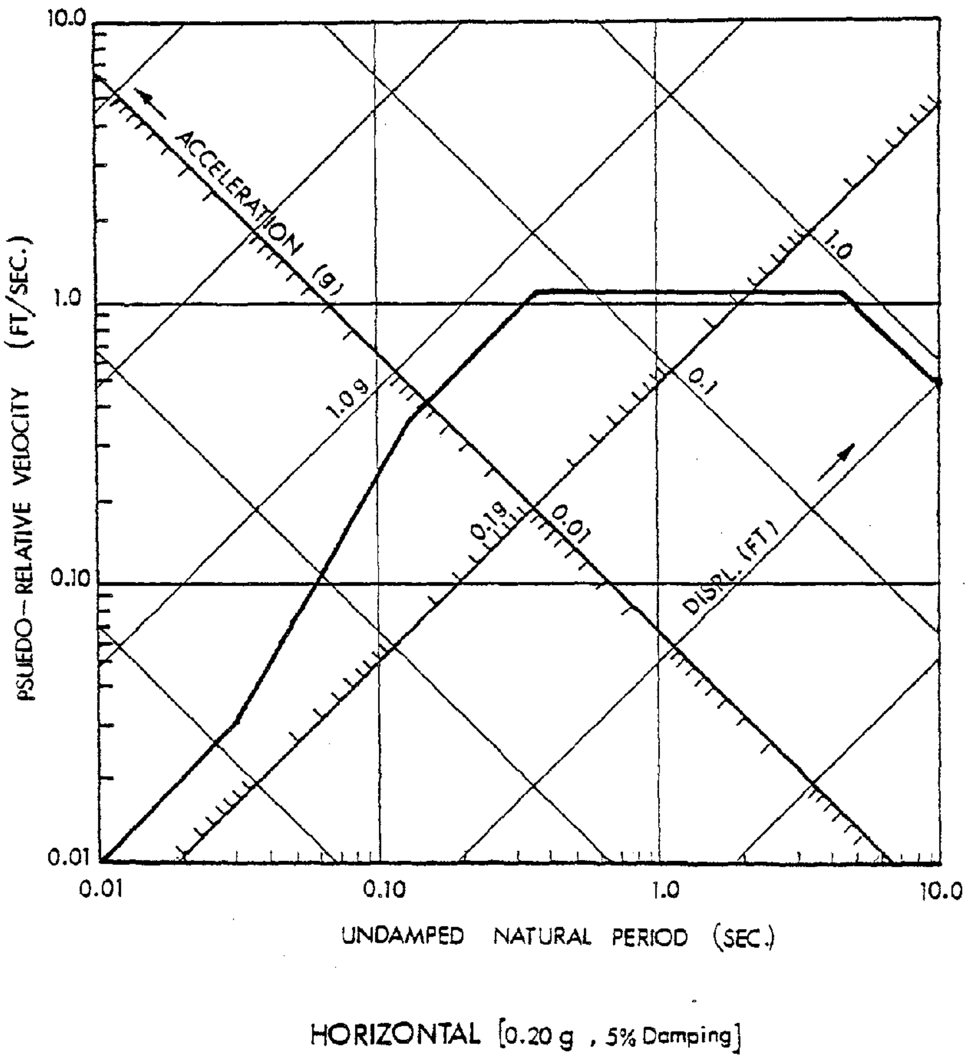

Figure 39. Horizontal Response Spectrum

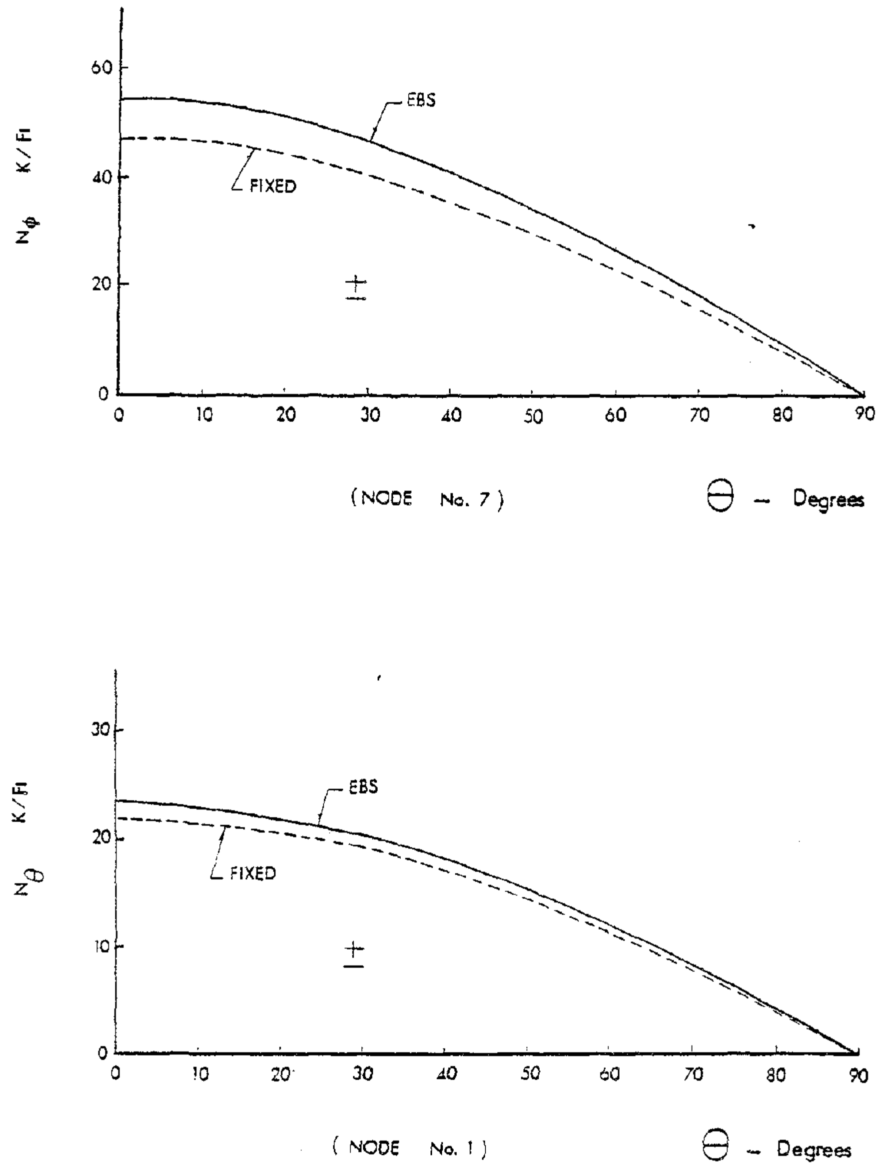

Figure 40. RSS of N_ϕ and N_θ

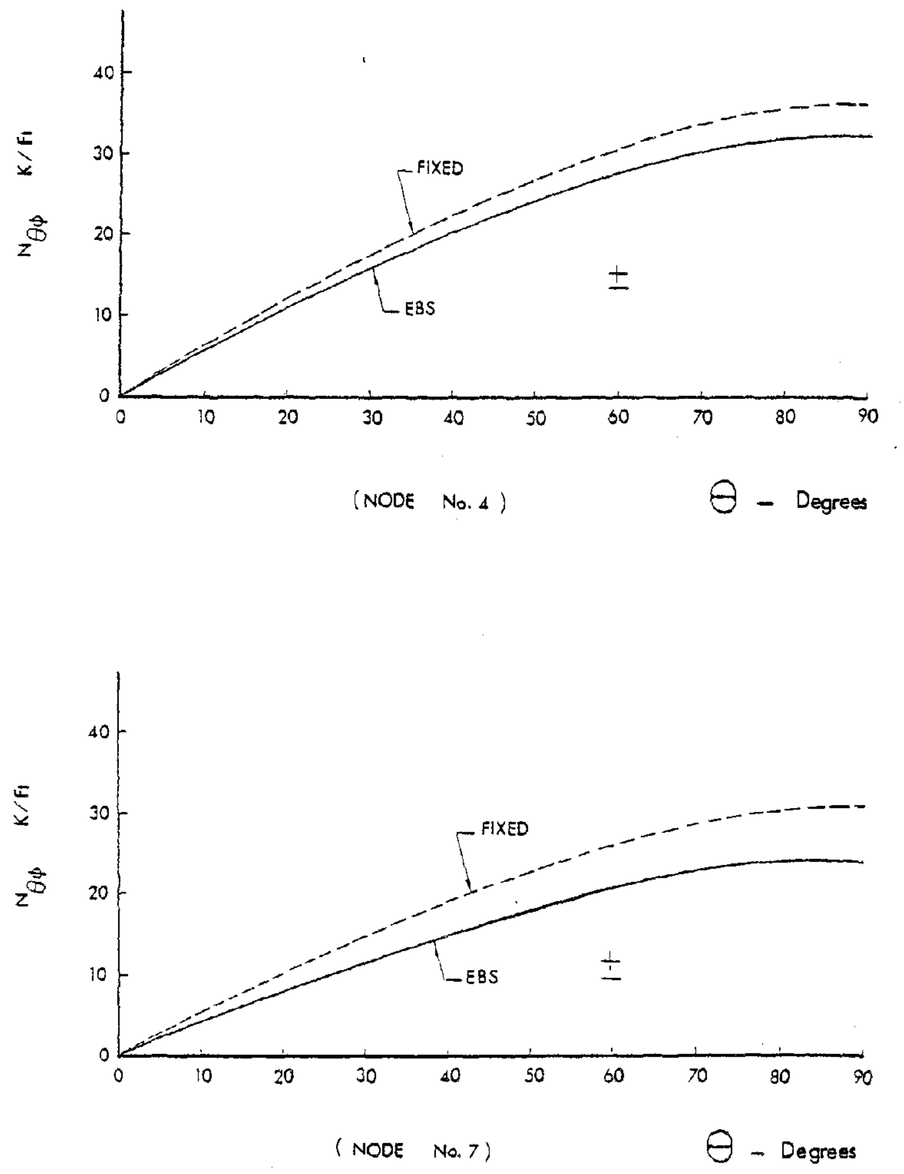

Figure 41. RSS of $N_{\theta\phi}$

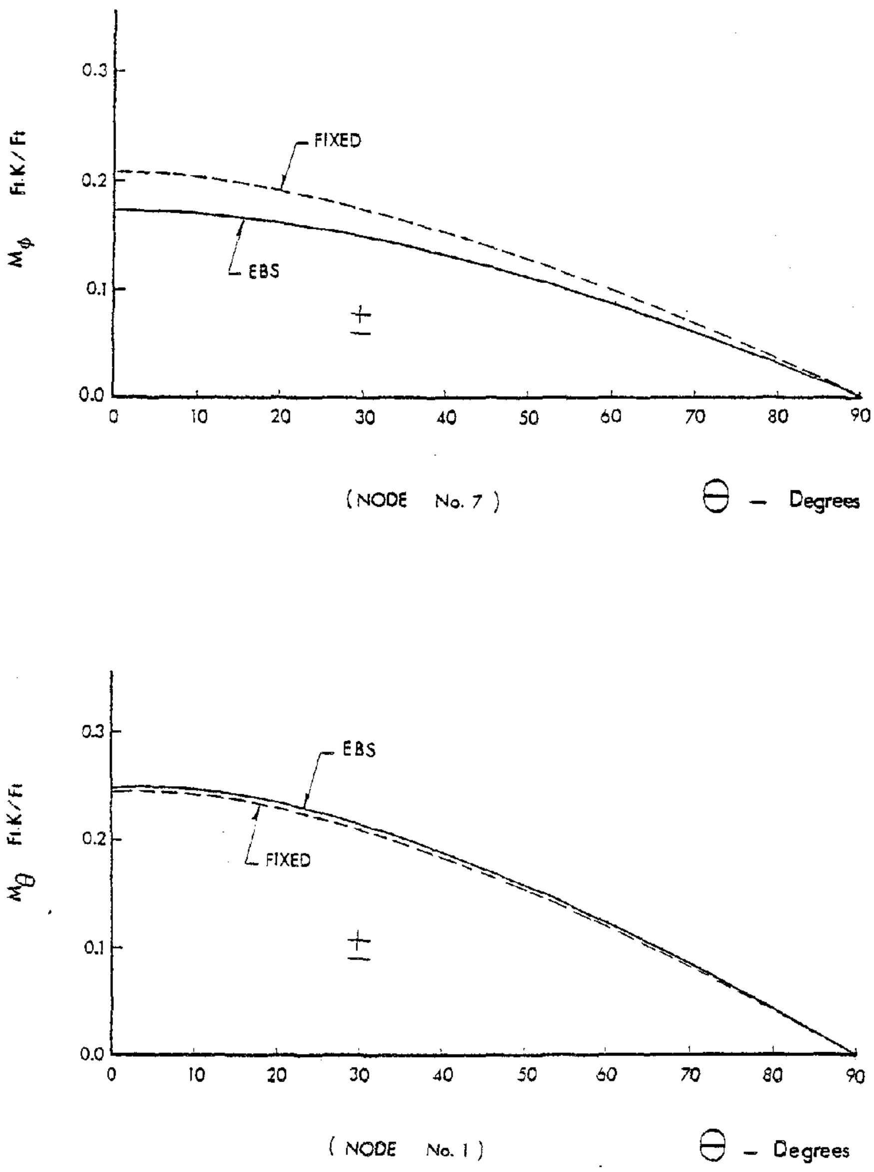

Figure 42. RSS of M_ϕ and M_θ

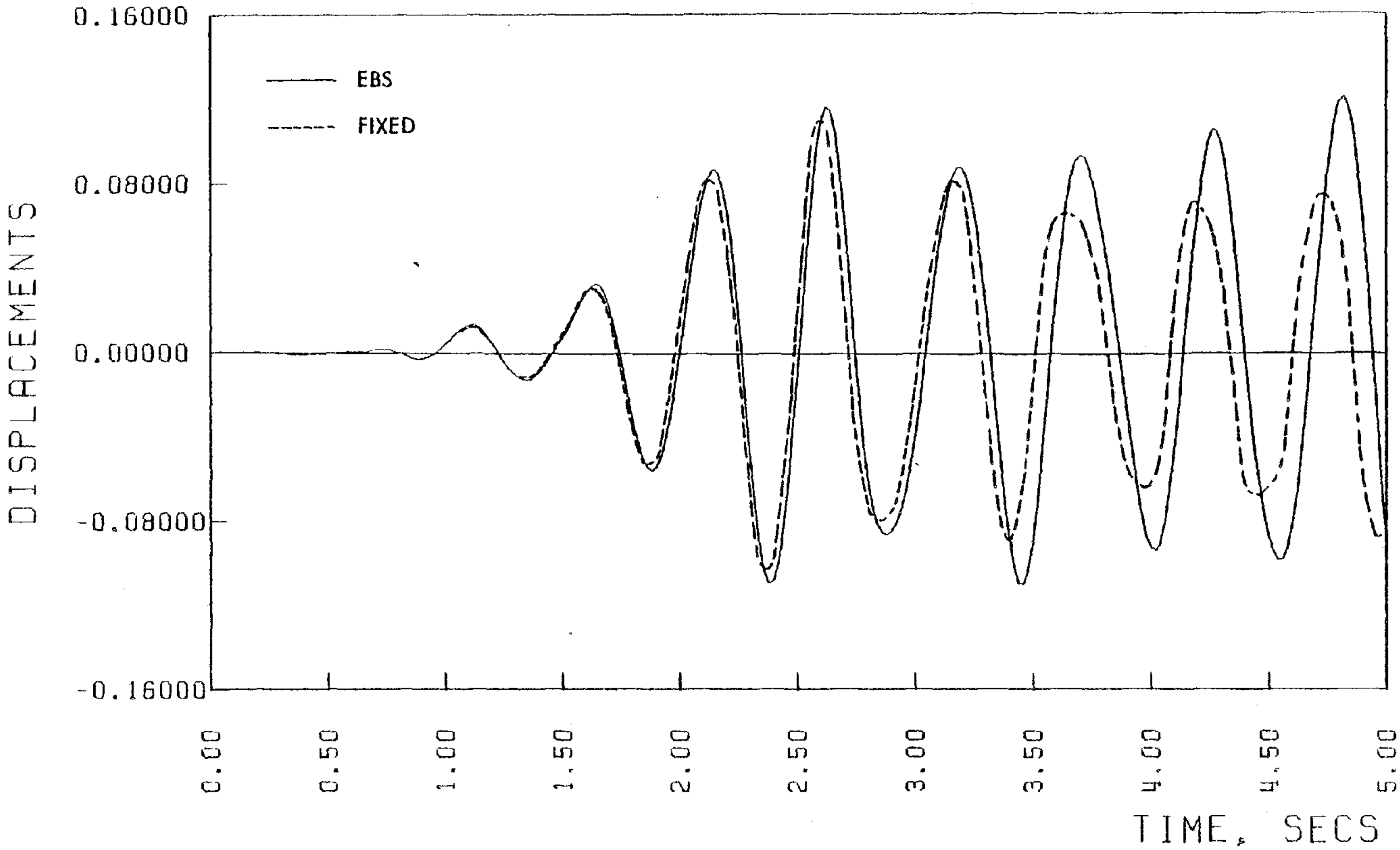

Figure 43. TIME HISTORY PLOT FOR HARMONIC NUMBER = 1

COMPONENT NO. 3 AT NODE NO. 1

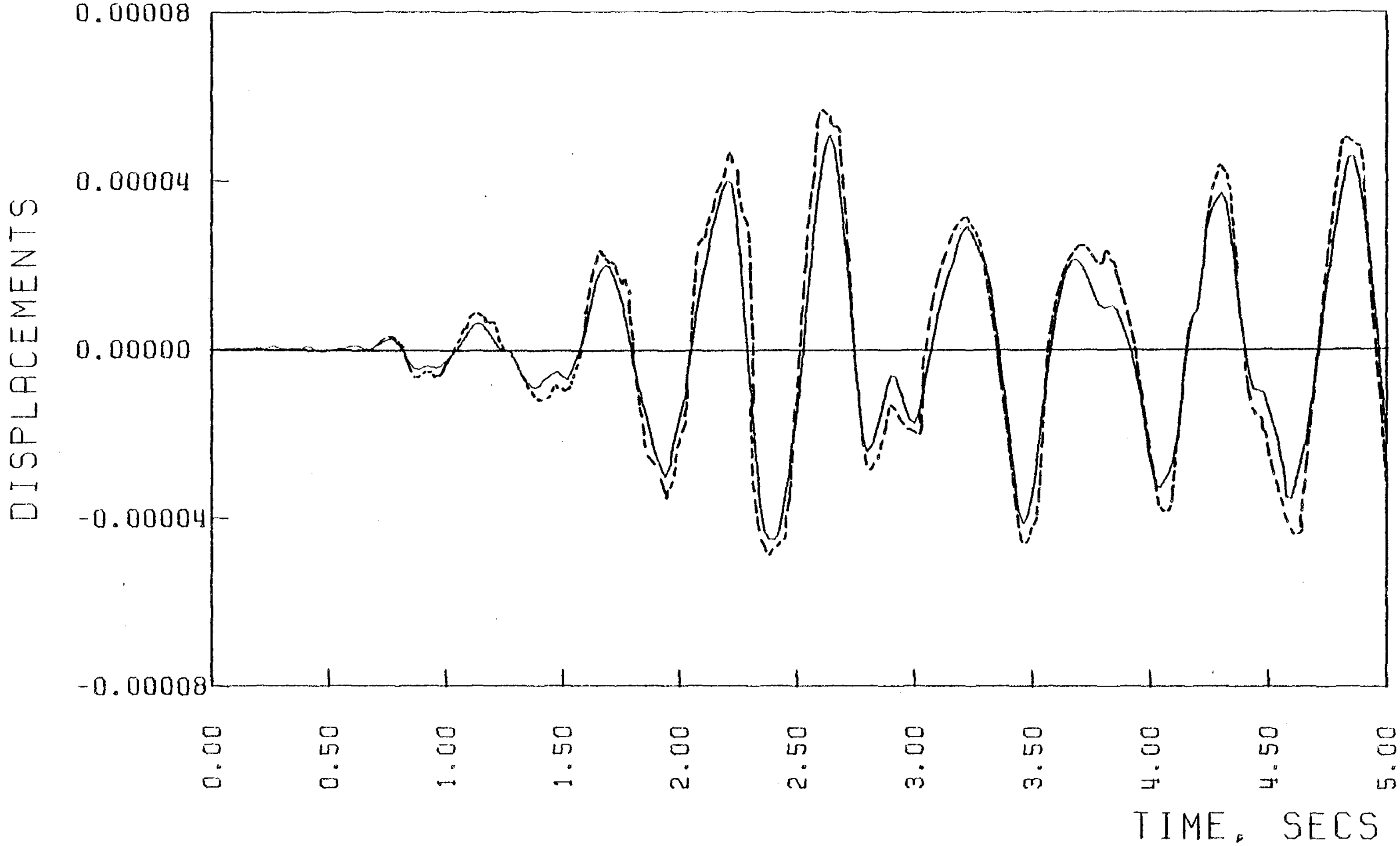

Figure 44. TIME HISTØRY PLØT FØR HARMØNIC NUMBER = 1

COMPØNENT NØ. 5 AT NØDE NØ. 1

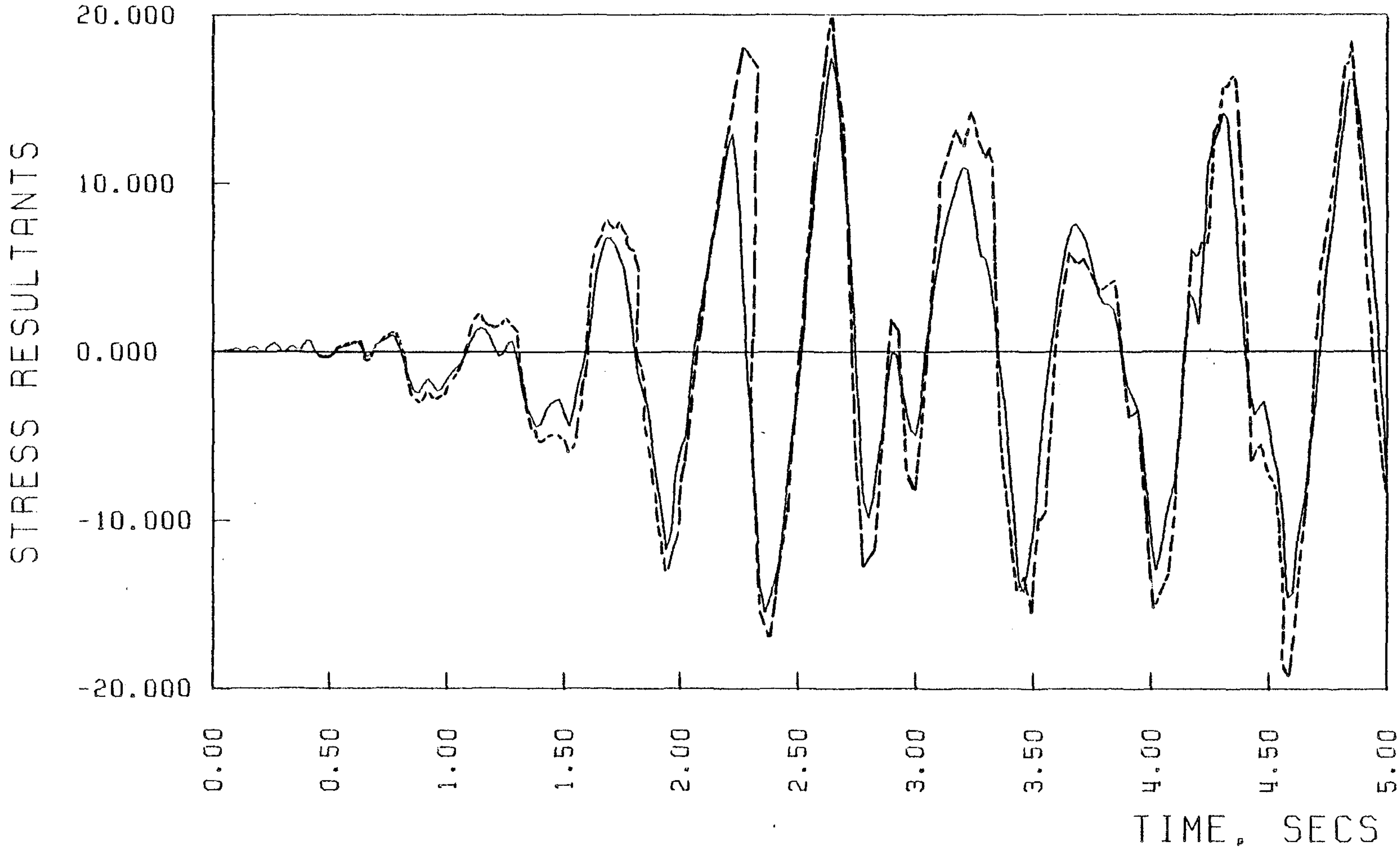

Figure 45. TIME HISTØRY PLØT FØR HARMØNIC NUMBER = 1
COMPØNENT NØ. 2 AT NØDE NØ. 1

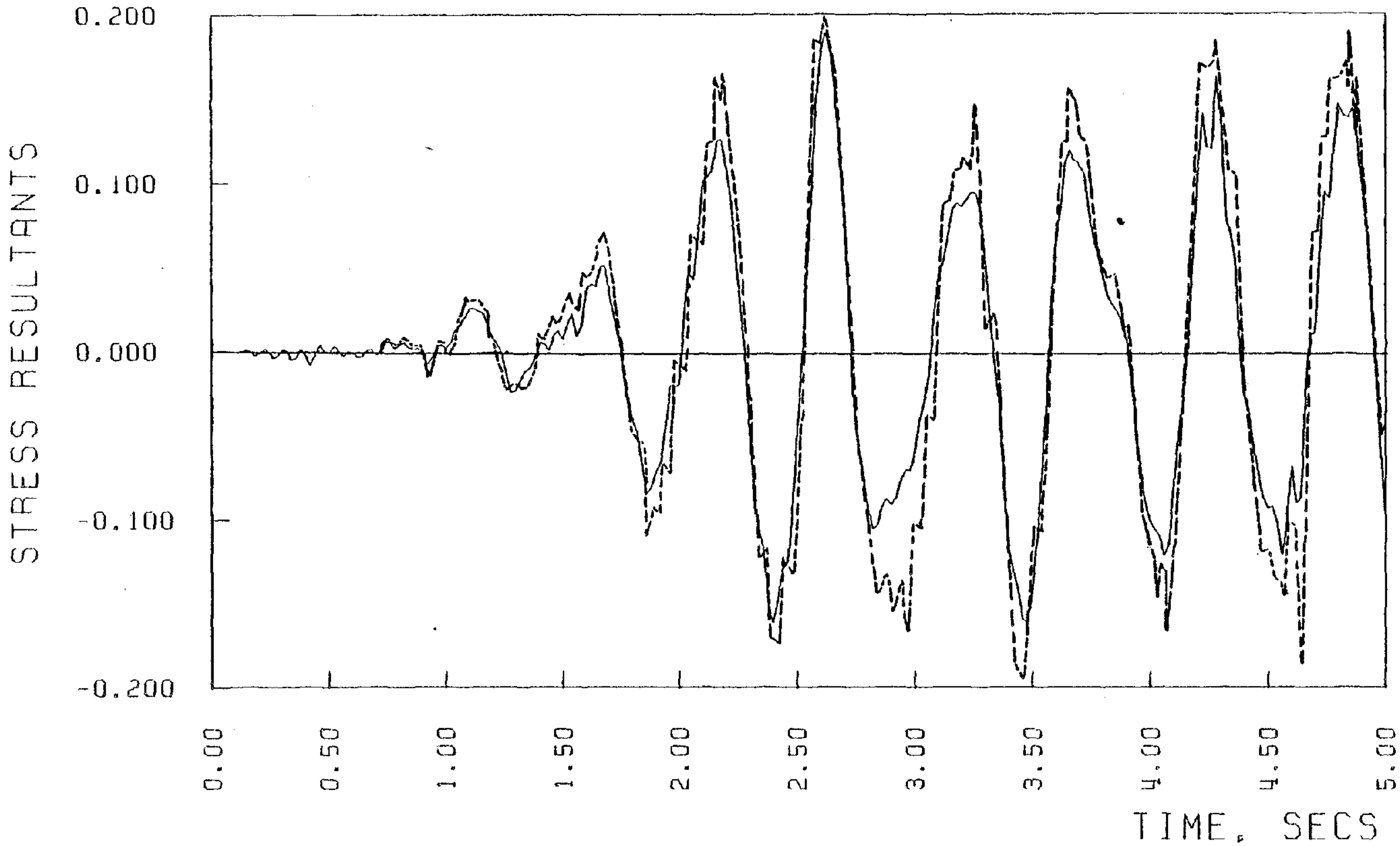

Figure 46. TIME HISTØRY PLØT FØR HARMØNIC NUMBER = 1

COMPØNENT NØ. 4 AT NØDE NØ. 1

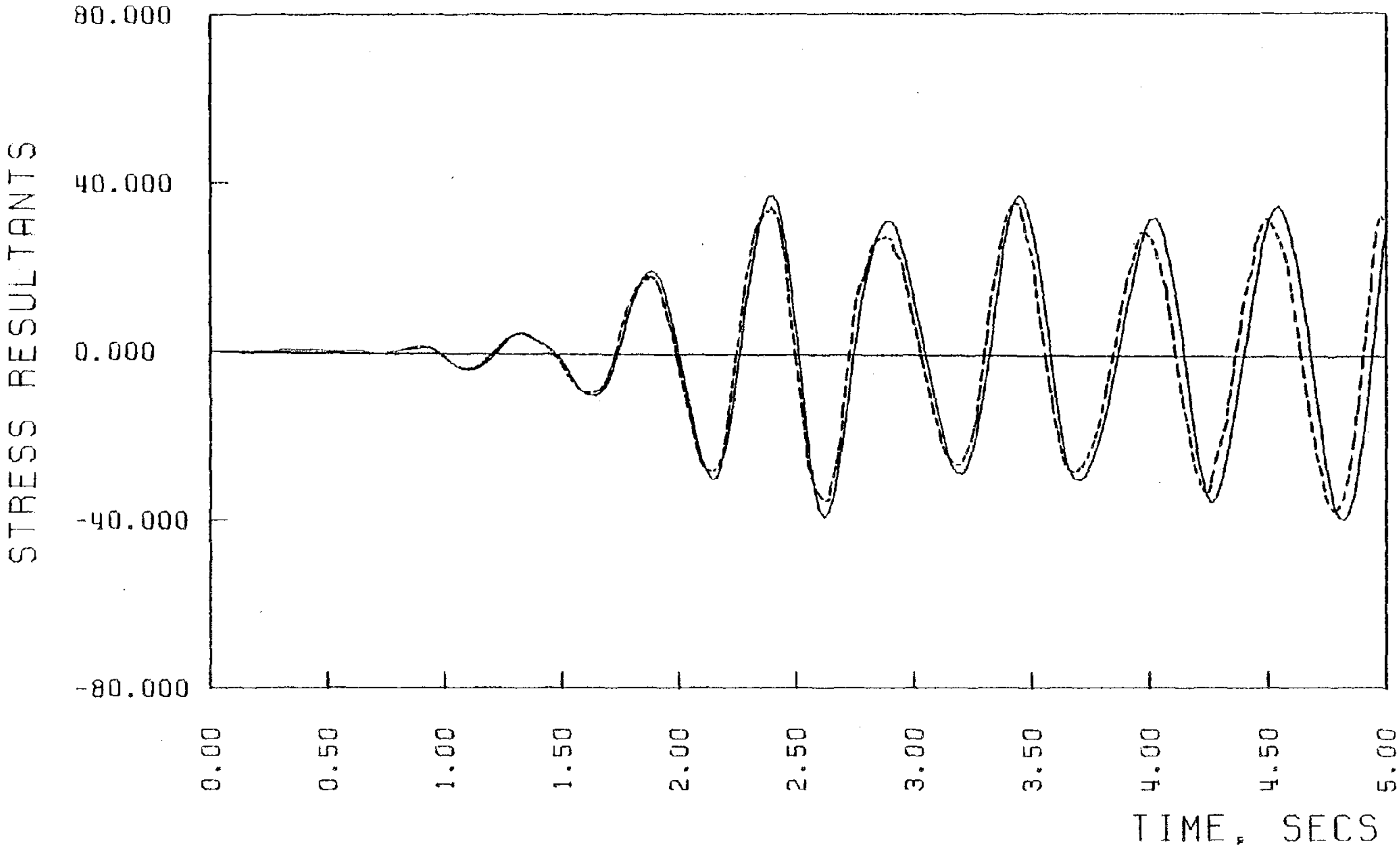

Figure 47. TIME HISTØRY PLØT FØR HARMØNIC NUMBER = 1

COMPØNENT NØ. 1 AT NØDE NØ. 7

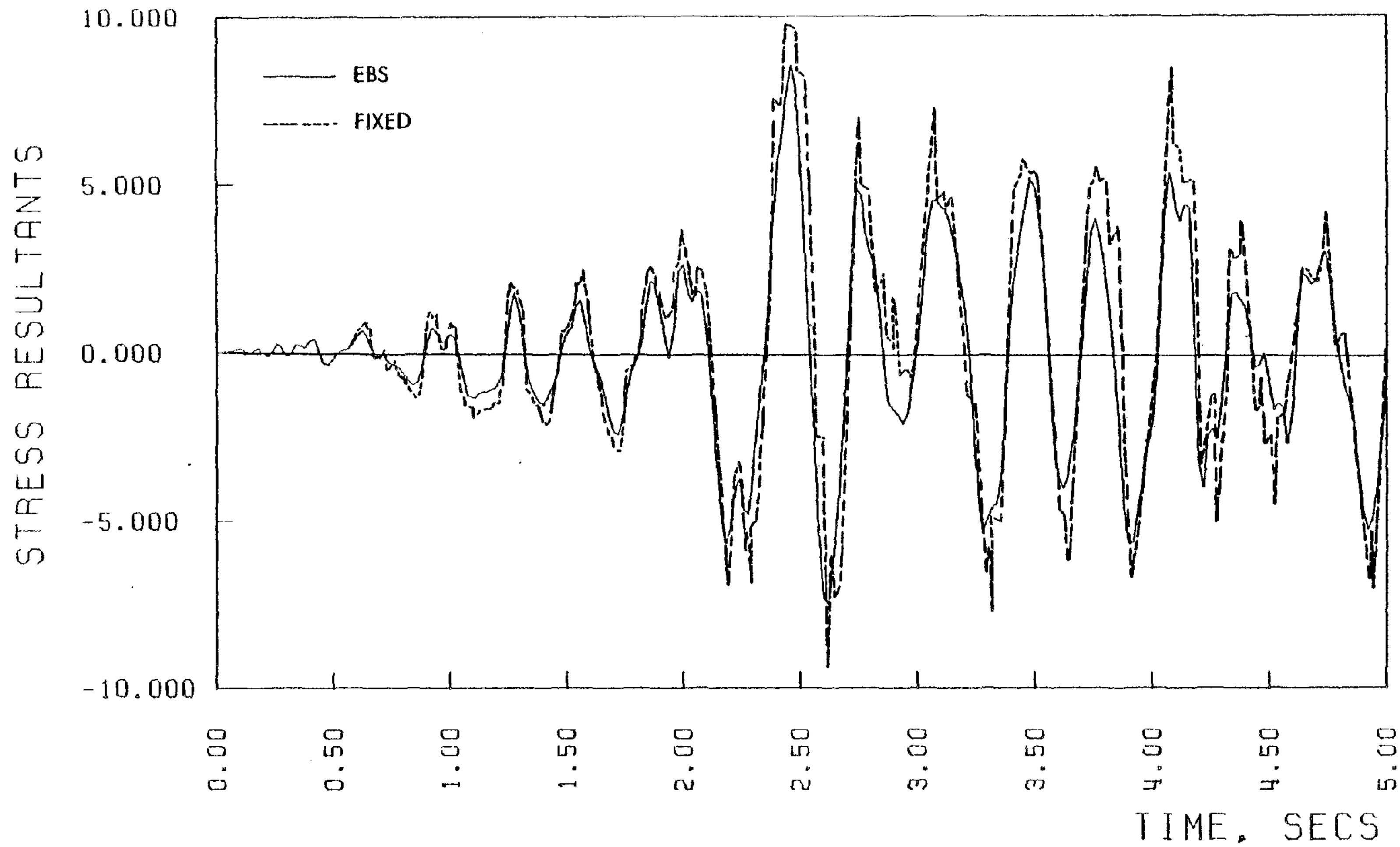

Figure 48. TIME HISTORY PLOT FOR HARMONIC NUMBER = 1

COMPONENT NO. 2 AT NODE NO. 7

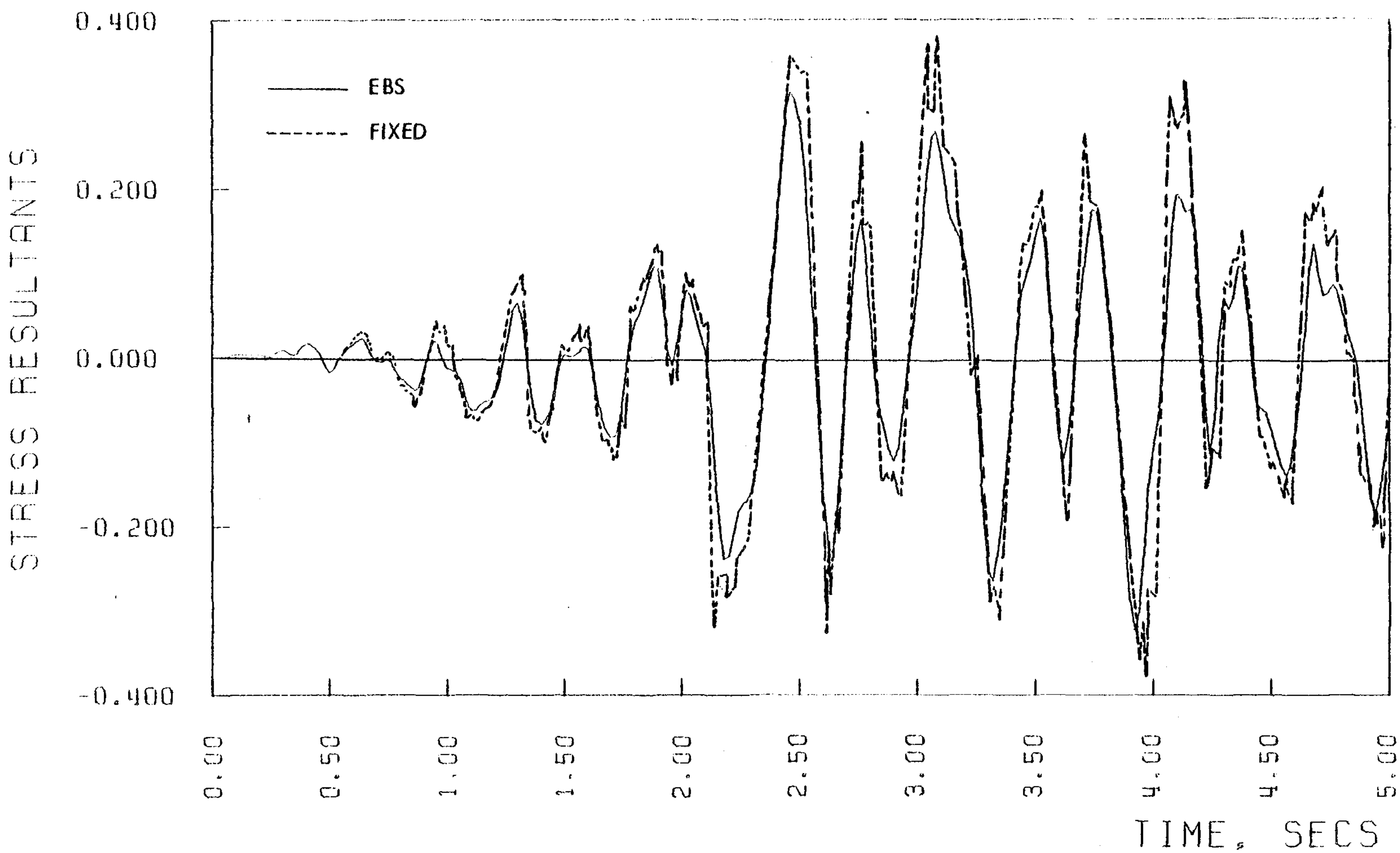

Figure 49. TIME HISTORY PLOT FOR HARMONIC NUMBER = 1

COMPONENT NO. 3 AT NODE NO. 7

APPENDIX A - STRAIN-DISPLACEMENT RELATIONSHIPS

$$\varepsilon_\phi = \frac{1}{L}\frac{\partial u}{\partial s} + \frac{w}{R_\phi}$$

$$\varepsilon_\theta = \frac{1}{R}\left(\frac{\partial v}{\partial \theta} + w \sin\phi + u \cos\phi\right)$$

$$\varepsilon_{\phi\theta} = \frac{1}{L}\frac{\partial v}{\partial s} + \frac{1}{R}\frac{\partial u}{\partial \theta} - \frac{v \cos\phi}{R}$$

$$\chi_\phi = \frac{1}{L}\frac{\partial \beta_\phi}{\partial s}$$

$$\chi_\theta = \frac{1}{R}\frac{\partial \beta_\theta}{\partial \theta} + \beta_\phi \cos\phi$$

$$\chi_{\phi\theta} = \frac{1}{R}\frac{\partial \beta_\phi}{\partial \theta} + \frac{1}{L}\frac{\partial \beta_\theta}{\partial s} - \beta_\theta \cos\phi$$

$$\gamma_\phi = \beta_\phi - \left(\frac{u}{R_\phi} - \frac{1}{L}\frac{\partial w}{\partial s}\right)$$

$$\gamma_\theta = \beta_\theta - \left(\frac{v \sin\phi}{R} - \frac{1}{R}\frac{\partial w}{\partial \theta}\right)$$

APPENDIX B – ELEMENTS OF CONSTITUTIVE MATRIX

The elements of constitutive matrix [H] for isotropic and single-layer orthotropic shells are given below.

	Isotropic	Single-layer Orthotropic
H_{11}	$A_i h$	$A_o h$
H_{12}	$\mu A_i h$	$\mu_{\phi\theta} A_o h$
H_{22}	$A_i h$	$\frac{\mu_{\phi\theta}}{\mu_{\theta\phi}} A_o h$
H_{33}	$(1-\mu)A_i h/2$	$G_{\phi\theta} h$
H_{44}	$A_i h^3/12$	$A_o h^3/12$
H_{45}	$\mu A_i h^3/12$	$\mu_{\phi\theta} A_o h^3/12$
H_{55}	$A_i h^3/12$	$\frac{\mu_{\phi\theta}}{\mu_{\theta\phi}} A_o h^3/12$
H_{66}	$(1-\mu)A_i h^3/24$	$G_{\phi\theta} h^3/12$
H_{77}	$\lambda(1-\mu)A_i h/2$	$\lambda G_{\phi n} h$
H_{88}	$\lambda(1-\mu)A_i h/2$	$\lambda G_{\theta n} h$

$A_i = E/(1-\mu^2)$; h = total shell thickness at any point in the meridian

λ = shear factor (to suppress transverse shearing strains, i.e. Kirchhoff hypothesis, set λ=100)

$A_o = E_\phi(1 - \mu_{\theta\phi}\cdot\mu_{\phi\theta})$

E_ϕ = Young's modulus in ϕ-direction

$\mu_{\phi\theta}$, $\mu_{\theta\phi}$ = Poisson's ratios for ϕ or θ directions with respect to θ or ϕ directions

$G_{\phi\theta}$, $G_{\phi n}$, $G_{\theta n}$ = the shear moduli for ϕ-θ, ϕ-n, and θ-n planes

The elements of the constitutive matrix [H] for symmetrical multi-layer layer orthotropic shells are given below.

	Multi-layer Orthotropic
H_{11}	$\sum_h (A_o)_k h_k$
H_{12}	$\sum_h (\mu_{\phi\theta} A_o)_k h_k$
H_{22}	$\sum_h (\frac{\mu_{\phi\theta}}{\mu_{\theta\phi}} A_o)_k h_k$
H_{33}	$\sum_h (G_{\phi\theta})_k h_k$
H_{44}	$\sum_h (A_o)_k (\zeta_k^2 + \frac{h_k^2}{12}) h_k$
H_{45}	$\sum_h (\mu_{\phi\theta} A_o)_k (\zeta_k^2 + \frac{h_k^2}{12}) h_k$
H_{55}	$\sum_h (\frac{\mu_{\phi\theta}}{\mu_{\theta\phi}} A_o)_k (\zeta_k^2 + \frac{h_k^2}{12}) h_k$
H_{66}	$\sum_h (G_{\phi\theta})_k (\zeta_k^2 + \frac{h_k^2}{12}) h_k$
H_{77}	$\lambda \sum_h (G_{\phi n})_k h_k$
H_{88}	$\lambda \sum_h (G_{\theta n})_k h_k$

$(A_o)_k$, etc. = the value of A_o, etc for layer 'k' at any point

h_k = thickness of layer 'k'

ζ_k = the distance from the centroid of layer k to middle surface, assuming symmetrical layers (see Fig

APPENDIX C-DIRECT INTEGRATION SCHEMES

1. Single Step Higher Derivative Schemes:

After the stiffness matrix [K] and mass matrix [M] has been formed, it is necessary to evaulate the following constants.

$$A_1 = \left(\frac{1}{P_1 \Delta t^2} + \frac{P_2 P_3}{P_1} \frac{\alpha}{\Delta t} \right) / \left(P_3^{\,2} + \frac{P_2 P_3}{P_1} \frac{\beta}{\Delta t} \right)$$

$$A_2 = P_3^{\,2} + \frac{P_2 P_3}{P_1} \frac{\beta}{\Delta t}$$

$$A_3 = \frac{1}{P_1 \Delta t^2} + \frac{P_2 P_3}{P_1} \frac{(\alpha - A_1 \beta)}{\Delta t} + \left(\frac{1}{P_3} - P_3^{\,2} \right) A_1$$

$$A_4 = \frac{1}{P_1 \Delta t} + \left(\frac{P_2 P_3}{P_1} - \frac{1}{P_3} \right)(\alpha - A_1 \beta) + (1 - P_3^{\,2}) A_1 \Delta t$$

$$A_5 = \left(\frac{1}{2P_1} - 1 \right) + \left(\frac{P_2 P_3}{2P_1} - 1 \right)(\alpha - A_1 \beta) \Delta t + (P_3 - P_3^{\,2}) A_1 \frac{\Delta t^2}{2} + \left(\frac{P_3 - 1}{P_3} \right)$$

$$A_6 = \left(A_2 - \frac{1}{P_3} \right)$$

$$A_7 = (A_2 - 1) \Delta t - \frac{\beta}{P_3}$$

$$A_8 = \left(\frac{P_2 P_3}{2P_1} - 1 \right) \beta \Delta t + \frac{P_3 (P_3 - 1)}{2} \Delta t^2$$

$$A_9 = \frac{1}{P_1 \Delta t^2}$$

$$A_{10} = \frac{1}{P_1 \Delta t}$$

$$A_{11} = \left(\frac{1}{2P_1} - 1 \right)$$

$$A_{12} = \frac{P_2}{P_1 \Delta t}$$

$$A_{13} = \left(\frac{P_2}{P_1} - 1 \right)$$

$$A_{14} = \left(\frac{P_2}{2P_1} - 1 \right) \Delta t$$

where

P_1, P_2, P_3 = the parameters of integration scheme

Δt = the time step

α, β = the coefficients of Rayleigh damping matrix

Next, it is necessary to form the modified stiffness matrix. It is followed by forward elimination.

$$[\tilde{K}] = [K] + A_1 [M]$$

Then, the modified load vector is formed as below.

$$\{\tilde{F}(t+\Delta t)\} = \{F(t+\Delta t)\} + \frac{1-P_3}{P_3} \{F(t)\}$$
$$+ [M] (A_3\{\Delta(t)\} + A_4\{\dot{\Delta}(t)\} + A_5\{\ddot{\Delta}(t)\})$$

Finally, the displacements $\{\tilde{\Delta}(t+\Delta t)\}$ are calculated by back substitution. Thus,

$$\{\tilde{\Delta}(t+ t)\} = [\tilde{K}]^{-1} \{\tilde{F}(t\Delta t)\}$$

and the true displacement vector at time 't+Δt' will then be

$$\{\Delta(t+\Delta t)\} = (\{\tilde{\Delta}(t+\Delta t)\} + A_6\{\Delta(t)\} + A_7\{\dot{\Delta}(t)\} + A_8\{\ddot{\Delta}(t)\}) / A_2$$

the corresponding velocity and acceleration vectors are then calculated from

$$\{\dot{\Delta}(t+\Delta t)\} = A_{12}\{\Delta(t+\Delta t)\} - A_{12}\{\Delta(t)\} - A_{13}\{\dot{\Delta}(t)\} - A_{14}\{\ddot{\Delta}(t)\}$$

$$\{\ddot{\Delta}(t+\Delta t)\} = A_9\{\Delta(t+\Delta t)\} - A_9\{\Delta(t)\} - A_{10}\{\dot{\Delta}(t)\} - A_{11}\{\ddot{\Delta}(t)\}$$

In the case of the Newmark-β method, $P_3 = 1$. For the Wilson-θ method, $P_1 = 1/6$ and $P_2 = 1/2$. For an unconditionally stable scheme, in the first case, one should take $P_1 = 1/4$ and $P_2 = 1/2$, and in the later case $P_3 = 1.4$.

2. Multistep (3-step) Schemes:

Here the constants to be evaluated are

$$\tilde{A}_1 = \left(\frac{P_5}{\Delta t} + P_1\alpha \right) / \left(\Delta t + P_1\beta \right)$$

$$\tilde{A}_2 = \left(1 + \frac{P_1\beta}{\Delta t} \right)$$

$$\tilde{A}_3 = -\frac{P_6}{\Delta t^2} - \frac{P_2(\alpha - \beta A_1)}{\Delta t}$$

$$\tilde{A}_4 = -\frac{P_7}{\Delta t^2} - \frac{P_3(\alpha - \beta A_1)}{\Delta t}$$

$$\tilde{A}_5 = -\frac{P_8}{\Delta t^2} - \frac{P_4(\alpha - \beta A_1)}{\Delta t}$$

$$\tilde{A}_6 = -\frac{P_2\beta}{\Delta t}$$

$$\tilde{A}_7 = \frac{P_3\beta}{\Delta t}$$

$$\tilde{A}_8 = -\frac{P_4}{\Delta t}$$

where P_1, P_2, etc. are the parameters of integration scheme.

Here the modified stiffness matrix and load vector will be

$$[\tilde{K}] = [K] + \tilde{A}_1 [M]$$

$$\{\tilde{F}(t+\Delta t)\} = \{F(t+\Delta t)\} + [M] (\tilde{A}_3\{\Delta(t)\} + \tilde{A}_4\{\Delta(t-\Delta t)\} + \tilde{A}_5\{\Delta(t-2\Delta t)\})$$

As in scheme 1, after solving the following for $\{\tilde{\Delta}(t+\Delta t)\}$

$$[\tilde{K}]\ \{\tilde{\Delta}(t+\Delta t)\} = \{\tilde{F}(t+\Delta t)\}$$

the displacement vector is calculated from

$$\{\Delta(t+\Delta t)\} = (\{\tilde{\Delta}(t+\Delta t)\} + \tilde{A}_6\{\Delta(t)\} + \tilde{A}_7\{\Delta(t-\Delta t)\} + \tilde{A}_8\{\Delta(t-2\Delta t)\}) \;/\; \tilde{A}_2$$

In the case of the first time step, i.e. at $t=\Delta t$, it is necessary to modify some of the aforementioned constants as below.

$$\tilde{C}_1 = (P_3 + 8P_4)\beta$$

$$\tilde{C}_2 = (P_7 + 8P_8) + (P_3 + 8P_4)\alpha$$

$$\tilde{C}_3 = (\tilde{C}_2 - A_1\tilde{C}_1) \;/\; (A_2 - \tilde{C}_1)$$

$$A_1{*} = (A_1A_2 - \tilde{C}_2) \;/\; (A_2 - \tilde{C}_1)$$

$$A_3{*} = (A_1A_2 - \tilde{C}_2) \;/\; (A_2 - \tilde{C}_1)$$

$$A_4{*} = (A_3 - P_2\tilde{C}_3)$$

$$A_5{*} = (A_5 - P_4\tilde{C}_3)$$

For this step, $\tilde{A}_1$, $\tilde{A}_3$, $\tilde{A}_4$, and $\tilde{A}_5$ are to be replaced by $A_1{*}$, $A_3{*}$, $A_4{*}$, and $A_5{*}$. Moreover, it is necessary to evaluate the following:

$$\{\Delta(-\Delta t)\} = \{\Delta(0)\} - \Delta t\ \{\dot{\Delta}(0)\} + \Delta t^2\ \{\ddot{\Delta}(0)\}/2.0$$

$$\{\Delta(-2\Delta t)\} = -\{\Delta(0)\} + 2\ \{\Delta(-\Delta t)\} + \Delta t^2\ \{\ddot{\Delta}(0)\}$$

In the case of Houbolt's scheme

$P_1 = 11/6$; $P_2 = -3.0$; $P_3 = 1.5$; $P_4 = 1/3$;

$P_5 = 2.0$; $P_6 = -5.0$; $P_7 = 4.0$; $P_8 = -1.0$

REFERENCES

(1) El-Shafee, O.M. and Gould, P.L., "Analytical Method for Determining Seismic Response of Cooling Towers on Footing Foundation", Research Report No. 55, Structural Division, Washington University, Sept. 1979.

(2) Gupta, K.K., "Eigenvalue Solution by a Combined Sturm Sequence and Inverse Iteration Technique", International Journal for Numerical Methods in Engineering, Vol. 7, 1973, pp. 17-42.

(3) Basu, P.K. and Gould, P.L., "SHORE II - Shell of Revolution Finite Element Program - Static Case - Theoretical Manual", Research Report No. 41, Structural Division, Washington University, St. Louis, March 1975.

(4) Brombolich, L.J., and Gould, P.L., "High-Precision Finite Element Analysis of Shells of Revolution," Research Report No. 16, Structural Division, Department of Civil and Environmental Engineering, Washington University, St. Louis, Missouri, Jan. 1973.

(5) Basu, P.K., "Dynamic and Nonlinear Analysis of Shells of Revolution", Doctoral Dissertation, Washington University, St. Louis, March 1977.

(6) Love, A.E.H., "A Treatise on the Mathematical Theory of Elasticity", Fourth Edition, Dover Publications, 1944.

(7) Weingarten, V.I., "Free Vibration of Thin Cylindrical Shells", Journal of the American Institute of Aeronautics and Astronautics, Vol. 2, No. 4, April 1964, pp. 717-722.

(8) Carter, R.L., Robinson, A.R., and Schnobrich, W.C., "Free and Forced Vibrations of Hyperboloidal Shells of Revolution", Structural Research Series No. 334, University of Illinois, Urbana, February 1968.

(9) Kraus, H., "Thin Elastic Shells", John Wiley & Sons, 1967.

(10) Kalnins, A. and Kraus, H., "Effect of Transverse Shear and Rotary Inertia on Vibration of Spherical Shells", Proc. 5th U.S. National Congress of Applied Mechanics, ASME, 1966, p. 134.

(11) Albasiny, E.L. and Martin, D.W., "Bending and Membrane Equilibrium in Cooling Towers", Journal of Engineering Mechanics Division, ASCE, Vol. 93, pp. 1-17.

(12) Johnson, D.E. and Grief, R., "Dynamic Response of a Cylindrical Shell: Two Numerical Methods", AIAA Journal, Vol. 4, No. 3, March 1966, pp. 486-494.

(13) Steinmetz, R.L., Billington, D.P., and Abel, J.F., "The Dynamic Response of Hyperbolic Cooling Towers to Wind", Research Report No. 76-SM-5, Princeton University, April 1976.

(14) Basu, P.K. and Gould, P.L., "SHORE - III, Shell of Revolution Finite Element Program - Theoretical Manual", Research Report No. 48, Structural Division, Washington University, St. Louis, MO, Sept. 1977.